Analysis of the set-down of structures onto the seabed

Interaction between structure, hydro-dynamic force and soil

J.J.F. Vogelzang

Delft University of Technology

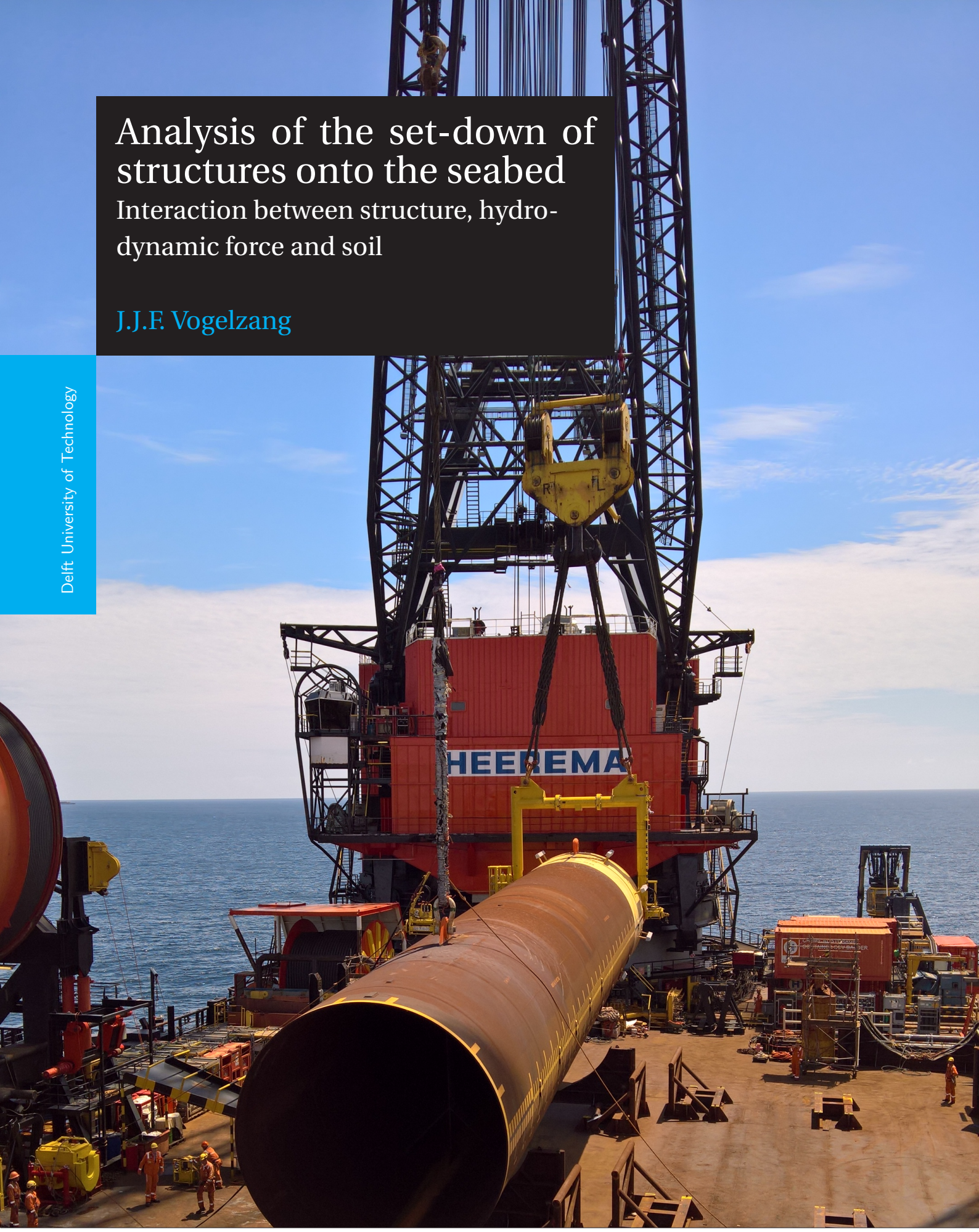

TU Delft Delft University of Technology

Challenge the future

ANALYSIS OF THE SET-DOWN OF STRUCTURES ONTO THE SEABED

INTERACTION BETWEEN STRUCTURE, HYDRODYNAMIC FORCE AND SOIL

by

J.J.F. Vogelzang

in partial fulfillment of the requirements for the degree of

Master of Science
in Offshore & Dredging Engineering

at the Delft University of Technology,
to be defended publicly on Thursday April 20, 2017 at 12:00 hours.

Chair:	Prof. Dr. A.V. Metrikine	TU Delft
Committee:	Dr. Ir. A. Jarquin Laguna	TU Delft
	Dr. Ir. K.N. van Dalen	TU Delft
	Ir. H. Siegersma	HMC
	D.M. Broekhuizen, MSc.	HMC

This thesis is confidential and cannot be made public until April 20, 2022.

TU Delft Delft University of Technology

The work in this thesis was supported by Heerema Marine Contractors. Their cooperation is gratefully acknowledged.

ABSTRACT

During an offshore installation procedure, a structure is lifted off the barge, lowered through the wave zone and water column and eventually set down on the seabed. As the structure reaches the seafloor, water will move out of the way, washing away soil underneath the structure. The resulting hydrodynamic pressure and disturbed soil play a role in the structure's set-down, motion behaviour and stability. It is expected that the allowable set-down velocity, for which safe installation can be guaranteed, is related to the occurring hydrodynamic force and to the (allowable) soil deformation.

This thesis focuses on the hydrodynamic forces during the set-down that cause the soil deformation. The objective of this thesis is to increase the understanding of how the set-down of structures on the seabed is influenced by the soil. To achieve this, a simplified dynamic model describing the lowering to and installation onto the seabed of a structure is established. Throughout this study the structure has been simplified to a disk.

The hydrodynamic force acting on the disk is similar to the method described in literature by Brennen. Brennen's flat plate analogy has been applied to derive a force acting on a closed disk (1D model) and one for an open disk (2D model). Whereas the 1D model includes only horizontal fluid flow velocity, the 2D model also takes vertical flow velocity through a central valve into account.

From the analysis on the behaviour of the hydrodynamic force it was observed that the hydrodynamic force rises with increasing proximity to the seabed. This is explained by the dominance of an extra added mass term in the derived function. Once the outside radius/height (R/z) ratio is bigger than 1, the force starts to behave like a water cushion, complicating the structure's set-down onto the seabed.

In the analysis of the closed 1D model, it was observed that the significant increase in the hydrodynamic force reduces the structure's velocity as it reaches the seabed. After landing onto the seabed, the structure, connected in a kinematic manner with the soil, starts to settle. The results for the 2D model, including a valve with vertical flow velocity, showed a smaller hydrodynamic force. The magnitude of the vertical flow velocity is shown to depend on the valve radius and structure's motion.

The sensitivity analysis reconfirmed that larger valves result in lower magnitudes of the hydrodynamic force, corresponding to a smaller amount of soil disturbance. No significant difference in the vertical flow velocity for different valve sizes was observed. The force's sensitivity to phasing and frequency was emphasized by the analysis for various crane tip heave motions. Larger heave motions correspond to a higher hydrodynamic force engendering the highest amount of soil disturbance. The force varies considerably for different phases. The influence of the structural mass and soil type is relatively small compared to the impact of the crane tip heave motions and the valve size.

Further work includes additional research on the expression for the 2D hydrodynamic force and analyzing the relation between the vertical and horizontal flow velocity. By including the skirts and adding length to the disk, a more realistic analysis of the set-down of suction piles onto the seabed is obtained. By varying the constant crane lowering velocity, optimizing the valve size and determining acceptable crane tip heave motions, the optimum scenario for the set-down of a suction pile on the seabed can be acquired.

PREFACE

Dear reader,

This report describes the research conducted at Heerema Marine Contractors as the final step for the Master of Science degree in Offshore & Dredging Engineering at Delft University of Technology. For the last 11 months I worked on this challenging research and throughout the process I was supported by several people, who I would like to thank.

I would like to thank my supervisors Harm Siegersma and Daan Broekhuizen from Heerema Marine Contractors. I felt supported by both supervisors and it was pleasant working with them. I am very thankful for their professional supervision, their critical eye and their useful advice. Your time, dedication and patience have not gone unnoticed. Furthermore, I would like to thank Alessio Pistidda for all the CFD work he conducted for me. Also many thanks to Marius Ottolini and Maaike van Slooten for giving input and valuable tips.

Next, I would like to take the opportunity to express my gratitude to Antonio Jarquin Laguna, my daily supervisor from the university. He was very engaged with my research and always made time to help whenever I asked. The many meetings we had were very pleasant and valuable. Your time, patience and advice in especially the theoretical part of this research are very much appreciated. Also the supervision done by Joao De Oliveira Barbosa in the first months of my graduation project are acknowledged. I would like to thank Andrei Metrikine, my professor and the chair of my committee, for supervising this thesis. Your academic expertise and useful comments during all the meetings have guided me through the graduation process.

The time I spent at HMC was certainly made enjoyable by the other graduate students. The many body pump lessons, the fun coffee and lunch breaks and all the Friday afternoon drinks we had made my time at HMC one to remember. I hope to stay in contact with you all!

Finally I would like to thank my family and friends for supporting me and for listening to the endless talks about the derivation of the hydrodynamic force and my Matlab script refusing to work. Your support was of tremendous value for me.

I wish you an interesting read.

J.J.F. Vogelzang
Leiden, April 2017

GLOSSARY

CFD Computational Fluid Dynamics.

DCV Deepwater Construction Vessel.

DNV Det Norske Veritas.

DOF Degree of Freedom.

EOM Equation of Motion.

FBD Free Body Diagram.

FPSO Floating Production Storage and Offloading.

HMC Heerema Marine Contractors.

MPM Most Probable Maximum.

STTR Single Top Tension Riser.

NOMENCLATURE

β	Sarpkaya-Beta number	–
$\ddot{z}$	Vertical acceleration	m/s^2
$\dot{z}$	Vertical velocity	m/s
$\frac{F_{subm}}{k_{crane}}$	Initial deflection	m
λ	Wave length	m
μ	Contraction coefficient	–
ν	Kinematic viscosity	m^2/s
ω	Angular velocity	rad/s
ω_0	Natural frequency	rad/s
ϕ	Phase difference	rad
ρ_s	Mass density of steel	kg/m^3
ρ_{soil}	Mass density of soil	kg/m^3
ρ_w	Mass density of sea water	kg/m^3
ζ	Damping ratio	–
A	Amplitude	m
a	Hydrodynamic mass coefficient or added mass	kg
A_{33}	Added mass	kg
A_p	Inner area of the suction pile	m^2
A_r	Reference area	m^2
A_v	Total area of vent valves	m^2
b	Hydrodynamic damping coefficient	kg/s
c	Restoring spring coefficient	kg/s^2
C_A	Non-dimensional added mass coefficient	–
C_D	Non-dimensional drag coefficient	–
D	Characteristic diameter	–
F	External force	N
F_{drag}	Drag force	N
F_{hyd}	Hydrodynamic force	N
$F_{inertia}$	Inertia force	N
F_{line}	Tension force from crane wire	N

F_{soil}	Soil reaction force	N
F_{subm}	Submerged weight	N
G	Elastic shear modulus	kPa
g	Gravitational acceleration, $g = 9.81$	m/s^2
H	Wave height	m
k	Correction factor	–
k_{crane}	Crane wire stiffness	N/m
k_{soil}	Soil stiffness	N/m
KC	Keulegan-Carpenter number	–
L	Length of structure	m
M	Structural mass	kg
m	Structural mass	kg
N_c	Bearing capacity factor	–
p	Pressure at chosen point	Pa
$p(r,t)$	Hydrodynamic pressure at variable position and time	Pa
P_{hyd}	Hydrodynamic pressure	Pa
R	Radius	m
R_v	Valve radius	m
Re	Reynolds number	–
S_u	Undrained shear strength	kPa
T	Oscillating flow period	s
T_0	Natural period	s
$u(r,t)$	Horizontal fluid flow velocity	m/s
u_o	Flow velocity	m/s
v	Fluid flow speed at a point on the streamline	m/s
$v(t)$	Vertical fluid flow velocity	m/s
V_c	Crane lowering velocity	m/s
V_R	Reference volume	m^3
z	Vertical displacement	m
z_0	Initial position suction pile	m
z_{ct}	Crane tip position	m
z_{soil}	Soil displacement	m
z_{sp}	Suction pile position	m

CONTENTS

1

INTRODUCTION

1.1. BACKGROUND

The world's population is expected to increase with 1.5 billion people to nearly 8.8 billion people by 2035. This population growth will generate a worldwide increasing energy demand [1]. Although the use of renewables will rise significantly as seen in figure 1.1, fossil fuels will remain the dominant source of energy powering the global economy.

Over the years, the exploitation of hydrocarbons has shifted from onshore production to shallow water production into deep-water fields. These fields are often located in remote and harsh environments. With this continuing trend [2], subsea engineering has taken a powerful role in the offshore industry resulting in more complex engineering. Deeper water and harsher weather conditions complicate installation of subsea structures. More knowledge on subsea installations allows for more safe and efficient offshore operations.

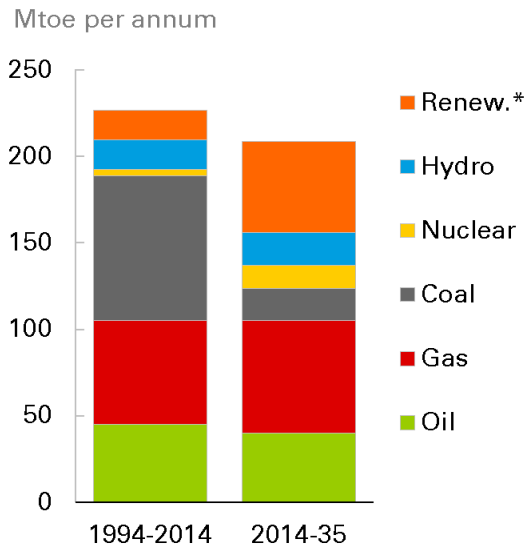

Figure 1.1: Annual demand growth by fuel [1]

Figure 1.2: HMC's DCV Balder

Within the offshore industry, Heerema Marine Contractors (HMC) is known for its semi-submersible crane vessels that can install offshore structures up to 14,000 ton in deep water fields [3]. In 2015, HMC's Deepwater Construction Vessel (DCV) Balder, seen figure 1.2, installed the world's largest and heaviest Floating Production Storage and Offloading (FPSO) buoy (3,000 ton) in the US Gulf of Mexico. For the permanent mooring, nine suction piles where installed in a water depth of 2,916 m: a world record.
With increasing water depths and number of subsea structure installations, the offshore industry has grown in complexity and size over the past years and will most likely continue to do so.

One of HMC's current projects is the Kaombo project, located offshore Angola in Block 32. This project encompasses six fields with an oil prediction of about 600 Mb over a twenty year license period. These six fields will be tied back to two FPSOs. At two locations, the Gengibre & Gindungo field, suction piles will be installed to support the Single Top Tension Riser (STTR) at a water depth of 1,750 m. All the data used in this thesis originates from HMC's Kaombo project.

1.2. PROBLEM DESCRIPTION

During a typical offshore installation procedure, a structure is lifted of the barge, lowered through the wave zone and water column and eventually is set down on the seabed. The set-down of a subsea structure on the seabed is governed by three critical parameters: the loads in the rigging, the set-down velocity and the soil disturbance of the installed structure. The last two critical parameters are the focus of this thesis, so no further elaboration on the first parameter is given.

The velocity with which a structure reaches the seabed is called the set-down velocity. The motion of the structure near the seabed is dependent on both the crane lowering speed as well as the motion of the installation vessel. This velocity is important to know in order to guarantee safe installation.

As the structure reaches the seabed, water will move out of the way resulting in soil being washed away underneath the structure. The resulting hydrodynamic pressure and possible soil deformation play a role in the structure's set-down, motion behaviour and stability. For suction piles, it is essential that the pile can penetrate into the soil without washing an excessive amount of soil away. Too much soil disturbance could reduce the holding capacity and therefore the pile's stability.

Generally accepted, e.g. Det Norske Veritas (DNV), there is a relation between the structure's geometry, the maximum velocity, the arising water pressure and the allowable soil deformation [4]. The DNV method includes a number of conservatisms and simplifications. Until now little is known about how the (non-linear) deforming seabed and valve sizes affect the generated fluid flow, which exerts a resistance force on the lowered structure. Presumably, the maximum allowable set-down velocity, for which a safe installation can be guaranteed, is related to an occurring hydrodynamic force and consequently to the (allowable) soil deformation. Better understanding of the relation between the water pressure and the set-down of a structure could optimize the allowable set-down velocity. Consequently, this could increase the operability and workability of the installation of subsea structures in deep water.

1.3. OBJECTIVE AND RESEARCH QUESTIONS

Based on the above problem description and the desire to gain more knowledge on the landing of a structure on a deforming seabed, possibly extending the installation weather window and/or optimizing the valve sizing, the research objective of this thesis is:

To increase the understanding of how the set-down of structures on the seabed is influenced by the soil.

The main objective is divided in the following sub-objectives and sub-questions:

1. What is the influence of the water pressure on the set down of suction piles near the seabed?
   (a) How is the water pressure created?
   (b) How much water pressure is there generated?
   (c) What influences the water pressure near the seabed?
   (d) What is the behaviour of water near the seabed?
   (e) Can we reduce conservatism in the calculation of set-down velocity?
2. What influence does the soil have on the hydrodynamics near the seabed?
   (a) How does the soil affect the water pressure generated?
   (b) What is the impact of the soil type?
   (c) What is the maximum allowed soil deformation?
   (d) What effect does the soil deformation have on the set-down of the structures?

1.4. APPROACH

To achieve the objective of this thesis, a simplified dynamic model will be constructed. The model will describe the system of a suction pile being lowered to and installed onto the seabed. The system can be divided into a fluid, structural and soil part, respectively. Fluid, structure and soil are modelled as shown in figure 1.3.

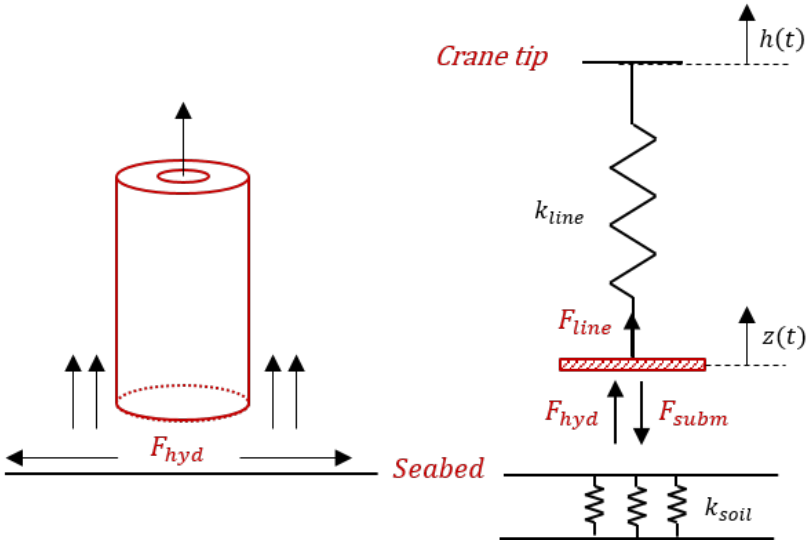

Figure 1.3: Modelling approach

The fluid flow close to the seabed is shown in figure 1.3 on the left. This fluid flow can be translated into a hydrodynamic force, which acts on the structure. The hydrodynamic force for a closed disk with 1D fluid flow is derived and used. Thereafter, the hydrodynamic force for a disk with a symmetric valve, including 2D cylindrically symmetric flow, is deduced.

The structure is modelled as a rigid body, representing a suction pile, and the soil is given as a linear spring. This is illustrated in figure 1.3 on the right. Both a closed disk and a disk with a valve in the middle are considered. The soil is modelled as a linear spring with certain spring stiffness. The spring stiffness is derived from Kaombo data.

1.5. REPORT OUTLINE

Chapter 2 starts with general background information on suction piles and elaborates on how subsea structures are installed on the seabed. A literature study has been done in chapter 3, in which first elaboration on the various calculation methods of the structure's motion is given. Next, the hydrodynamics near the seabed and the basics of soil mechanics are explained. In chapter 4, the derivation of the hydrodynamic force for a closed (1D flow) and an open (2D flow) disk is given as the 1D and 2D model, respectively. These forces have been implemented into a structural model in chapter 5 and the expectations concerning the set-down procedure are also given here. The results for a base case situation for both models are discussed in chapter 6. In chapter 7, a sensitivity analysis has been done, in which the influential parameters are illustrated. Chapter 8 describes the verification of the hydrodynamic force with CFD results. Finally, conclusions and recommendations are given in chapter 9.

2

GENERAL BACKGROUND

This chapter gives background information on suction piles and the installation of a subsea structure. First, elaboration on suction piles and the use of a valve is given. Thereafter, the installation steps of subsea structures are explained. Especially the final step, the set-down, is relevant for this thesis. Therefore that step is explained in more detail.

2.1. SUCTION PILES

A suction pile, seen in figure 2.1, is an open ended circular shaped tube with a closed top, which is embedded in the soil. A suction pile can function as part of a mooring system or as a foundation for subsea structures, e.g.manifolds and jackets.

Suction piles were first introduced in the offshore industry in 1980. However, only after further research and development in the early 90's, were they extensively used in mooring applications for floating production units. Nowadays, suction piles are widely used in the offshore oil industry. The advantages of using a suction pile as a preferred foundation are [5][6]:

- Cost effectiveness of the installation method
- Possible to install in deep and shallow water
- Reusability, i.e. installation may be reversed and repeated
- Extensive experience
- Removal is easy if planned for
- Environmental friendly, i.e. silent installation method

(a) Suction piles, with valves on the top plate

(b) Butterfly valve

Figure 2.1: Suction piles & butterfly valve

The key parameters that define the holding capacity of a suction pile are the geometry, length and the aspect ratio or length/diameter (L/D) ratio. The aspect ratio for a typical suction pile ranges between one and five. Different ratio's are used for different soil types. In sand and hard clays, a low aspect ratio is sufficient, while in soft clay higher ratio's are necessary.[5]

When a suction pile is in close proximity with the seabed, the soil may wash away and a crater may form. To minimize this, a vent valve is added to the top of the suction pile. This allows water to flow through the pile as it moves up and down. There are several different types of valves used in practice, e.g. gate valves and butterfly valves, seen in figure 2.1b. The diameter and number of valves are expected to have impact on the size of the crater, that is the amount of soil washes away. Valves are generally expensive and thus decisions concerning the use and amount of valves need to be carefully taken.

A suction pile is installed onto the seabed in two steps: first the pile penetrates the soil due to its self weight. This penetration continues until the self weight and the soil resistance reach an equilibrium. Next, water is pumped out of the pile through a vent valve, at the top of the pile, creating a pressure difference over the top plate. Because of this pressure difference, the pile is pushed further into the soil until the required penetration depth is reached [7]. In the next section, further elaboration on the installation of structure is given.

2.2. INSTALLATION OF STRUCTURES

The installation of subsea structures is a complex procedure. It can be divided into four phases [8]:

1. Lift off from the barge
2. Lowering through the wave zone
3. Lowering through the water column
4. Landing on the seabed

All phases must be considered to ensure a safe operation and the structural integrity of the structure. In this section a short description of the installation steps and governing parameters is given. The final installation step, the landing on the seabed, is the focus of this thesis and thus a more detailed explanation is given in section 2.2.4.

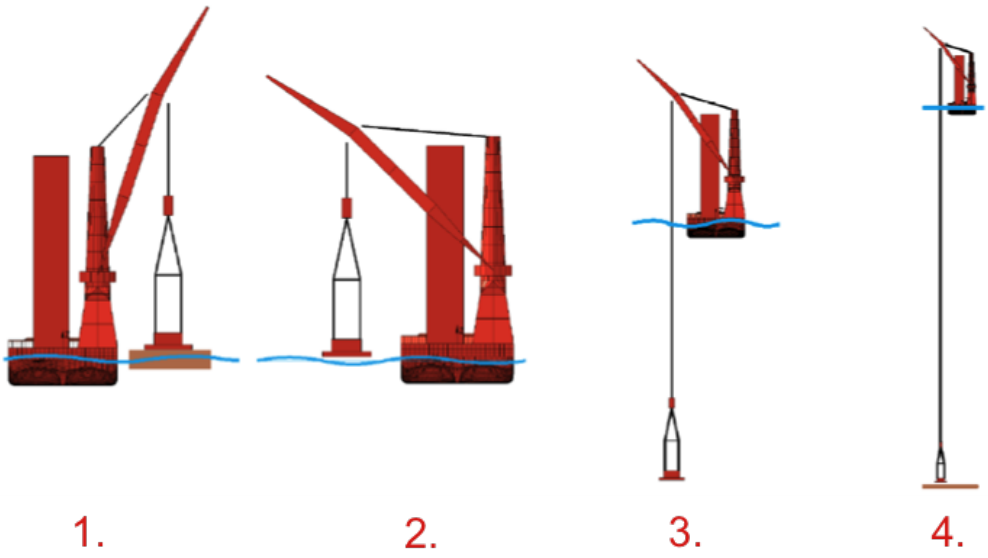

Figure 2.2: Installation steps

2.2.1. LIFT OFF FROM THE BARGE

In the first phase, a crane vessel lifts the suction pile from a barge moored alongside, step 1 in figure 2.2. To prevent recontact between the lifted structure and the barge, the relative vertical motions need to be assessed.

The feasibility of the lift-off is determined by the following parameters [4] [8]:

- The hoisting speed of the crane
- The combined motion characteristics of barge and crane vessel
- The weather conditions, combined with the orientation of the installation vessels

To lift the structure of the barge, use is made of pre-heeling, crane pre-tensioning and ballasting [8]. Once a pre-tension in the wire is given, the DCV is re-ballasted and the module comes loose from the barge.

2.2.2. LOWERING THROUGH THE WAVE ZONE

Once the structure is lifted off the barge, it is lowered through the wave zone, indicated as step 2 in figure 2.2. This means that the structure enters the water and eventually fully submerges. The critical aspects of this phase are the possibility of slack rigging and the exceedance of crane capacity. During this operation the structure is exposed to several environmental loads. These loads are non-linear and therefore it is difficult to predict what their effect is on the structure's motion. DNV gives a simplified method to conservatively estimate the forces acting on the object. They can be found in the DNV standard on 'Modelling and Analysis of Marine Operations' [4].

2.2.3. LOWERING THROUGH THE WATER COLUMN

Next, the structure is lowered through the water column to the seabed, step 3 in figure 2.2. The resonance period of the hoisting arrangement increases with increasing water depth. Therefore, resonance with the crane tip heave period or wave period may occur. This may lead to excessive structural motions. In order to avoid resonance, close investigation into the natural frequency of the system through the whole water column is essential.

2.2.4. LANDING ON THE SEABED

In the last step, the structure is placed on the seabed, visualized as step 4 in figure 2.2. As the structure approaches the seabed, the water underneath moves sideways. As the clearance to the seabed decreases, the area for water to escape reduces and therefore the hydrodynamic pressure rises. This pressure exerts a force on the structure and on the soil: the hydrodynamic force. The soil interaction and the amount of water, which may escape through the valves, influence the generated pressure. The hydrodynamic force increases as the structure gets closer to the seabed and is expected to decelerate the suction pile and deform the soil.

During the landing on the seabed several challenges need to be dealt with. The heave motions of the structure, originating from motions of the installation vessel, can be large and therefore reduce the visibility and complicate handling. A large heave velocity of the structure can result in excessive soil disturbance. If the soil displacement is too high, the holding capacity reduces, compromising pile stability. Besides, the dynamic loads during the landing can be high, resulting in possible slack rigging and exceedance of crane capacity.

Detailed analysis of the landing on the seabed is necessary to ensure that:

- Foundation failure does not occur;
- No structural damage occurs.

Similar to the lowering through the wave zone, the DNV standard [4] is used to provide a conservative approach of the loads on the structure.

STAGES OF LANDING

The landing of a suction pile on the seabed can be divided in four stages. Once the suction pile gets closer to the seabed and the skirts start to penetrate, the force equilibrium changes. For each stage, a momentum balance with corresponding forces can be determined. The four different phases and corresponding forces in the vertical direction are schematically visualized in 2D in figures 2.3 and 2.4, respectively. In chapter 5, the physical meaning of these forces is given.

During the first stage seen on the left in figure 2.3, the suction pile is unaffected by the seabed. The forces acting on the pile include the structure's submerged weight F_{subm}, the viscous drag force F_{drag}, the inertia force $F_{inertia}$ and a resistance force coming from the line connected to the structure F_{line}. At his point, the resistance force from the water originating between the structure and the soil is (negligibly) small. .

Once the structure gets closer to the seabed, as is seen on the right in figure 2.3, the extra added mass or hydrodynamic force F_{hyd} starts to play a role. The presence of a solid boundary will cause a rise in added mass. This is due to the increase in the fluid acceleration in the region between the fluid and the boundary. This increase in added mass results in an upward hydrodynamic resistance force.

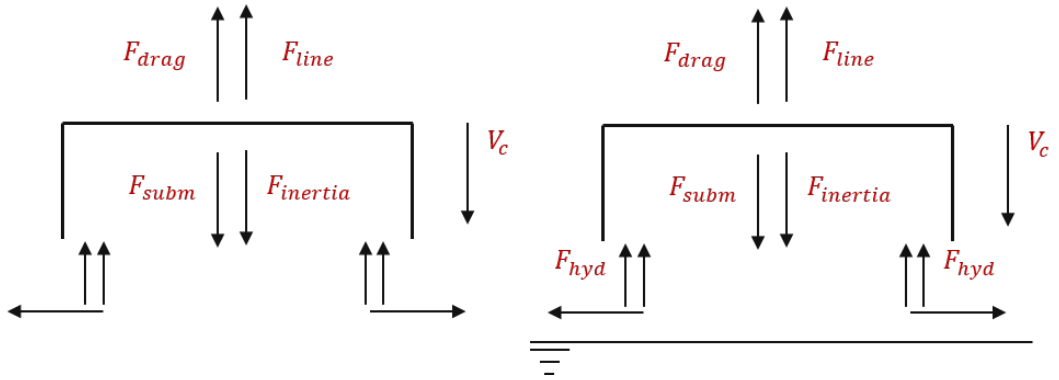

Figure 2.3: Landing stages 1 & 2 of the installation process.
Left side: forces on structure, unaffected by the seabed. Right side: forces on structure, close to the seabed.

In stage three, seen on the left in figure 2.4, the skirts start to penetrate the soil, leading to a further reduction of structure velocity and a maximum value for added mass. The only possibility for water to escape is through the valves on top of the suction pile. There is also a possibility that the line becomes slack and thus the line force would become zero.

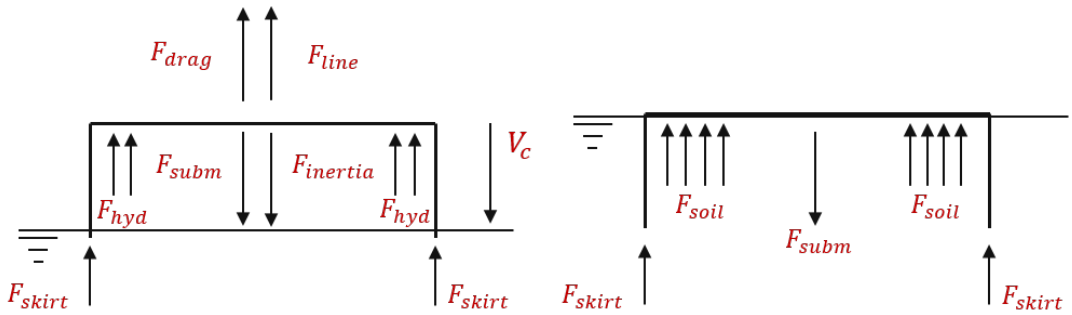

Figure 2.4: Landing stages 3 & 4 of the installation process.
Left side: forces on structure, with penetrating skirts. Right side: forces on structure, for full installation.

In the final stage, the skirts of the suction pile are fully embedded and the hydrodynamic force is not present anymore. The remaining forces are the soil reaction coming from the skirts and the foundation, and the submerged weight.

3

LITERATURE STUDY

This chapter describes the literature research that is essential to achieve the main goal of this thesis. A study on the structure's motion, the hydrodynamics in close proximity to the seabed and on soil mechanics has been conducted.
In the first section, the different ways of calculating the maximum set-down velocity is explained. Next, elaboration on the hydrodynamics of a structure close to the seabed is given. Finally, research was done on the different soil types, their behaviour and at which moment they fail.

3.1. STRUCTURE'S MOTION

One of the important aspects to thoroughly analyse is the vertical motion of the lowered structure. To guarantee safe installation and to minimize the soil disturbance, often a maximum set-down velocity is set.

The vertical motion of a suction pile is described by a constant downward velocity plus an oscillatory heave motion, which comes from the wave induced motion of the installation vessel. There are alternative ways to calculate the maximum allowable vertical velocity. Since the velocity is dependent on e.g. structural dimensions, weather conditions and soil conditions, the allowable velocity differs per situation. Next, elaboration on two different applied approaches of calculating the maximum allowable set-down velocity is given.

3.1.1. SIMPLIFIED CALCULATION

This simplified method, often used within HMC, is based on Bernoulli's principle. This law states that an increase in fluid flow speed appears simultaneously with a decrease in pressure. The principle is named after Daniel Bernoulli, who published it in his book 'Hydrodynamica' in 1738.
It is possible to apply Bernoulli's principle to various types of fluid flow, leading to several forms of Bernoulli's equations. A common form, valid for incompressible fluid flow, is described as follows [9] :

$$\frac{1}{2}v^2 + \frac{p}{\rho_w} + gz = constant \tag{3.1}$$

Where

- v : Fluid flow speed at a point on the streamline $[m/s]$
- p : Pressure at chosen point $[Pa]$
- ρ_w : Mass density of sea water, $\rho_w = 1025$ $[kg/m^3]$
- g : Gravitational acceleration, $g = 9.81$ $[m/s^2]$
- z : Elevation of the point above the reference plane $[m]$

For the calculation of the maximum allowable set-down velocity, HMC uses a similar equation, taking soil properties, valve dimensions and pressure losses into account. While the suction pile penetrates the soil, an overpressure inside of the pile is created. In case the pressure inside the pile is higher than the soil strength, a crater is expected until the depth with sufficient soil strength is reached. The allowed crater is dependent on the design requirement and on what the client finds acceptable.

Based on Bernoulli's principle and taking e.g. structural dimensions and soil properties into account, the maximum allowable set-down velocity for a certain soil strength can be described by [10]:

$$v = \sqrt{\frac{2N_c S_u k g}{\rho\left(\frac{1}{\mu^2}\left(\frac{A_p}{A_v}\right)^2 - 1\right)}} \tag{3.2}$$

In which:

N_c : Bearing capacity factor [-]
S_u : Undrained shear strength [kPa]
k : Correction factor [-]
μ : Contraction coefficient [-]
A_p : Inner area of the suction pile [m^2]
A_v : Total area of vent valves [m^2]

The derivation of this equation basically consists of two parts; one related to the flow capacity of the vent valve and one related to the soil strength.
In the first section, the ratio $\frac{A_p}{A_v}$ together with the correction factor k and contraction coefficient μ, determine the maximum possible flow through a valve. Based on this, it can be stated that the maximum set-down velocity is among others defined by the pile/valve dimensions and the pressure losses through the valve. Appropriate choices concerning especially the size and amount of the valves is essential.
The part related to the soil strength concerns the pressure inside the pile. The soil conditions set a limit to the maximum acceptable pressure inside the pile. The soil strength can no longer be guaranteed in case the pressure surpasses the limiting pressure. The soil strength, determined by among others the undrained shear strength S_u, is variable per location and depth. In figure 3.1, this can be seen in the Design Profile [11].

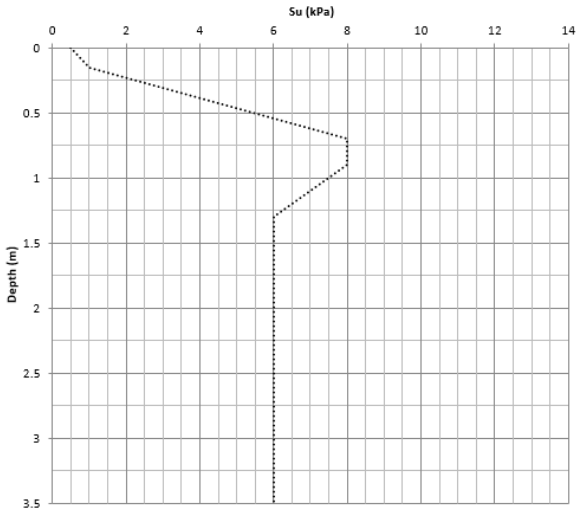

Figure 3.1: Design Profile from Kaombo soil data specification report

Within HMC, a Design Profile like in figure 3.1, is used to calculate what the corresponding soil disturbance is for a structure lowered with a certain velocity. By means of equation 3.2, a value for the occurring water pressure pushing on the seabed and the corresponding velocity can be calculated. Dividing the pressure by a bearing capacity factor of 5.14, the corresponding shear strength can be found. Consequently, a vertical line downward can be drawn from that specific S_u point until it intersects with the Design Profile. This point can be translated into a crater depth, seen on the y-axis in figure 3.1.

This simplified method does not include how the soil (disturbance) and the occurring water cushion, located between the structure and the seabed, affect the set-down velocity. Furthermore, this method considers worst timing and the 20 minutes Most Probable Maximum (MPM) is used, corresponding to a conservative estimation. This simplified method is used in chapter 6 to compare with two different methods, which are explained in section 3.3.

3.1.2. ITERATIVE CALCULATION

Based on a method described by R.D. Blevins in the 'Applied Fluid Dynamics Handbook' [12] in 1984, DNV established a method to iteratively determine the allowable set-down velocity of a suction pile [4].
In a time domain analysis, the structure's velocity is determined, taking non-linear soil behaviour into account. In figures 3.2 and 3.3, the iteration procedure is illustrated in a flowchart. In appendix A, a stepwise explanation of the whole procedure is given.

By going through this flowchart, the structure's velocity can be calculated for each time step. The velocity calculation in this iterative analysis procedure is based on the change in kinetic energy. One of the requirements for using this analysis is the fact that the crane lowering velocity V_c remains constant until the pile comes to rest.

The procedure begins with a time domain part, where the initial input parameters are determined. These are inserted into an iteration part (highlighted in figure 3.2), which solves for the change rate of the soil displacement. Figure 3.3 zooms in on a specific section of this iteration part. The calculation of the rate of change of soil displacement depends on the 'mode' you are in, seen in figure 3.3. The mode indicates whether the soil is in mobilisation phase or in unloading/reloading phase.
Once the iteration has been solved for the rate of change of soil displacement, the values are used to calculate the new lowering velocity by means of time domain. Together with this new lowering velocity, the development of the soil displacement is perceived and can be analyzed.

Compared to the simplified method described in section 3.1.1, the iteration method is expected to give a less conservative estimation of the allowable set-down velocity. Still some conservatism is expected to be present in this method. To investigate this, the results from the iteration method can be compared with the results from the dynamic model, established in this thesis and explained in chapter 6.
In this thesis, the dynamic model is only analyzed for a disk, taking no skirts and thus actual suction pile into consideration. Since, the iteration method describes the set-down of a suction pile, the comparison between the DNV iteration analysis and the dynamic model is not made within the research of this thesis. It is highly recommended to analyze the dynamic model for an actual suction pile and compare those results with both the simplified method and DNV iteration method.

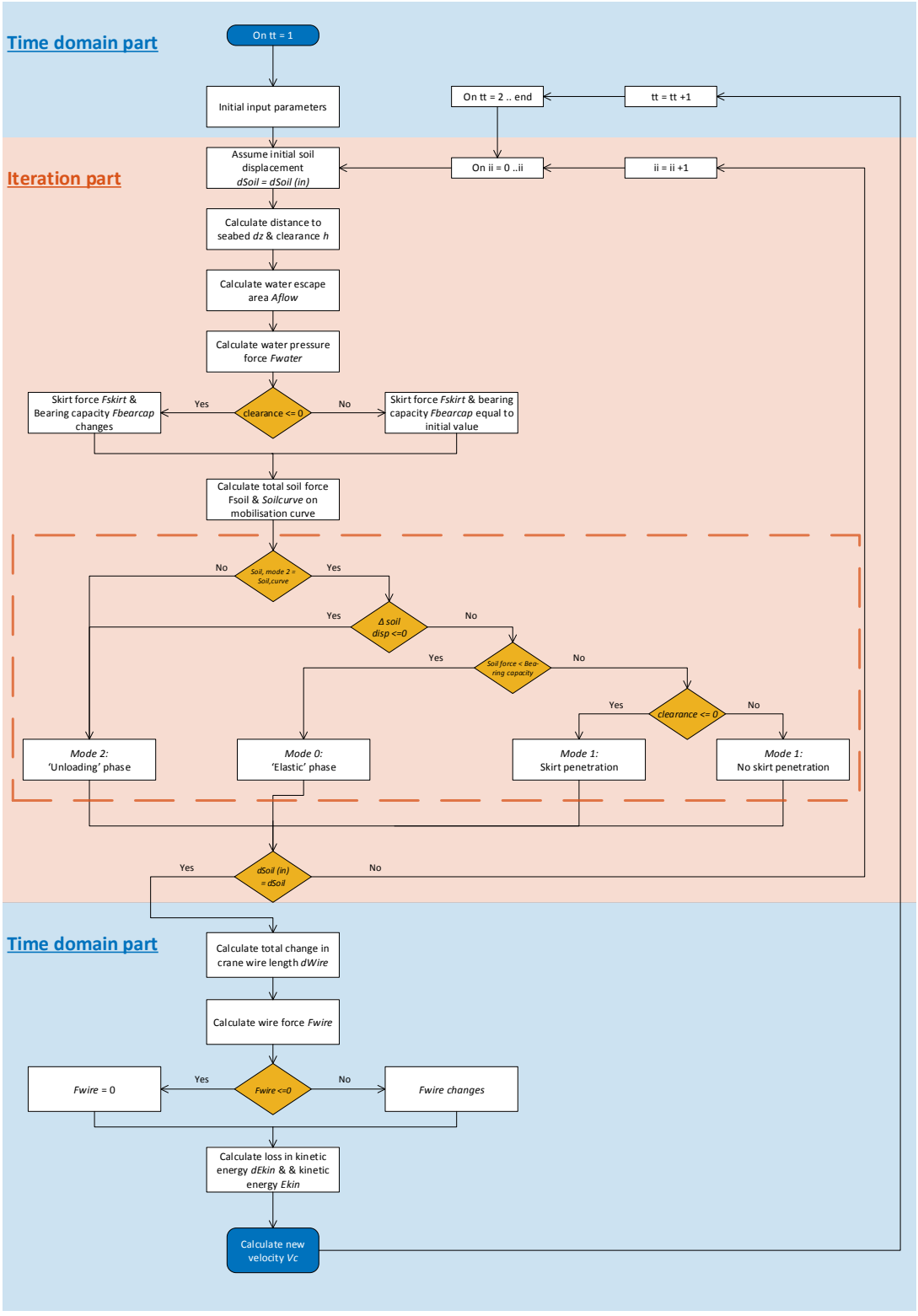

Figure 3.2: Flowchart describing the DNV iteration analysis, part 1

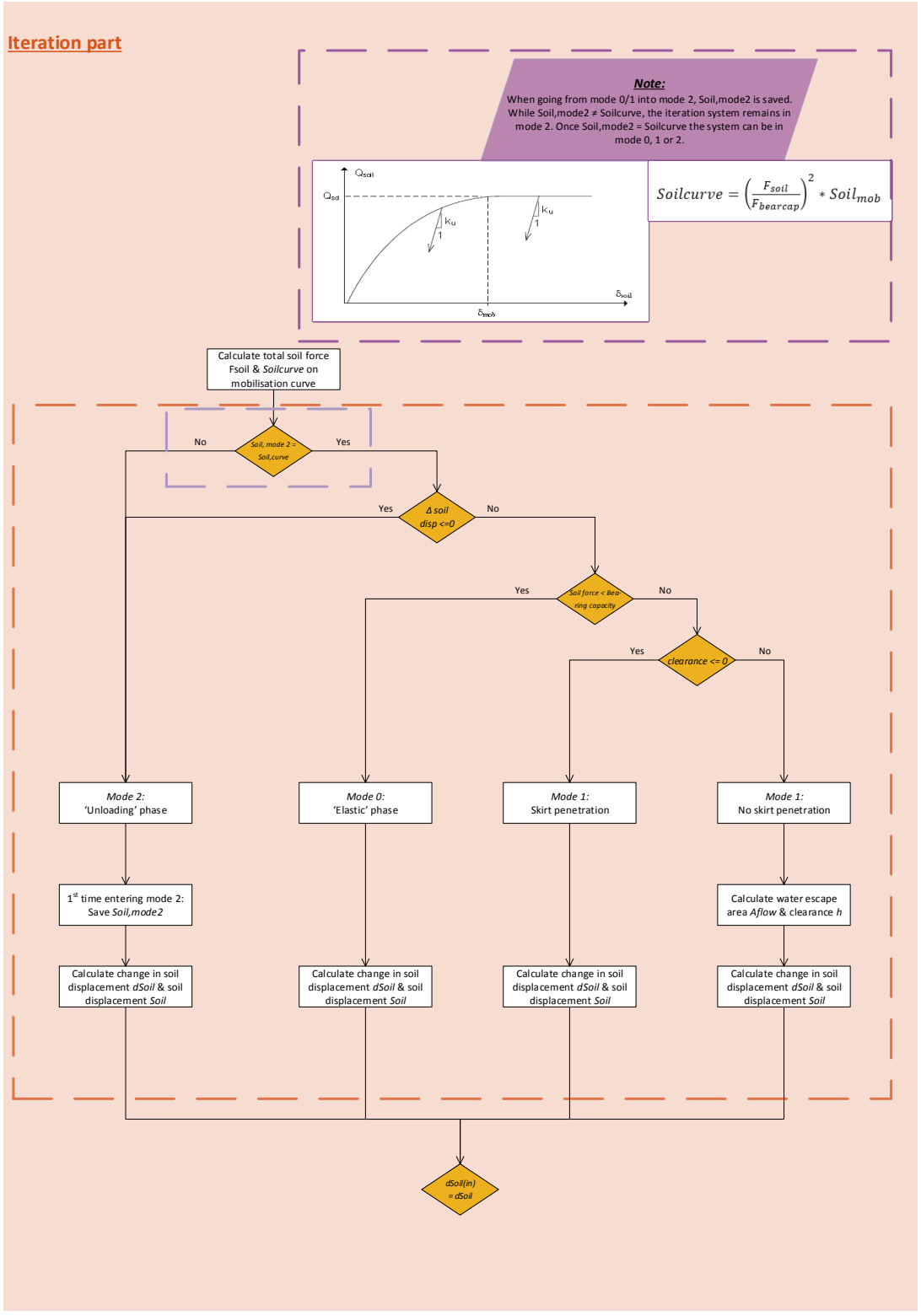

Figure 3.3: Flowchart describing the DNV iteration analysis, part 2

3.2. HYDRODYNAMICS NEAR SEABED

During an offshore installation, external forces act on the submerged suction pile. These loads can be divided into static and dynamic components. The static loading consists of the gravity- & hydrostatic loads, while the dynamic part is compelled of the waves, currents and the structural motions of the suction pile.

In the event of an offshore installation operation, the environmental conditions are naturally defined by constant currents in combination with (irregular) waves [9]. The installation vessel is constantly excited by these waves. The induced motions of the installation vessel are passed on to the crane wire, which is connected to pile. As explained in section 3.1, the pile's velocity is composed of this static lowering speed and the heave oscillating motion induced by the waves. As the structure gets closer to the seabed, the hydrodynamic loading on the structure will increase due to the increasing proximity.

In this section, elaboration on the physical meaning of the involved hydrodynamic forces is given. The hydrodynamic loading is composed of inertia, drag and diffraction forces. These forces depend on a range of parameters, including the structure dimensions and wave characteristics. To describe the characteristics of these force, traditional non-dimensional numbers have been established.

$Re = \frac{u_o D}{\nu}$	The Reynolds number measures the relative contribution of the inertia and drag forces in constant flow.
$KC = \frac{u_o T}{D}$	The Keulegan-Carpenter number measures the relative contribution of inertia and drag forces in oscillating flow.
$\beta = \frac{D^2}{\nu T} = \frac{Re}{KC}$	The Sarpkaya-Beta measures the relative contribution of inertia and drag forces.

As Re is increased from zero, the flow changes tremendously. Low Reynolds numbers correspond to laminar flow, which is characterized by a smooth and steady flow. Between $10^3 \leq Re \leq 10^4$, the transition from laminar to turbulent flow takes place. Turbulent flow is identified by fluctuating and agitated flow [13].

In his book 'Hydrodynamics for Offshore Structures', Chakrabarti (1987) [14] defined regions, in which the different types of hydrodynamic loads are applicable. Nowadays these different regions, illustrated in figure 3.4, are widely recognized and used by among others the offshore classification society DNV.
These regions are described by the characteristic diameter D, the wave height H and the wave length λ, respectively. This proves that the non-dimensional numbers depend on wave characteristics.

In the graph established by Chakrabarti, shown in figure 3.4, both axis dimensions are defined by a rate between structure's diameter and wave dimensions. These determine the hydrodynamic loading type. Offshore structures can be characterized as either large and small or slender structures. A slender structure implies that its diameter is small to the wave length, thus $D/\lambda < 0.1-0.2$. Large structures, having $D/\lambda > \pm 1$, correspond to the diffraction wave force regimes, while small & slender structures match the drag & inertia dominated areas.

To determine the appropriate regime for suction piles from figure 3.4, a range of dimensional and environmental conditions is considered. The range for the wave length is based on the deep water assumption ($\lambda = \frac{gT^2}{2\pi}$).

$$1 \leq D \leq 10m$$

$$0.5 \leq H \leq 2.5m$$

$$8 \leq T \leq 16s$$

$$100 \leq \lambda \leq 400m$$

Automatically, the ranges for H/D and $\pi D/\lambda$, respectively result into:

$$0.05 \leq H/D \leq 2.5$$

$$0 \leq \pi D/\lambda \leq 0.31$$

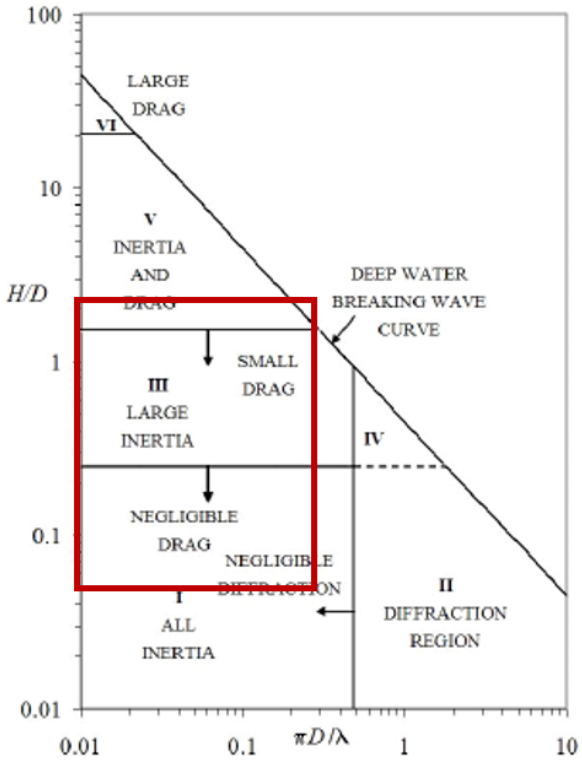

Figure 3.4: Different wave force regimes (Chakrabarti, 1987)

Based on the assumed dimensional and environmental conditions and the ranges for H/D and $\pi D/\lambda$, the corresponding regime is highlighted in figure 3.4. The indicated area does not include diffraction. Since a suction pile is typically recognized as a small and slender cylinder, this results was expected.

It can be concluded that the hydrodynamic loading on a suction pile is identified by drag and inertia forces. This was also proven by J.R. Morison in 1950 [15]. To determine the magnitude and influence of these forces, hydrodynamic coefficient need to be defined. In the next section, an explanation of the determination of these coefficients is given.

3.2.1. HYDRODYNAMIC COEFFICIENTS

The hydrodynamic loading is composed of inertia and drag forces. These loadings depend on hydrodynamic coefficients, which stem from the dimensions and geometries of the structure and various flow conditions. These coefficients have to be tuned for specific situations. They can be based on measurements from full scale testing, from model scale testing or from Computational Fluid Dynamics (CFD) analysis. Thorough research on the behaviour of these coefficients for different shapes in various flow conditions has been performed. As a result, a general characteristic behaviour of hydrodynamic coefficients for changing dimensionless and varying flow regimes has been established.
This section elaborates on the origin of added mass and drag and their corresponding hydrodynamic coefficients.

ADDED MASS COEFFICIENT

In fluid mechanics, the added mass is described as the mass of the extra volume a body displaces as it moves through a fluid. The structure and the surrounding fluid can never be at the same physical location simultaneously. Therefore, the fluid is inevitably accelerated, creating this extra volume virtually attached to the object. This virtual mass is incorporated into Newton's second law ($F = Ma$), representing the inertia of the system .

$$F_{inertia} = (M + A_{33})\ddot{z} \tag{3.3}$$

With:

M : Structural mass $[kg]$
A_{33} : Virtual added mass $[kg]$
$\ddot{z}$: Acceleration $[m/s^2]$

According to the DNV guidelines, the heave added mass of a two-dimensional flat circular disk can be described as the equation given in equation 3.4. The component C_A represents the non-dimensional added mass coefficient and the component V_R the reference volume.

$$A_{33} = \rho_w C_A V_R \tag{3.4}$$

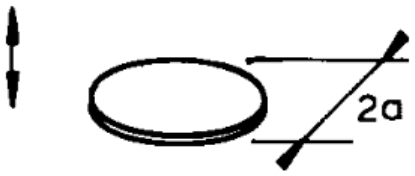

Figure 3.5: Definition reference volume

Where

C_A : $2/\pi$ $[-]$
V_R : $4/3\pi a^3 [m^3]$

For this simplified disk, the value for C_A of $2/\pi$ is determined independently from flow conditions. This value is accepted and used by the DNV guidelines. For an actual suction pile, the added mass coefficient C_A is dependent on specific shape and characteristic dimensions relative to the flow conditions.

DRAG COEFFICIENT

The drag or fluid resistance is the force working opposite to the relative motion of a structure and can be described as follows:

$$F_{drag} = 0.5\rho_w C_D A_r \dot{z}|\dot{z}| \tag{3.5}$$

In which:

C_D : Non-dimensional drag coefficient [-]
A_r : Reference area $[m^2]$
$\dot{z}$: Vertical velocity $[m/s]$

The drag coefficient C_D is dependent on shape, flow type, structural motion and roughness. Also here, extensive research has been done and many laboratory test have been conducted to determine realistic values for C_D. Once the KC-number is known, the drag coefficient for a disk can be read from the graph shown in figure 3.6. The graph was published by Keulegan and Carpenter in their paper 'Forces on Cylinders and Plates in an Oscillating Flow' in 1958 [16].

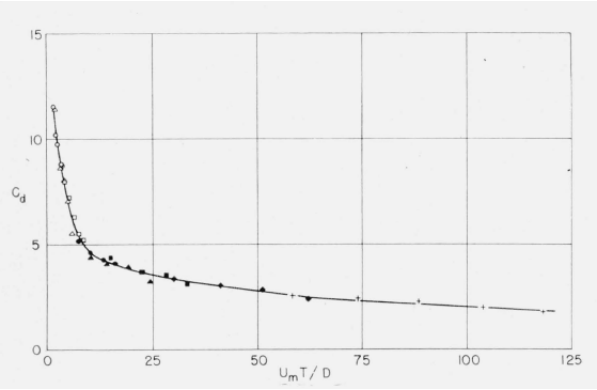

Figure 3.6: Variation of drag coefficients for disks

Equation 3.4 is used to determine the added mass coefficient for a flat disk. From figure 3.6, a drag coefficient of 10 is defined for a flat disk with a diameter of 5.5 m positioned in an oscillating flow with a period of 10 s. These values are used to calculate the added mass and drag forces in chapter 5.

3.3. SOIL MECHANICS

Offshore structures are installed onto the soil and therefore some basic understanding of soil mechanics is necessary. Due to a number of the special properties that characterize soils, soil mechanics belongs to a separate branch of engineering.
During the preparation phase of an offshore installation project, an extensive geotechnical survey on the soil at the installation field is done. A soil data specification report is published in which a summary of the soil conditions from the field development area is given. This information can be used for the design analysis of the relevant offshore structures. This section describes the basic and relevant information on soil mechanics necessary for this study.

3.3.1. SOIL TYPES

Generally, soils can be categorized into various types. One of the most common ways to classify different soil types is by means of grain size of the particles that form the soil [17]. These grain size particles are often divided into four groups, given in figure 3.1.

Soil type	Min	Max
Clay		0.002 mm
Silt	0.002 mm	0.063 mm
Sand	0.063 mm	2 mm
Gravel	2 mm	63 mm

Table 3.1: Grain sizes

The behaviour of each type of soil is somewhat different. Nevertheless, for all soil types applies that their behaviour is unpredictable, irregular and can be different at every location within an offshore field. Sand is rather permeable and quite stiff, especially after the pre-loading phase. Clay is much softer and less permeable for water compared to sand. Water can flow freely through sand, where the grains are rounded and the numerous pore spaces are large. In clay, on the other hand, the water moves much slower through the small particles. The water functions to hold the grain particles together, which results in additional strength.
Next to the grain size classification, the properties stiffness and strength are also necessary to distinguish. These can be determined from mechanical test, such as triaxial and direct simple shear tests [17] [18].

3.3.2. SOIL FAILURE

In order to assure safe offshore installation, it is necessary to make some predictions when the soil at the specific operational location fails.
In geotechnical engineering, the bearing capacity is said to be the capacity the soil has to support the forces acting on the ground. Once the structure is landed on the seabed and starts to penetrate into the seabed, the loads will be transferred to the soil. If these loads exceed the bearing capacity of the soil, the settlement or cavity formation will increase further until a new equilibrium is found.

In figure 3.1 in section 3.1, an example of a Design Profile describing the undrained shear strength S_u was given. The undrained shear strength, given in terms of lower/upper bound and best estimate, changes with the depth of penetration. This clarifies the non-linear behaviour of the soil. As seen in figure 3.1, the soil will fail directly for $S_u > 8$ kPa.

Although modelling soil is rather complex, an attempt has been made to include soil in the structural model in chapter 5. The soil is included as a spring behaving in a linear way. The expression for the soil reaction force, used as input for the model, was derived from the API standard given in 'Geotechnical and Foundation Design Consideration'[19].

$$F_{soil} = \frac{1}{\left(\frac{1-\nu}{4GR}\right)} z_{soil} \tag{3.6}$$

Where:

ν : Poisson's ratio of the soil, $\nu = 0.5$ [-]
G : Elastic shear modulus of the soil $[kPa]$
z_{soil} : Soil displacement $[m]$

The elastic shear modulus G is defined in the soil data specification report for the Kaombo project as $G = 80S_u$ and $G = 200S_u$ for large and small strains, respectively. The value for the large strains is assumed. The shear strength S_u change over depth in the following way:

$$S_u = 1 + 1\,(z_{soil}) \tag{3.7}$$

To include the soil as a linear spring, the z_{soil} is set equal to 1, and thus $S_u = 2$ is used leading to a linear function for equation 3.6. The linear description for the soil is used in the structural model in chapter 5.

3.3.3. SOIL DISTURBANCE

Soil as a spring is too simplistic, alternatively the Design Profile from figure 3.1 can be used to calculate soil displacement. This soil profile is used within HMC to calculate the estimated soil disturbance. In this method the maximum hydrodynamic force is converted into a corresponding shear strength S_u. The graph in figure 3.1 can be used to give an estimation of the amount of soil that will displace. The maximum magnitude of the hydrodynamic force can be converted into a corresponding S_u value in the following way:

$$P_{hyd} = \frac{F_{hyd}}{A_r} \quad \Rightarrow \quad S_u = \frac{P_{hyd}}{N_c} \tag{3.8}$$

For the bearing capacity value N_c a value of 5.14 is taken. By using the S_u and the Design Profile from figure 3.1, the estimated soil disturbance can be read from the graph.

An alternative and less conservative way to calculate the soil displacement resulting from the hydrodynamic force is a method based on the conservation of energy. The soil is modelled as a 1 Degree of Freedom (DOF) mass spring system with viscous damping, onto which a general disturbing force is acting: the hydrodynamic force [20]. The situation is illustrated in figure 3.7.

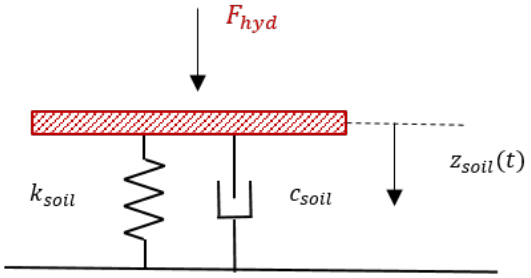

Figure 3.7: 1 DOF system with viscous damping under general disturbing force

The 1 DOF system with viscous damping under a general disturbing force can be explained by the equation of motion given in equation 3.9 and can be rewritten into equation 3.10 [21]. The terms m, c and k in expression 3.9 represent soil properties instead of structural characteristics.

$$m\ddot{z}_{soil} + c\dot{z}_{soil} + kz_{soil} = F_{hyd}(t) \tag{3.9}$$

$$\ddot{z}_{soil} + 2\zeta\omega_0\dot{z}_{soil} + \omega_0^2 z_{soil} = \frac{1}{m}F_{hyd}(t) \tag{3.10}$$

With

ω_0 : Natural period of soil, $\omega_0 = \sqrt{\frac{k_{soil}}{m}}$ $[rad/s]$
ζ : Damping ratio, $\zeta = 0.7..1.3$ [-]

The natural period of the soil is calculated by the ratio between the soil stiffness and the mass of the soil. The damping ratio is taken between the range of 0.7 - 1.3, which will result in a lower, median and upper bound of soil. To describe the maximum soil displacement by means of the conservation of energy, equation 3.10 is integrated between the starting time t_0 and the collision time t_{col}. The collision time t_{col} is the moment at which the hydrodynamic force is maximum. This is just before the structure lands on the seabed. With respect to the starting time t_0, the following requirement should hold:

$$(t_{col} - t_0) < T_0 \tag{3.11}$$

The natural period T_0 is calculated by $\frac{2\pi}{\omega_0}$. By taking that requirement into account, the integration is described by the following equation:

$$\int_{t_0}^{t_{col}} \left(\ddot{z}_{soil} + 2\zeta\omega_0 \dot{z}_{soil} + \omega_0^2 z_{soil} = \frac{1}{m} F_{hyd}(t) \right) dt \tag{3.12}$$

The energy balance in equation 3.12 is solved for the soil displacement at the time of collision: $z_{soil}(t_{col})$. The full derivation has been done in Maple and is given in appendix B. The final expression for the soil displacement at the time of collision is described by:

$$z_{soil}(t_{col}) = \frac{-\left(m\omega_0^2 z_{soil}(t_0)\,(t_{col} - t_0) - 4m\omega_0 z_{soil}(t_0) + \left(F_{hyd}(t_0) + F_{hyd}(t_{col})\right)(t_0 - t_{col}) - 2m\dot{z}_{soil}(t_0)\right)}{m\omega_0\,(-\omega_0 t_0 + \omega_0 t_{col} + 4\zeta)} \tag{3.13}$$

Based on the method of conservation of energy, expression 3.13 represents the maximum soil displacement which results from the momentum of the hydrodynamic force. Compared to the Design Profile, this is a less conservative method to estimate the maximum soil disturbance and thus expected to be more realistic. In this method an average of the hydrodynamic force over a specific time period is taken instead of the maximum hydrodynamic force, which is used in the Design Profile. The results for the estimated soil disturbance generated by this method are expected to be lower and thus less conservative compared to the Design Profile.

Both methods are used in chapter 6 to calculate the soil disturbance corresponding to the occurring hydrodynamic force.

4

HYDRODYNAMIC FORCE

As was seen in the different stages of landing in chapter 2, a hydrodynamic force occurs in close proximity to the seabed and acts on the structure. This chapter discusses the fundamental derivation of this hydrodynamic force, which will serve as an input for the structural model, described in chapter 5.

A short overview of the equation of motion and reference to the fundamental origin of the derivation of the hydrodynamic force is given. The so-called '1D model' in section 4.3 discusses the derivation of the fundamental equations needed to describe the hydrodynamic force for 1D fluid flow. In order to understand the behaviour of the hydrodynamic force, an analysis has been done in section 4.3.2. The derivation of the 2D fluid flow and the corresponding force is given as '2D model' in section 4.4. Section 4.4.2 gives an overview of the assumptions made in derivation of the hydrodynamic force with 2D fluid flow.

4.1. EQUATION OF MOTION

As will be elaborated in chapter 5, the structural system for a disk can be described by the following equation of motion:

$$F_{inertia} + F_{drag} = F_{hyd} + F_{line} - F_{subm} \tag{4.1}$$

This chapter focusses on the derivation of the hydrodynamic force F_{hyd}. This force, resulting from the water pressure underneath the disk, acts on the structure opposite to direction the structure moves in. A detailed explanation of the other forces is given in chapter 5.

4.2. BRENNEN'S FLAT PLATE ANALOGY

As the structure is lowered to the seabed, water is forced to move away to allow the structure to move down. Since it is assumed that water is incompressible, the fluid will generate an upward resistance force acting on the structure. This phenomenon is known as the 'cushioning effect'. As the gap between the structure and the boundary becomes very small, the water starts to behave like a water cushion. This water cushion results into a resistance force acting on the structure and decelerates the system. This doesn't mean that the force dissipates energy from the system, it only slows the system down

The presence of a solid boundary will cause an increase in this force, which basically results in extra added mass. This is a result of the increase in the fluid accelerations in the area between the fluid and the boundary (seabed). The total hydrodynamic force consists of the force caused by the proximity of the seabed and the force coming from the added mass. Since this force is related to the position of the suction pile, its value changes over time and thus location.

A description of the function for the hydrodynamic force acting on a flat plate close to a boundary was first obtained by Brennen [22]. In his paper, Brennen explains a two dimensional problem of a flat plate lying on

an ocean floor, which is lifted from the floor. This problem is comparable to the set-down of a suction pile, however in opposite direction and in a cylindrical shape.

4.2.1. FLAT PLATE ON OCEAN FLOOR

In his model, Brennen considers a flat plate of width, $2a$, lying on the ocean floor. This plate is lifted away from the floor by a vertically upward force F and rises to a uniform height $h(t)$ above the floor at time t. Figure 4.1 illustrates the situation described by Brennen in his paper 'A review of added mass and fluid inertial forces' [22].

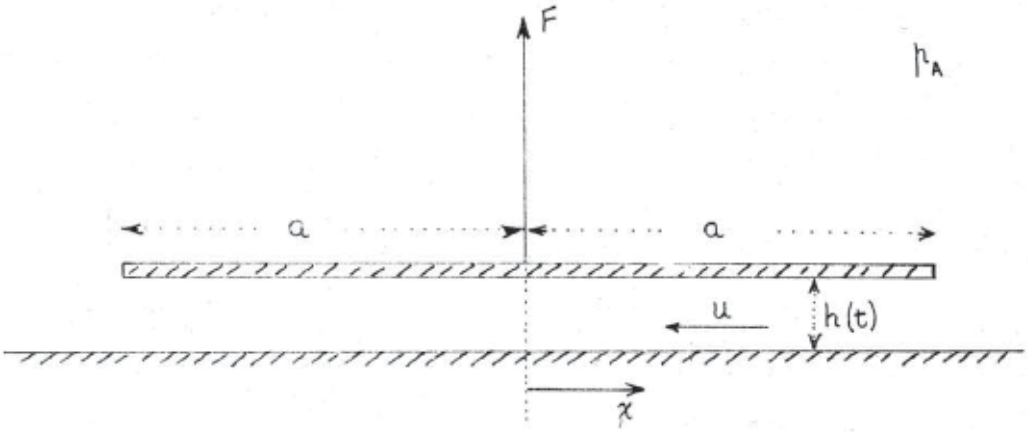

Figure 4.1: Brennen's flat plate near the sea floor

By lifting the plate, the small separation distance generates a larger fluid inflow velocity than the vertical velocity of the plate. It is necessary to mention that this approach is only applicable when the structure is in close proximity with the seabed, $a/h >> 1$. As Brennen explains in his paper, the force can best be described by making use of the fundamental principles of mass and momentum conservation, given by White [13].

The full derivation of the hydrodynamic force acting on a flat plate obtained by Brennen is given in appendix C. For simplicity, only the three relevant equations derived by Brennen have been given here.
Function for the 1D horizontal fluid flow velocity $[m/s]$:

$$u(x,t) = -\frac{x}{h}\frac{dh}{dt} \tag{4.2}$$

Function for the pressure distribution $[Pa]$ underneath the plate:

$$p(x,t) = p|_{x=a} + \frac{\rho}{2}\left(a^2 - x^2\right)\left(\frac{2}{h^2}\left(\frac{dh}{dt}\right)^2 - \frac{1}{h}\frac{d^2h}{dt^2}\right) \tag{4.3}$$

Function for the hydrodynamic force $[N]$ acting on the plate in close proximity with the seabed:

$$F = \frac{2}{3}\rho\frac{a^3}{h}\left(\frac{2}{h}\left(\frac{dh}{dt}\right)^2 - \frac{d^2h}{dt^2}\right) \tag{4.4}$$

4.2.2. CYLINDRICAL MODEL

The situation of a hydrodynamic force acting on a disk is similar to the situation of Brennen. Therefore, the Brennen's flat plate analogy is applied and adjusted into a cylindrical model for three different situations:

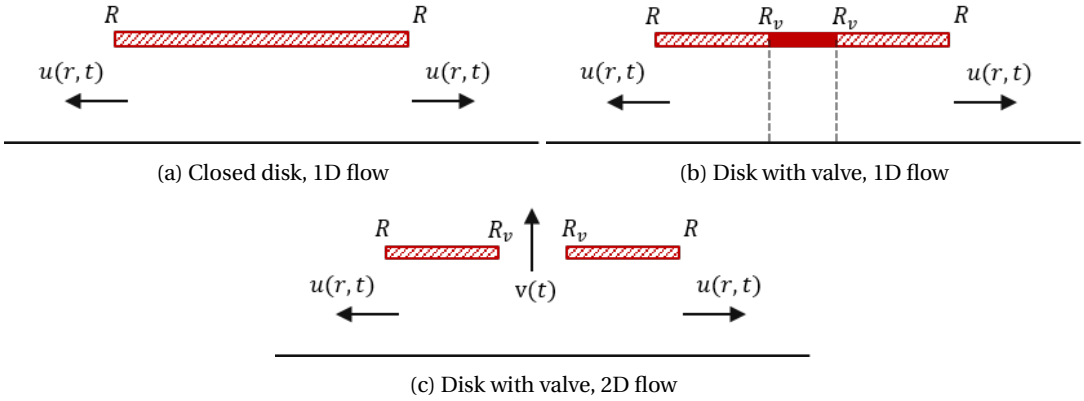

(a) Closed disk, 1D flow

(b) Disk with valve, 1D flow

(c) Disk with valve, 2D flow

Figure 4.2: Three situations for cylindrical model

These cases describe three different situations in which a disk approaches the seabed. The first situation, seen in figure 4.2a, is directly derived from Brennen's flat plate analogy, but for a disk with 1D fluid flow $u(r,t)$. Figure 4.2b shows the situation where the hydrodynamic force only acts between the valve radius R_v and the outside radius R with 1D fluid flow. In this situation, a valve has been created with radius R_v, however there is no fluid going through the valve. The last situation, seen in figure 4.2c, describes a hydrodynamic force acting between R_v and R with horizontal fluid flow $u(r,t)$ escaping underneath the disk and vertical fluid flow $v(t)$ through the valve.

As the situations in figure 4.2a and 4.2b are very similar, the derivation of the hydrodynamic force for both cases is explained in the 1D model in section 4.3. The derivation for the hydrodynamic force with 2D fluid flow for situation three is described as the 2D model in section 4.4. The force derivation for both models is based on the derivation for the hydrodynamic force from Brennen's flat plate. In both models, the suction pile is simplified to a disk.

4.3. 1D MODEL: CLOSED & OPEN DISK

As explained in section 4.2, the 1D model describes the landing of a closed and open disk on the seabed. In this model, just like in the flat plate of Brennen, only 1D horizontal flow occurs. The 1D model is comparable to Brennen's model, however it has a cylindrical shape instead of rectangular and the disk moves downwards instead of upwards. For the open disk a valve is applied between 0 and R_v. This model is assumed to estimate the impact of a valve on the hydrodynamic force and the motions of the structure.

4.3.1. DERIVATION OF HYDRODYNAMIC FORCE

Lowering the structure increases the horizontal outflow of water. This generates a hydrodynamic fluid force, which acts on the structure and the seabed. It can be derived in the same way as Brennen's flat plate.
In this section, a brief derivation of this force for a closed and open disk is given. As this derivation is based on Brennen, a more detailed stepwise description can be found in appendix C.
It should be emphasized that the disk is lowered in a perfectly vertical direction. Therefore the displacement $z(t)$ is only a function of time t and not of the horizontal position r.

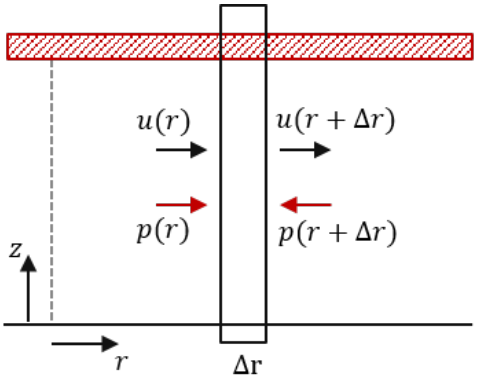

Figure 4.3: Visualization of the flow elements, derived by White, in the gap with horizontal velocities u and pressures p at the elemental boundaries of r and $r+\Delta r$. The conservation of mass and conservation of momentum both relate back to this figure, as the mass or momentum both flow from r to $r+\Delta r$.

CONSERVATION OF MASS

The derivation of the hydrodynamic force is based on the fundamental principle of mass and momentum conservation in accordance with literature on 'Fluid Mechanics' from White [13]. The fluid flow between a closed disk and the sea floor can be represented by a channel flow, see figure 4.3.
Consider a closed disk with radius R and height $z(t)$ from the seabed. Similar to Brennen's situation seen in figure 4.1, use is made of mass conservation from White, given as:

$$\frac{\partial}{\partial t}\iiint_V \rho dV + \iint_A \rho\,(\vec{u} * \vec{n}) dA = 0 \tag{4.5}$$

The first term describes the change in mass over time and the second term the mass flow in and out of the control volume. If a disk with outside radius R is examined along its position r, the mass change is obtained in equation 4.6.

$$\frac{\partial}{\partial t}\iiint_V \rho dV = \frac{\partial}{\partial t}\int_0^{z(t)} \rho\,(\pi r \Delta r) dz = \rho \pi r \Delta r \frac{dz}{dt} \tag{4.6}$$

The mass flow integral is accounted to sign convention. As visualized in figure 4.3, the unit normal vector $\vec{n}$ is prescribed outward positive and therefore the velocities are positive in the x-direction. The mass flow is defined as the difference between the mass flows in and out of the control volume, expressed in equation 4.7. The quantity $\rho A u$ represents the mass flow $\dot{m}$ [kg/s] passing through the 1D medium. To solve this equation, use is made of the Taylor expansion [1].

$$\iint_A \rho(\vec{u} * \vec{n}) dA = (\rho A u)_{out} - (\rho A u)_{in} \tag{4.7}$$

$$= \rho 2\pi r z\,(u(r+\Delta r) - u(r)) \approx \rho 2\pi r z \left(\left(u(r) + \frac{\partial u}{\partial r}\Delta r\right) - u(r)\right) = 2\pi \rho r z \frac{\partial u}{\partial r}\Delta r \tag{4.8}$$

When substituting equations 4.6 and 4.8 into the law for mass conservation, it describes the velocity gradient, seen in equation 4.10.

$$\rho \pi r \Delta r \frac{dz}{dt} + 2\pi \rho r z \frac{\partial u}{\partial r}\Delta r = 0 \tag{4.9}$$

$$\frac{\partial u}{\partial r} = -\frac{1}{2z}\frac{dz}{dt} \tag{4.10}$$

[1] Taylor series: $u(r+\Delta r) \approx u(r) + \frac{\partial u}{\partial r}\Delta r$

In order to find the expression describing the horizontal fluid flow velocity passing between the disk and the seabed, it is necessary to integrate equation 4.10 with respect to its position r. This leaves us with an expression for the horizontal fluid velocity for a closed disk, given as:

$$\int_0^r \frac{\partial u}{\partial r} dr = \int_0^r -\frac{1}{2z}\frac{dz}{dt} dr \tag{4.11}$$

$$\boxed{u(r,t) = -\frac{r}{2z}\frac{dz}{dt}} \tag{4.12}$$

Just like in Brennen's model, the horizontal fluid velocity in the centre of the disk, $u(0,t)$, is zero. Since there is no possibility for water to escape vertically, the vertical fluid flow $v(0,t)$ is zero.

The fluid velocity is expected to have the highest magnitude on the outside of the disk and zero magnitude right in the middle. To give function 4.12 a physical meaning, one could plot equation 4.12 for an imposed motion. As this horizontal flow velocity is expected to behave in the same way as Brennen's velocity, a similar visualisation as in figure C.2 is expected. Here indeed it was observed that the flow velocity is maximum on the outside and zero in the middle. It is presumed that the motion parameters play an important role in the behaviour of the fluid underneath the disk.

CONSERVATION OF MOMENTUM

Similar to the mass conservation, the conservation of momentum from White[**?**], and therefore the situation shown in figure 4.3, holds. The fundamental equation for the momentum conservation is given here:

$$\sum F = \frac{\partial}{\partial t}\iiint_V \rho \vec{u} dV + \iint_A \rho(\vec{u}\cdot\vec{n})\vec{u} dA \tag{4.13}$$

This equilibrium is also recognized as Newton's second law of motion ($F = ma$). The terms on the right-hand side of equation 4.13 represent the change in momentum over time and the momentum flux, respectively. The $\sum F$ expresses the sum of all the external forces acting on the free body. Since only the flow in horizontal direction is considered, gravitational forces are neglected. The only external force comes from the pressure at the boundary.
Using the change in volume $dV = \rho\pi r\Delta r$ from equation 4.6, the change in momentum is expressed as:

$$\frac{\partial}{\partial t}\iiint_V \rho \vec{u} dV = \frac{\partial}{\partial t}\int_0^{z(t)} \rho\pi r\Delta r u dz = \rho\pi r\Delta r \frac{\partial}{\partial t}(zu) \tag{4.14}$$

Similar to the mass flow in equation 4.7, the 1D momentum flux is defined as the difference between the inlet and outlet flux. To solve for the momentum flux, the Taylor series [2] is applied again.

$$\iint_A \rho(\vec{u} * \vec{n})\vec{u} dA = \left((\rho A u)\vec{u}\right)_{out} - \left((\rho A u)\vec{u}\right)_{in} \tag{4.15}$$

$$= \rho 2\pi r z\left((u(r+\Delta r))^2 - (u(r))^2\right) \approx \rho 2\pi r z\left(u^2 + 2u\frac{\partial u}{\partial r}\Delta r + \left(\frac{\partial u}{\partial r}\Delta r\right)^2 - u^2\right) \tag{4.16}$$

$$\approx 4\pi\rho r z u\frac{\partial u}{\partial r}\Delta r \tag{4.17}$$

It is presumed that the mesh size of the system is very small, $\Delta r << 1$. Therefore, the term including $(\Delta r)^2$ can be neglected.

Next, the external force coming from the pressure at the boundary is derived. The pressure at the boundaries, seen in figure 4.3, is again calculated by means of the Taylor series and given in equation 4.19. As indicated in figure 4.3, the pressure at the boundaries is acting inward, whereas the normal vector $\vec{n}$ is positive in outward

[2] Taylor series: $(u(r+\Delta r))^2 \approx u^2 + 2u\frac{\partial u}{\partial r}\Delta r + \left(\frac{\partial u}{\partial r}\Delta r\right)^2$

direction. Therefore it is consistently in opposite direction to the normal vector, hence the minus sign within the integral.

$$\sum F = \iint_A p\,(-\vec{n})\,dA \tag{4.18}$$

$$\approx 2\pi r z\big(p(r) - p(r+\Delta r)\big) \approx 2\pi r z\left(p - \left(p + \frac{\partial p}{\partial r}\Delta r\right)\right) = -2\pi r z \frac{\partial p}{\partial r}\Delta r \tag{4.19}$$

Consequently, the three terms to solve the conservation of (linear) momentum have been found and can be substituted into equation 4.13. By reorganizing the equation, the momentum equilibrium can be written as in equation 4.21.

$$-2\pi r z \frac{\partial p}{\partial r}\Delta r = \rho \pi r \Delta r \frac{\partial}{\partial t}(zu) + 4\pi\rho r z u \frac{\partial u}{\partial r}\Delta r \tag{4.20}$$

$$\boxed{\frac{1}{\rho}\frac{\partial p}{\partial r} + 2u\frac{\partial u}{\partial r} + \frac{1}{2z}\frac{\partial}{\partial t}(zu) = 0} \tag{4.21}$$

From expression 4.21, clearly the time t and position r dependency on the horizontal fluid flow velocity $u(r,t)$ can be seen. By inserting equation 4.12 into this equation, the next step towards finding the hydrodynamic force can be made.

PRESSURE CALCULATION

Before finding an expression for the pressure distributed underneath the plate, the horizontal flow velocity $u(r,t)$ is inserted into equation 4.21, illustrated in equations 4.22 and 4.23.

$$\frac{1}{\rho}\frac{\partial p}{\partial r} + 2\left(-\frac{r}{2z}\frac{dz}{dt}\right)\left(-\frac{1}{2z}\frac{dz}{dt}\right) + \frac{1}{2z}\frac{\partial}{\partial t}\left(-\frac{r}{2}\frac{dz}{dt}\right) = 0 \tag{4.22}$$

$$\frac{1}{\rho}\frac{\partial p}{\partial r} + \frac{r}{2z^2}\left(\frac{dz}{dt}\right)^2 - \frac{1}{4z}\frac{d^2z}{dt^2} = 0 \tag{4.23}$$

The velocity $\frac{dz}{dt}$ and acceleration $\frac{d^2z}{dt^2}$ terms are clearly recognizable in equation 4.23. The velocity squared term originates from the composition of the flow velocity. Since the flow velocity in equation 4.12 is accounted to both the plate's velocity and the gap height, it gives rise to squared velocity term.

Subsequently, the pressure gradient $\frac{\partial p}{\partial r}$ from equation 4.23 is integrated over the width of the structure between r and R. Finally, the hydrodynamic pressure inside the gap between the disk and the seabed can be expressed as in equation 4.26.

$$\int_r^R \frac{\partial p}{\partial r}dr = \int_r^R -\left(\frac{r}{2z^2}\left(\frac{dz}{dt}\right)^2 - \frac{1}{4z}\frac{d^2z}{dt^2}\right)\rho r\,dr \tag{4.24}$$

$$p|_{r=R} - p(r,t) = -\frac{\rho}{8}(R^2 - r^2)\left(\frac{2}{z^2}\left(\frac{dz}{dt}\right)^2 - \frac{1}{z}\frac{d^2z}{dt^2}\right) \tag{4.25}$$

$$\boxed{p(r,t) = p|_{r=R} + \frac{\rho}{8}\frac{(R^2 - r^2)}{z}\left(\frac{2}{z}\left(\frac{dz}{dt}\right)^2 - \frac{d^2z}{dt^2}\right)} \tag{4.26}$$

The term $p|_{r=R}$ represents the pressure at the edges of the suction pile, at $r = R$. The assumption is made that the pressure at the edges is equal to the ambient water pressure, thus $p|_{r=R} = 0$. The ambient water pressure is assumed to be uniform over the whole surface of the structure and thus is not included in the determination of the hydrodynamic force.

It is expected that the pressure on the outside of the disk is equal to zero and maximum in the middle underneath the disk. Again, this pressure distribution is assumed to be similar to Brennen's flat plate. In appendix C, a plot of the pressure distribution is given. The plot is in line with the expectation for the behaviour of the pressure.

FORCE CALCULATION

The final step in the derivation of the hydrodynamic force involves an integration of the pressure equation over the surface of the disk. At this point, distinction is made between situation 1 and situation 2 from figure 4.2 by integrating the hydrodynamic pressure between different limits. The polar system representation is used to obtain the force acting on a disk with a valve in close proximity to the seabed:

$$F = \iint_A p(r,t)\,dA = \int_0^{2\pi}\int_{R_v}^{R} p(r,t)\,r\,dr\,d\theta \tag{4.27}$$

The hydrodynamic force, imposed by the fluid, acting on a disk with a valve in close distance to the seabed boundary is derived as follows:

$$F_{hyd1} = 2\pi\int_{R_v}^{R}\frac{\rho}{8}\frac{(R^2 r - r^3)}{z}\left(\frac{2}{z}\left(\frac{dz}{dt}\right)^2 - \frac{d^2z}{dt^2}\right)dr \tag{4.28}$$

$$\boxed{F_{hyd1} = \frac{\pi}{16}\rho\frac{\left(R^2 - R_v^2\right)^2}{z}\left(\frac{2}{z}\left(\frac{dz}{dt}\right)^2 - \frac{d^2z}{dt^2}\right)} \tag{4.29}$$

Expression 4.29 illustrates the hydrodynamic force, or added mass force, for an open disk. The force acts as a resistance force on the structure with a valve at the top. When R_v is set to zero, the function of the hydrodynamic force for a closed disk is obtained:

$$\boxed{F_{hyd1_{closed}} = \frac{\pi}{16}\rho\frac{R^4}{z}\left(\frac{2}{z}\left(\frac{dz}{dt}\right)^2 - \frac{d^2z}{dt^2}\right)} \tag{4.30}$$

It can be observed that as the plate is lowered, the added mass for the closed disk starts at a small value of the order ρR^3 (when z is of the order R) and will rapidly increase with z to a value of the order $\rho\frac{R^4}{z}$. Comparing this expression with the one from Brennen in equation 4.4, it is observed that the velocity and acceleration switched signs. This is correct, as Brennen considers the force to be in downward direction in his paper.

In his paper, Brennen gave the expression for the inertial force in absence of a solid, i.e. moving in free open water. The equation for Brennen's flat plate is given here (it is also given in appendix C):

$$F_{free} = -\rho\pi a^2\frac{d^2h}{dt^2} \tag{4.31}$$

Brennen illustrated it to emphasize the dominance of the presence of the boundary on the magnitude of the force. The presence of the boundary results in an increase in the magnitude of the hydrodynamic force. Close to the seabed, the hydrodynamic force is dominated by the solid boundary. This is expected to be seen in the behaviour of the hydrodynamic force and also applies for the expression derived for the disk.

The function for the hydrodynamic force is used as one of the input components for the structural model, which eventually is used to analyze the motion behaviour and set-down of the structure.

4.3.2. BEHAVIOUR OF HYDRODYNAMIC FORCE

To better understand the behaviour of the hydrodynamic force from the 1D model, equations 4.29 and 4.30 are plotted for several imposed motions with a period $T = 10$ s, an outside radius $R = 2.75$ m and a valve radius $R_v = 1$ m:

1. $z(t) = 0.5sin(\omega t) + 2$
2. $z(t) = 0.5sin(\omega t) - 0.1t + 2$
3. $z(t) = 0.5sin(\omega t + \pi) - 0.1t + 2$

The first motion describes the force in a free hanging situation. The second and third motions represent a lowering situation in which the imposed motions differ in phase, $\phi = 0$ and $\phi = \pi$, respectively.

Initially an oscillation with amplitude $A = 0.5$ m and period $T = 10$ s is imposed at a distance of 2 m to the seabed (rigid underground). A constant lowering of 0.1 m/s is added to the motion. Whereas the first two appointed oscillations start in an upward direction, the third motion begins with a downward movement. This is intended to see if the hydrodynamic force is sensitive to phase difference. The results for the imposed motion $z(t) = 0.5sin(\omega t) + 2$, plotted for a time period of 10 s, are given in the figure 4.4 and figure 4.5.

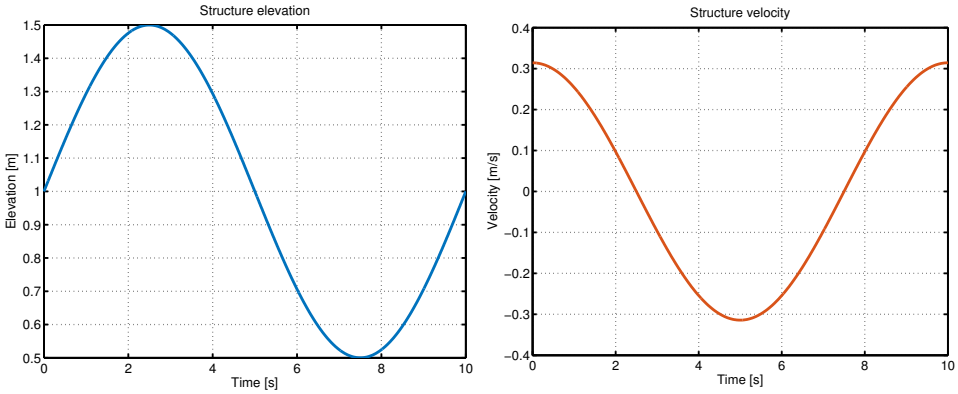

(a) Structure's elevation

(b) Structure's velocity

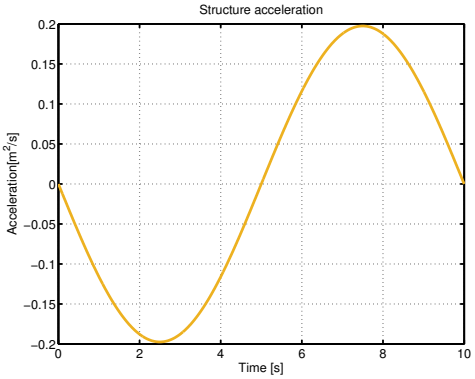

(c) Structure's acceleration

Figure 4.4: Motion behaviour with input $z(t) = 0.5sin(\omega t) + 2$

The displacement, velocity and acceleration are used to calculate the hydrodynamic force, seen in the figure 4.4. In figure 4.5, the force induced by the fluid inside the gap during one oscillation is illustrated for both models. The total force, indicated with the blue line, is plotted together with the terms it is composed of. The red line is the squared conservative velocity $(\frac{dz}{dt})^2$ term and the yellow line the linear acceleration $\frac{d^2z}{dt^2}$ term. In the graph, the first half of the period shows an overpressure and the second half an underpressure. The structure's acceleration works opposite to the acceleration term (yellow line), which contributes to the hydrodynamic force.

For this imposed motion, F_{hyd} is dominated by the acceleration term. This is in line with the expectation based on Brennen's hydrodynamic force for moving in free open water (equation 4.31).

The difference between figures 4.5a and 4.5b is the magnitude of the total force. The force for the disk with a valve is lower than the one without valve. This shows the first evidence that the presence of a valve results in a lower resistance force.

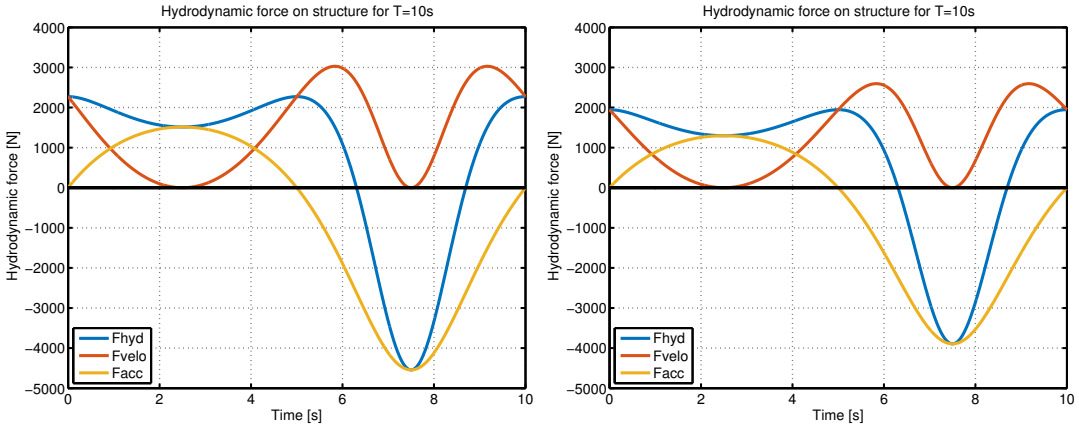

(a) Hydrodynamic force, without valve

(b) Hydrodynamic force, with $R_v = 1m$

Figure 4.5: Hydrodynamic force with input $z(t) = 0.5sin(\omega t) + 2$

Figures 4.6a and 4.6b show the results for the hydrodynamic force for the disk without valve for the two lowering cases. The left graphs shows the results from the motion with an upward starting direction and the right one the results for the motion beginning in downward direction. In both situations, the motion/force moves towards a rigid boundary. This is reflected in the increasing value of the force, which is dominated by the velocity term. The results for the disk with a valve showed the same development but for a lower magnitude. They have been given in appendix G.

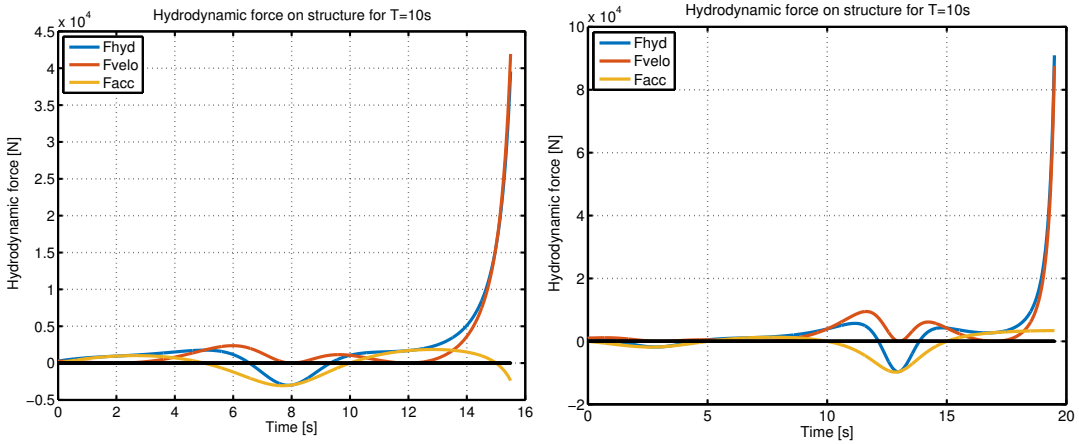

(a) Hydrodynamic force, without valve for $z(t) = 0.5sin(\omega t) - 0.1t + 2$

(b) Hydrodynamic force, without valve for $z(t) = 0.5sin(\omega t + \pi) - 0.1t + 2$

Figure 4.6: Hydrodynamic force

What is interesting to see is the fact that a different phase in the input motion can lead to different behaviour of the force. The change in phase is reflected in the time it takes for the force to increase significantly. For both cases, still the clear dominance of the velocity term (red line) is seen in close proximity to the seabed. From this analysis it became clear that the hydrodynamic force is sensitive to phasing.

4.3.3. CONCLUSIONS

During the process of lowering, the structure is exposed to drag and inertia forces. Close to the seabed, the inertia or added mass force increases. This increase originates from a force imposed by the fluid on the structure in close proximity to the seabed. Physically the hydrodynamic force represents a water cushion. This water cushion works as a resistance force onto the structure and therefore decelerates the system. It is important to emphasize that this force does not dissipate energy from the system.

Recall equation 4.29 for the hydrodynamic force on disk with radius R, valve radius R_v and at a height of $z(t)$:

$$F_{hyd1} = \frac{\pi}{16}\rho\frac{\left(R^2 - R_v^2\right)^2}{z}\left(\frac{2}{z}\left(\frac{dz}{dt}\right)^2 - \frac{d^2z}{dt^2}\right) \tag{4.32}$$

From this equation, a squared velocity term $(\frac{dz}{dt})^2$ and a single linear acceleration term $\frac{d^2z}{dt^2}$ can clearly be seen. The contribution of both terms to the total hydrodynamic force can be explained in the following way:

- The acceleration term is an open water added mass, which remains dominant as long as the distance between the structure and the boundary (seabed) is large enough.
- The velocity term represents an extra added mass, rising with increasing proximity. The closer the structure gets to the boundary, the bigger the effect of this extra term. This is a direct result of the division the squared velocity $(z)^2$ term and that makes the velocity part a nonlinear conservative term.

The forces coming from velocity and acceleration terms are never in phase. This is because one term is squared and the other is single. Whichever z is prescribed, the two parts of the force will never be in phase and there will always be a sign switch. The fact that one term is quadratic and the other is not, makes the force also frequency dependent.

The presence of the valve is reflected in the magnitude of the corresponding hydrodynamic force, which is lower than for a disk without a valve. In this case this is also expected, as the area where the fluid can act on is less compared to a completely closed disk.

Overall it can be stated that the hydrodynamic force for a disk with radius R and height $z(t)$ rises with increasing proximity to a solid boundary. From $R/z >> 1$, a clear increase in the force was observed. Just before the structure hits the seabed, the force reaches its maximum. The fluid force is sensitive to phasing, frequency and valve size. It is expected to also see this sensitivity in the results of the structural model, elaborated on in chapter 6.

4.4. 2D MODEL: DISK WITH ONE SYMMETRIC VALVE

The 2D model describes the situation of a disk with a symmetric valve in the middle, as was shown in figure 4.2c. The difference between this situation and the situation seen in figure 4.2b, is that 2D fluid flow is included. In this case, the fluid can escape vertically through the valve or horizontally underneath the plate. Just like the 1D model, the pile is simplified to a flat symmetric disk with outer radius R and valve radius R_v.

In the next section, an explanation of the derivation of the hydrodynamic force and assumptions is given. Similar to Brennen's derivation and the 1D model, the fundamental equations are used to derive the force.

4.4.1. DERIVATION OF HYDRODYNAMIC FORCE

Other than the 1D model, the derivation of the hydrodynamic force for the 2D model can be divided into two sections: one related to the plate and one to the valve.

The situation of the 2D model is visualized in figure 4.7a. Since the disk and the valve are symmetric, only one side of the disk is assumed. In this situation, water can escape horizontally, as $u(r,t)$, and vertically through the valve, as $v(t)$. According to White, you can speak of a 2D fluid flow situation, since flow can escape in $r-$ & $z-$direction, respectively. Again it is assumed that the disk is lowered in a perfectly vertical direction, resulting in a time dependent displacement $z(t)$.

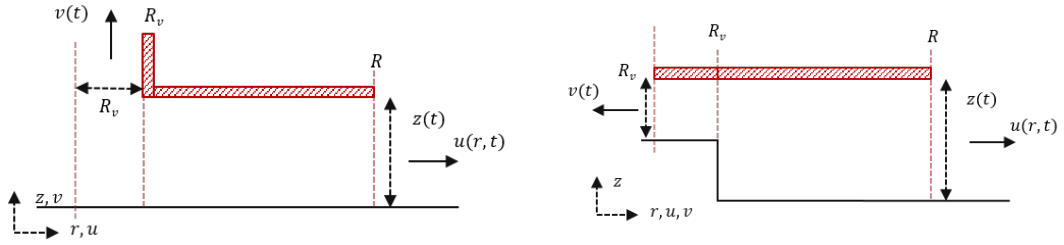

(a) Disk with a valve, one side

(b) Disk with a valve, one side & simplified

Figure 4.7: One side of disk with one symmetric valve

As the derivation of the hydrodynamic force with 2D fluid flow becomes quite complex, a simplification has been made. It is assumed that the valve part is rotated 90 ° to the left, illustrated in figure 4.7b. In this way, the fluid flow in the system remains 1D, instead of the earlier 2D, but actual vertical fluid velocity is still considered.
On the right side in figure 4.7b, fluid can escape horizontally through the time-changing opening between the disk and the seabed. On the left side, flow can escape 'vertically' through a constant area described by πR_v^2. Whereas the height of the plate side changes with $z(t)$ over time, the valve side has a constant height R_v. This is due to the simplification made between figure 4.7a and figure 4.7b. It is assumed that the vertical fluid velocity through the valve is constant over the position, therefore the vertical fluid velocity is only a function of time, $v(t)$.
Figure 4.8 illustrates the flow elements underneath the plate and in the valve. The elemental boundaries and related u and p for the plate side are shown. The same can be visualized for the valve side for v and p.

Next, the derivation of the equations for mass and momentum conservation for the plate side and the valve side are explained. With use of these equations, the hydrodynamic pressure and finally hydrodynamic force can be derived. Due to complexity, the full derivation has been obtained by making use of the numerical software Maple. The Maple code can be found in appendix E.

CONSERVATION OF MASS

Recall equation 4.5 describing the conservation of mass from White, including the change in mass over time and the mass flow in and out of the control volume.

$$\frac{\partial}{\partial t}\iiint_V \rho dV + \iint_A \rho(\vec{u} * \vec{n}) dA = 0 \tag{4.33}$$

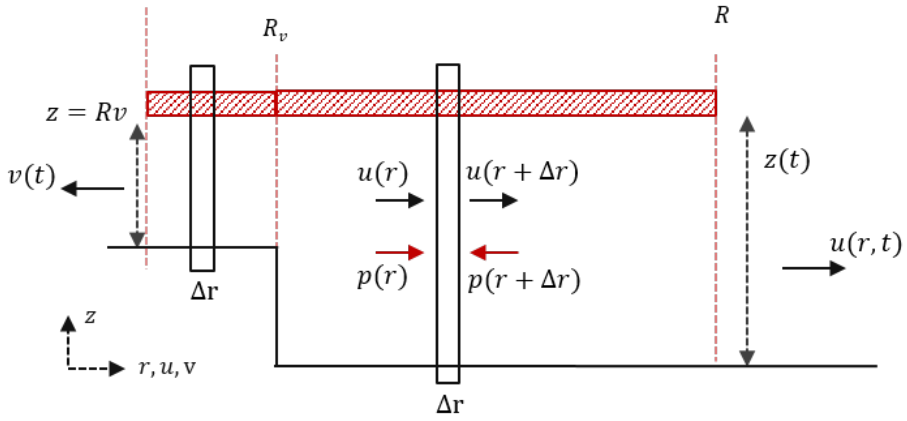

Figure 4.8: Visualization of the fluid flow under the disk with horizontal flow velocity u and pressure p at the boundaries of r and $r+\Delta r$ at the plate side. In a similar way, this can be visualized for the valve side, with vertical velocity v and pressure p.

For both the plate side and the valve side an expression for the conservation of mass can be derived.

Plate side
Exact to model 1, the change in mass for the plate side is described by:

$$\frac{\partial}{\partial t}\iiint_V \rho dV = \frac{\partial}{\partial t}\int_0^{z(t)} \rho(\pi r \Delta r) dz = \rho \pi r \Delta r \frac{dz}{dt} \tag{4.34}$$

The mass can flow through the valve side or the plate side, resulting in two equations for the mass flow in and out of the system. Since the fluid flow is assumed to be positive to the right, the mass flow going through the valve is negative. Equations 4.35 and 4.36 describe the mass flow going to the plate side and the valve side, respectively.

$$\iint_A \rho\,(\vec{u} * \vec{n}) dA = \int_0^{z(t)} \rho\,(2\pi\Delta r)\,u dz = 2\pi\rho\Delta r z u \tag{4.35}$$

$$\iint_A \rho\,(\vec{u} * \vec{n}) dA = \int_0^{R_v} -\rho\,(\pi\Delta r)\,v dz = -\rho\pi R_v \Delta r\, v \tag{4.36}$$

From equations 4.35 and 4.36, it can be noticed that the mass flowing through the plate side is related to the horizontal flow $u(r,t)$ and the mass through the valve to the vertical flow $v(t)$. Since the valve is assumed to have a constant height, the equation for the mass flow was obtained by an integration to R_v instead of $z(t)$.

Subsequently equations 4.34, 4.35 and 4.36 can be substituted into the mass conservation law of equation 4.33. By rearranging and clearing the equilibrium, the expression for the horizontal fluid flow velocity $u(r,t)$ is obtained in equation 4.38.

$$\rho\pi r\Delta r\frac{dz}{dt} + 2\pi\rho\Delta r z u - \rho\pi R_v \Delta r\, v = 0 \tag{4.37}$$

$$\boxed{u(r,t) = \frac{R_v v(t) - r\frac{dz}{dt}}{2z}} \tag{4.38}$$

It can be noted that the horizontal fluid flow is time t and position r dependent. Furthermore, the horizontal flow is influenced by the time-dependent vertical fluid flow $v(t)$. In case no valve is present, i.e. $R_v = 0$, the equation is simplified to $u(r,t) = -\frac{r}{2z}\frac{dz}{dt}$, which is exactly the same as the one derived for the 1D model in equation 4.12, based on Brennen.

Valve side

In the same manner, an equation for the vertical fluid flow velocity can be derived. The change in mass, described by equation 4.39, is equal to zero as it is assumed that the vertical velocity $v(t)$ is constant over the position.

$$\frac{\partial}{\partial t}\iiint_V \rho dV = \frac{\partial}{\partial t}\int_0^{R_v} -\rho(\pi R_v \Delta r)dz = 0 \tag{4.39}$$

In this case, the mass can flow through the valve or through the medium at $r = R_v$ to the plate side. Again this results in two equations for the mass flow, one related to the plate and one to the valve. To derive the mass flow at the plate side, use is made of the horizontal fluid velocity at the position of $r = R_v$, $u(R_v, t)$. Also notice that the mass flow related to the valve side is integrated over 'height' R_v.

$$\iint_A \rho\,(\vec{u} * \vec{n})dA = \int_0^{z(t)} \rho\,(2\pi R_v)\,u(R_v, t)dz = 2\pi\rho R_v z u(R_v, t) \tag{4.40}$$

$$\iint_A \rho\,(\vec{u} * \vec{n})dA = \int_0^{R_v} -\rho\,(\pi R_v)\,v dz = -\rho\pi R_v^2 v \tag{4.41}$$

By inserting the derived equations 4.39, 4.40 and 4.41 into the mass conservation law, an expression for the vertical fluid flow velocity $v(t)$ is found.

$$2\pi\rho R_v z u(R_v, t) - \rho\pi R_v^2 v = 0 \tag{4.42}$$

$$\boxed{v(t) = \frac{2z}{R_v}u(R_v, t)} \tag{4.43}$$

Because of the assumption made that the flow in the valve does not change over its position, the vertical fluid flow velocity is only dependent on time t. As can be seen from equation 4.43, the vertical fluid velocity is related to the time-changing $z(t)$ and $u(R_v, t)$ terms and the valve size R_v. In case there is no valve present, $R_v = 0$, the vertical fluid velocity becomes zero. As expected, the vertical velocity is directly related to the horizontal flow velocity $u(r, t)$, presumable at position $r = R_v$.

CONSERVATION OF MOMENTUM

Recall equation 4.13 describing the law for momentum conservation. Again, it consists of the change in momentum, the momentum flux and external forces, respectively. Similar to the conservation of mass, an equation for the conservation of momentum for both sides can be derived.

$$\sum F = \frac{\partial}{\partial t}\iiint_V \rho\vec{u}dV + \iint_A \rho\,(\vec{u}\cdot\vec{n})\vec{u}dA \tag{4.44}$$

Plate side

Using the change in volume $dV = \rho\pi r\Delta r$ from equation 4.34, the change in momentum for the plate side can be derived, seen in equation 4.45. Similar to the 1D model, use is made of the Taylor expansion in order to derive the term describing the momentum flux, seen in equation 4.46.

$$\frac{\partial}{\partial t}\iiint_V \rho\vec{u}dV = \frac{\partial}{\partial t}\int_0^{z(t)} \rho\,(\pi r\Delta r)\,u dz = \rho\pi r\Delta r\frac{\partial}{\partial t}(zu) \tag{4.45}$$

$$\iint_A \rho\,(\vec{u}\cdot\vec{n})\,\vec{u}dA = 2\pi\rho r z\left(2u\frac{\partial u}{\partial r}\Delta r\right) = 4\rho\pi r z u\frac{\partial u}{\partial r}\Delta r \tag{4.46}$$

Likewise to the 1D model, the external force comes from the pressure acting at the boundary of the system. In this case that boundary is at the right outside of the plate side. The force is acting inward, opposite to the unit normal vector $\vec{n}$, seen in figure 4.8. Therefore the external force in equation 4.47 contains a minus sign. By applying the Taylor series, a definition for the external pressure force is deduced.

$$\iint_A p\,(-\vec{n})\,dA = -2\pi r z\frac{\partial p}{\partial r}\Delta r \tag{4.47}$$

All the derived equations related to the momentum are substituted into equation 4.44 and by rearranging and clearing, it is possible to describe the conservation of (linear) momentum between the plate and the seabed, as follows:

$$\rho\pi r\Delta r\frac{\partial}{\partial t}(zu)+4\rho\pi rzu\frac{\partial u}{\partial r}\Delta r=-2\pi rz\frac{\partial p}{\partial r}\Delta r \tag{4.48}$$

$$\boxed{\frac{1}{\rho}\frac{\partial p}{\partial r}+2u\frac{\partial u}{\partial r}+\frac{1}{2z}\frac{\partial}{\partial t}(zu)=0} \tag{4.49}$$

From equation 4.49, the position r and time t dependency on horizontal velocity $u(r,t)$ clearly be seen. Notice that this expression is similar to the (linear) momentum derived in equation 4.21 for the 1D model.

Valve side

Similar to the plate side, a conservation of momentum for the valve can be derived. The volume change $dV=-\rho\pi R_v\Delta r$ from the conservation of mass is used to derive the momentum change of equation 4.50. As stated earlier, the vertical flow velocity is independent of position r. Therefore the momentum flux, seen in equation 4.51, will be equal to zero. For the valve, the external force comes from the pressure working inward to the system, described in equation 4.52.

$$\frac{\partial}{\partial t}\iiint_V\rho\vec{u}dV=\frac{\partial}{\partial t}\int_0^{R_v}-\rho\left(\pi R_v\Delta r\right)v\,dz=-\rho\pi R_v^2\Delta r\frac{\partial v}{\partial t} \tag{4.50}$$

$$\iint_A\rho\left(\vec{u}\cdot\vec{n}\right)\vec{u}dA=\rho\pi R_v^2\left(2v\frac{\partial v}{\partial r}\Delta r\right)=0 \tag{4.51}$$

$$\iint_A p\left(-\vec{n}\right)dA=-\pi R_v^2\frac{\partial p}{\partial r}\Delta r \tag{4.52}$$

Again, these equations are implemented into the momentum law from White, which results in a description for the conservation of (linear) momentum in the valve:

$$-\rho\pi R_v^2\Delta r\frac{\partial v}{\partial t}=-\pi R_v^2\frac{\partial p}{\partial r}\Delta r \tag{4.53}$$

$$\boxed{\frac{1}{\rho}\frac{\partial p}{\partial r}-\frac{\partial v}{\partial t}=0} \tag{4.54}$$

Equation 4.54 indicates that the vertical velocity is only dependent on time t. Now that the conservation of mass and momentum for both sides have been derived, it is necessary to connect them. This is done through an equilibrium between the conservation of momentum from both sides, explained in the next section.

EQUILIBRIUM BETWEEN EQUATIONS OF MOMENTUM CONSERVATION

To connect both parts of the system, it is assumed that the pressure gradient of both the plate and the valve side need to be in equilibrium at position $r=R_v$. Because of this assumption, the phenomenon that the horizontal flow velocity is zero somewhere under the disk will not be valid anymore.
For the connection, the following equilibrium must hold:

$$\frac{\partial p}{\partial r}\Big|_{plate}=\frac{\partial p}{\partial r}\Big|_{valve} \tag{4.55}$$

When setting the position r equal to the valve radius R_v, the terms $\frac{\partial p}{\partial r}$ describe the pressure gradient at $r=R_v$ for both the plate and the valve side. The pressure gradients for the plate and the valve, respectively, can be defined as:

$$\frac{\partial p}{\partial r}\Big|_{plate}=\rho\left(-2u\frac{\partial u}{\partial r}-\frac{1}{2z}\frac{\partial}{\partial t}(zu)\right) \tag{4.56}$$

$$\frac{\partial p}{\partial r}\Big|_{valve}=\rho\frac{\partial v}{\partial t} \tag{4.57}$$

Before solving this equilibrium, the horizontal fluid flow velocity $u(r,t)$ derived in equation 4.38 is inserted into equation 4.56 at $r = R_v$. Due to complexity, this has been done in the numerical software program Maple and the exact steps can be found in appendix E. Finally, this equilibrium was solved and rewritten into a first order non-linear differential equation for $v(t)$, as follows:

$$\boxed{A\left(\frac{\partial v}{\partial t}\right) + Bv(t) + C = 0} \tag{4.58}$$

With the term A, B & C, respectively, as:

$$A = -1 - \frac{R_v}{4z} \qquad B = \frac{R_v}{z^2}\frac{dz}{dt} \qquad C = -\frac{R_v}{z^2}\left(\frac{dz}{dt}\right)^2 + \frac{R_v}{4z}\left(\frac{d^2}{dt^2}z\right)$$

Equation 4.58 was solved in Maple for the derivative of the vertical fluid flow velocity $v(t)$ with respect to time. This results in the vertical fluid flow acceleration as:

$$\boxed{\frac{\partial v}{\partial t} = \frac{R_v\left(4\left(\frac{dz}{dt}\right)v(t) + z\left(\frac{d^2}{dt^2}z\right) - 4\left(\frac{dz}{dt}\right)^2\right)}{z(R_v + 4z)}} \tag{4.59}$$

This function is necessary in order to write the final equation for the hydrodynamic force as function of z, $\frac{dz}{dt}$, $\frac{d^2z}{dt^2}$ and v. In the next step, the hydrodynamic pressure acting under the plate was deduced.

PRESSURE CALCULATION

The function for the hydrodynamic pressure acting under the disk was derived through integration with respect to the position r. It is assumed that the hydrodynamic pressure only acts on the disk, i.e. between R_v and R, meaning that $r \geq R_v$ and that only equation 4.49 is relevant. Like the 1D model, the magnitude of the pressure is changing with the position underneath the plate. The equation for the pressure distribution, derived in the same way as the 1D model, is too long and complex to display in this report, therefore only the short expression is preserved.

$$\int_r^R \frac{\partial p}{\partial r}\Delta r = \int_r^R \rho\left(-2u\frac{\partial u}{\partial r} - \frac{1}{2z}\frac{\partial}{\partial t}(zu)\right)dr \tag{4.60}$$

$$p(r,t) = p|_{r=R} + \int_r^R \rho\left(-2u\frac{\partial u}{\partial r} - \frac{1}{2z}\frac{\partial}{\partial t}(zu)\right)dr \tag{4.61}$$

$$\boxed{p(r,t) = C_1(r,z)\left(\frac{dz}{dt}\right)^2 - C_2(r,z)\frac{d^2z}{dt^2} - C_3(r,z)v - C_4(r,z)\frac{dv}{dt}} \tag{4.62}$$

Here $p|_{r=R}$ is the pressure at the edge of the disk, $r = R$. Again it can be assumed that the pressure at the outside radius of the disk is equal to the ambient water pressure, i.e. $p|_{r=R} = 0$. This pressure distribution is only valid for $R_v \leq r \geq R$ and will be used to deduce the function for the hydrodynamic force. The pressure as described in equation 4.62 is used to calculate the function for the hydrodynamic force.

FORCE CALCULATION

Comparable to the pressure distribution, the hydrodynamic force is presumed to only be exerting on the plate, and is therefore ignored in the part of the valve. Like the 1D model, the pressure equation is integrated over the surface of the disk. Use polar coordinates, equation 4.62 is integrated with respect to 2π and R. The shortened notation obtained by Maple is given here. To make the expression readable, the terms proportional to the velocity squared, the acceleration, the vertical flow velocity and the vertical flow acceleration have been collected in C_5, C_6, C_7 and C_8, respectively. These terms still carry a dependency on the structure's elevation $z(t)$.

$$F_{hyd2} = \int_0^{2\pi}\int_{R_v}^R p(r,t)\,r\,dr\,d\theta \tag{4.63}$$

$$= 2\pi \int_{R_v}^{R} \left(C_1(r,z) \left(\frac{dz}{dt} \right)^2 - C_2(r,z) \frac{d^2z}{dt^2} - C_3(r,z)\, v - C_4(r,z) \frac{dv}{dt} \right) r\, dr \tag{4.64}$$

$$= C_5(z) \left(\frac{dz}{dt} \right)^2 - C_6(z) \frac{d^2z}{dt^2} - C_7(z)\, v - C_8(z) \frac{dv}{dt} \tag{4.65}$$

In order to use the force as input for the structural model, the hydrodynamic force F_{hyd2} should only consist of the terms z, $\frac{dz}{dt}$, $\frac{d^2z}{dt^2}$ and v. Hence the vertical flow acceleration of equation 4.59 was substituted into equation 4.65. This changes the terms C_5, C_6, C_7 and C_8 into C_9, C_{10}, C_{11}, respectively.
Obtained through Maple, the short notation for the hydrodynamic force, imposed by the fluid, acting on a disk with a symmetric valve in close proximity to the seabed, is given by:

$$\boxed{F_{hyd2} = C_9(z) \left(\frac{dz}{dt} \right)^2 - C_{10}(z) \frac{d^2z}{dt^2} - C_{11}(z)\, v} \tag{4.66}$$

Similar to the added mass force derived by Brennen, the velocity squared and acceleration term can clearly be seen. Recall equation 4.29 expressing the hydrodynamic force F_{hyd1} for an open disk in the 1D model:

$$F_{hyd1} = \frac{\pi}{16} \rho \frac{\left(R^2 - R_v^2\right)^2}{z} \left(\frac{2}{z} \left(\frac{dz}{dt} \right)^2 - \frac{d^2z}{dt^2} \right) \tag{4.67}$$

Both expressions look similar to each other. The difference is the extra term concerning the vertical fluid flow velocity v in F_{hyd2}. It is expected that the function, including the vertical fluid velocity through the valve, is a more realistic expression for the hydrodynamic force acting on the structure in close proximity of the seabed.

4.4.2. OVERVIEW ASSUMPTIONS

An overview of the assumptions made in order to derive the function for the hydrodynamic force with 2D fluid flow is given here.

- The difference between the 1D and 2D model is the flow direction. In the 1D model, fluid flow can only escape horizontally underneath the plate. The fluid behaviour is different for the 2D model, in which the flow can either escape horizontally underneath the disk or vertically through the valve. Because of the simplification made in figure 4.7b, the flow actually remains 1D and some of the mass flow in the valve may have been lost/ignored.
- The vertical fluid flow velocity is taken only as function of time t. The assumption has been made that the flow through the valve is constant and independent along the position in the valve. In reality, the flow in the valve is different for each position.
- Normally, there is a stagnation point underneath the disk, which is expected to change its position over time. At this point, the fluid flow velocity is zero and thus maximum pressure occurs. For a structure with a valve, two stagnation points, one left and one right of the valve, are expected. Due to the assumption made in equation 4.55, it is predicted that the stagnation point has been fixed at $r = R_v$ and therefore will not change over time.
- During the installation of a suction pile, vortices and turbulent flow occur underneath the structure. These vortices and turbulences have been ignored in the derivation of the hydrodynamic force of equation 4.66.

4.4.3. CONCLUSIONS

Different to the 1D model, the hydrodynamic force from the 2D model includes both vertical fluid flow $v(t)$ and horizontal fluid flow $u(r,t)$. Its origin and function is similar to the 1D model, which is described in section 4.3.3.

Similar to the 1D model, a squared velocity $(\frac{dz}{dt})^2$ and a single linear acceleration term $\frac{d^2z}{dt^2}$ can be recognized. In this case a third term is present: one related to the vertical flow velocity $v(t)$, indicating the presence of the valve.
Originally, a function only consisting of z, $\frac{dz}{dt}$, $\frac{d^2z}{dt^2}$ and known constants was expected. However, due to the assumptions made in the derivation of the force, the term $v(t)$ remained present in the final expression of the hydrodynamic force. This makes it difficult to analyze the behaviour of the hydrodynamic force for an imposed motion, like what was done for the 1D model, and therefore is not given for the 2D model. The derived expressions for $v(t)$ and $u(r,t)$ are directly related to each other. Therefore it is complex to calculate the steady state condition for an imposed motion. This is the reason why the system for the 2D model is initialized before actual analysis is performed. This is described in chapter 6.

Since the force also represents an extra added mass force, the behaviour of the force is predicted to be comparable to the behaviour seen in the 1D model in section 4.3.2. The presence of the valve is expected to be reflected in a lower magnitude of the hydrodynamic force. Like the 1D model, the hydrodynamic force is phase and frequency dependent, which can be seen from the squared velocity and single acceleration term in equation 4.66.

In the next chapter, the hydrodynamic force, defined as in equations 4.29 and 4.66, will be implemented into the structural model. Furthermore, an overview of expectations for the results of the base case situation, described in chapter 6, and for the results of the sensitivity analysis, explained in chapter 7, is given here.

5

STRUCTURAL MODEL

By implementing the hydrodynamic force from the 1D and 2D model into the structural model, the set-down of a structure can be modelled and analyzed.
In this chapter the Equation of Motion (EOM) for the structure and the corresponding soil reaction is obtained and elaboration on all components is given. A short list of the important input parameters for the base case is provided. Also, an overview of expectations for the results of the base case situation and the sensitivity analysis is presented.

5.1. EQUATION OF MOTION

Illustrated in figure 1.3 on the right side, the system is divided into two situations; 'above' the seabed and 'settling' on the seabed, referred to as phase 1 and phase 2, respectively. The EOMs are derived for a flat disk and thus the force related to skirts is not included.

Phase 1 is separated into two coupled equations of motion, one related to the structure and one to the soil. These need to be in equilibrium. The one related to the structure describes the forces acting on the structure. The EOM specifying the soil defines the equilibrium between the hydrodynamic force pushing on the seabed and the soil resistance. This means that there is an interaction between the structure and the displaced soil. Phase 1 describes the EOM for both the structure and the soil.

It is not allowed for the structure to bounce, so a 'smooth' landing is expected. Once the structure lands on the seabed, the hydrodynamic force becomes zero and is replaced by the soil force. The soil starts to exerts a force on the object. Once the structure's submerged weight and the soil resistance force reach an equilibrium, the module is settled on the seabed. This situation defines phase 2. Both the soil equilibrium of phase 1 and the EOM for phase 2 is explained in the section referred as soil equilibrium.

5.1.1. STRUCTURAL EQUILIBRIUM

As described by Journée and Massie [23], the equation of motion for a rigid body moving vertically through a fluid is given as:

$$(m+a)\ddot{z}+b\dot{z}+cz=F \tag{5.1}$$

In which

- a : Hydrodynamic mass coefficient or added mass $[kg]$
- b : Hydrodynamic damping coefficient $[kg/s]$
- c : Restoring spring coefficient $[kg/s^2]$

The equation of motion can be segregated into four components. On the left-hand side of the equation, the term including $\ddot{z}$ represents the inertial forces, the second term the damping forces and the last term the restoring force, respectively. The term on the right-hand side describes the sum of all external forces acting on the structure.

To describe the motion behaviour of the disk, a Free Body Diagram (FBD) is used to indicate the forces acting on it. The forces acting on the structure need to be in equilibrium. From the FBD in figure 5.1, the equation of motion for the structure during the landing phase is obtained (skirt force is not included).

$$F_{inertia} + F_{drag} = F_{hyd} + F_{line} - F_{subm} \tag{5.2}$$

Where

$F_{inertia}$: Inertia force $[N]$
F_{drag} : Drag force $[N]$
F_{hyd} : Hydrodynamic force acting on the structure $[N]$
F_{line} : Tension force from crane wire $[N]$
F_{subm} : Submerged weight $[N]$

When looking at this EOM, it is different than the equation used by Journée and Massie. In this resulting equation, the external forces acting on the structure are F_{hyd}, F_{line} and F_{subm}. The hydrodynamic force F_{hyd}, caused by the proximity of the seabed, can behave like a suction or resistance force, as was described in chapter 4. The spring or restoring force term cz is included in the upward directed tension force F_{line}, coming from the crane wire. The structure is assumed to be fully submerged. This generates a force F_{subm} acting in downward direction. This was also seen in section 2.2.4 in figures 2.3 and 2.4.

Since the position of the disk, $z(t)$, is time dependent, the inertia force $F_{inertia}$, the drag force F_{drag}, the hydrodynamic force F_{hyd} and the line force F_{line} are a function of time.

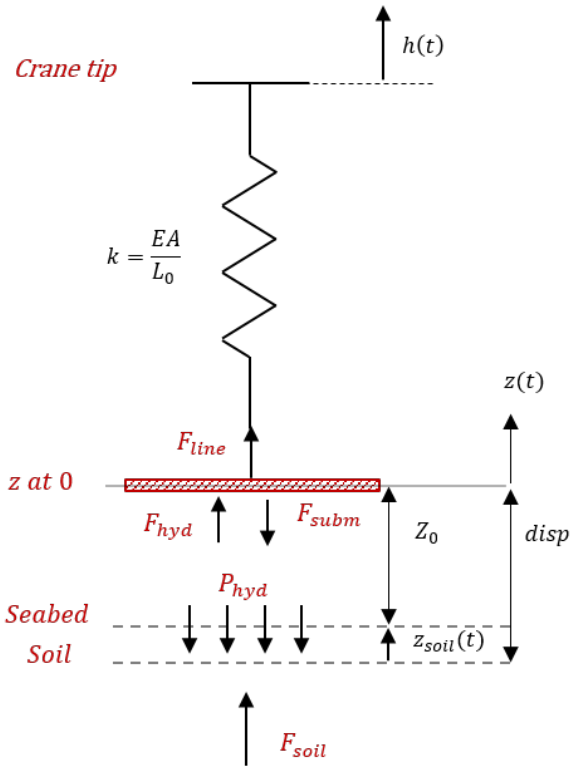

Figure 5.1: Free body diagram of structural model

As indicated in chapter 4, the hydrodynamic force is different for a disk with 1D or 2D fluid flow, represented by equations 4.29 and 4.66. The other equations are identical for both the 1D model and 2D model. A short elaboration on all the other forces is given next.

INERTIA FORCE

At the moment a structure starts to move in a fluid, a resistance or inertia force in opposite direction to the structure is created. The magnitude of the inertia force is proportional to the structure's acceleration and the increase in added mass due to seabed proximity. In section 3.2, the added mass term was explained and the inertia force was given as:

$$F_{inertia} = (M + A_{33})\ddot{z} \tag{5.3}$$

DRAG FORCE

The viscous drag force results from the vertical motion of the structure and gives quadratic damping to the system. Once the structure comes to rest, this force becomes zero. Referring back to section 3.2, the viscous drag force can be calculated by:

$$F_{drag} = 0.5\rho_w C_D A_r \dot{z}|\dot{z}| \tag{5.4}$$

LINE FORCE

The structure is connected to a crane with a crane wire, which is positioned on an oscillating barge. The crane lowers the structure to the seabed, which results in a tension force on the structure. The line force, originating from the change in length between the crane tip z_{ct} and the suction pile z_{sp}, is described by:

$$F_{line} = k_{line}\Big(z_{ct} - z_{sp}\Big) \tag{5.5}$$

$$F_{line} = k_{line}\Big(\big(z_0 + \frac{F_{subm}}{k_{line}} - V_c t - Asin(\omega t + \phi)\big) - z\Big) \tag{5.6}$$

In which:

k_{line} : Crane wire stiffness, $k_{line} = EA/L\ [N/m]$

z_0 : Initial position suction pile $[m]$

$\frac{F_{subm}}{k_{line}}$: Initial deflection suction pile $[m]$

V_c : Crane wire velocity $[m/s]$

A : Amplitude $[m]$

ω : Angular velocity, $\omega = \frac{2\pi}{T}\ [rad/s]$

ϕ : Phase difference $[rad]$

The structure starts at an initial position z_0 from the seabed, with an initial deflection of the crane wire, represented by $\frac{F_{subm}}{k_{line}}$. The crane wire is lowered with a certain constant lowering velocity V_c. The oscillating component, $Asin(\omega t + \phi)$, is a result of the heave oscillation which the crane experiences. This heave motion directly results from the vessel, on which the crane is positioned.

SUBMERGED WEIGHT

The difference between the weight in air of the structure and the weight of the displaced volume is the submerged weight [4]. It is obtained by looking at the difference between the density of sea water ρ_w and of steel ρ_s. For a fully submerged structure, the force, independent of time, is calculated by:

$$F_{subm} = Mg\frac{\rho_s - \rho_w}{\rho_s} \tag{5.7}$$

5.1.2. SOIL EQUILIBRIUM

PHASE 1

During the lowering of the structure, fluid is pushing onto the soil and thus an equilibrium between the fluid and the soil must hold. The equation of motion can be derived using the hydrodynamic pressure distribution, which is directly related to the hydrodynamic force acting on the structure.

Literature [17] tells us that the behaviour of soil is very unpredictable and irregular. Therefore soil is difficult to precisely model. Initially, the soil is described as a linear spring with certain soil stiffness k_{soil}. In a next stage, non-linear soil behaviour will be included, as was discussed in section 3.3. The following soil equilibrium between the soil force F_{soil} and the hydrodynamic force F_{hyd} can be derived:

$$F_{hyd} = F_{soil} \quad \Rightarrow \quad P_{hyd} A_r = k_{soil} z_{soil} \tag{5.8}$$

The pressure is distributed differently at each point along the disk. Since the soil reaction force is given as a point force, the retroactive pressure is a point force too. The maximum hydrodynamic pressure P_{hyd} is taken. This maximum pressure is multiplied with the reference area A_r, which results in the hydrodynamic force F_{hyd}, seen in equation 5.8. The reference area A_r is the area of the disk minus the area of the valve.

By searching for the equilibrium between the structure's EOM in equation 5.2 and the soil's EOM in equation 5.8 of phase 1, the structure's motion behaviour and corresponding reaction forces before the set-down can be determined.

PHASE 2

Once the structure lands on the seabed, the hydrodynamic force becomes zero and consequently is replaced by the soil force. In phase 2, the structure is settled onto the seabed and finally comes to rest. For phase 2, the EOM is changed into:

$$F_{inertia} + F_{drag} = F_{soil} + F_{line} - F_{subm} \tag{5.9}$$

While the structure settles on the seabed, it reduces in velocity and finally the forces $F_{inertia}$, F_{drag} and F_{line} decrease to zero. Once the soil force is equal to the submerged weight, the structure has fully come to rest and is finally settled.

5.2. INPUT DATA BASE CASE

The input data comes from HMC's Kaombo project. In table 5.1, the most relevant input data for the base case situation for the 1D and 2D model can be found. A list of all the input data for the base case situation is given in appendix F.

	Input data	Value
Structural	Structural mass	M = 222 ton
	Radius	R = 2.75 m
	Valve radius	R_v = 0.75 m
Crane	Period	T = 10 s
	Amplitude	A = 0.5 m
	Crane lowering velocity	V_c = 0.1 m/s
Soil	Soil stiffness	k_{soil} = 3.52 MN/m

Table 5.1: Overview of most relevant input data

5.3. VALIDATION

Before running and analyzing the whole system, i.e. the set-down of a structure, it is essential to check the accuracy of the obtained equilibrium. The following simple checks were done as validation:

- Free fall test : $k_{line} = 0$
- Free decay test : $V_c = 0$, $A = 0$
- Constant lowering test : $A = 0$, $V_c > 0$

The results of all three tests for the 1D and 2D model are given in appendix G.
In a free fall test, there is no line attached to the structure ($k_{line} = 0$), so the structure experiences a free fall towards the seabed in which the structure's velocity and acceleration becomes zero eventually. This was indeed observed for both the 1D and 2D model. In a free decay test, the structure starts in an out of equilibrium position without any crane tip heave motion. Eventually the structure needs to get back into equilibrium and the velocity and acceleration need to become zero. In the constant lowering test, the structure is lowered without heave oscillation and with a constant velocity ($A = 0$, $V_c = 0.1$ m/s) towards the seabed.

5.4. EXPECTATIONS

Based on the conducted literature research in chapter 3 and the insight gained on the hydrodynamic force in chapter 4, the following expectations are made:

HYDRODYNAMIC FORCE

- The hydrodynamic force increases in close proximity with the seabed.
- The presence of a valve in the disk, resulting in 2D fluid flow, results in a lower hydrodynamic force compared to a closed disk. This means that the results of the 1D model are expected to be higher compared to the 2D model.
- Including a valve results in a lower horizontal fluid flow velocity and pressure underneath the disk. The vertical fluid flow velocity going through the valve is expected to decrease in magnitude as the valve radius reduces. For a valve size nearly as big as radius of the disk, the vertical flow velocity is expected to have the same magnitude as the structure.
- The stagnation point for a closed disk is expected in the centre of the disk. For a disk with a valve, on both sides of the valve a stagnation point is predicted.
- The size/number of valves will have an impact on the amount of soil displacement caused by the set-down of the subsea structure.

SET-DOWN OF STRUCTURE

- Far away from the seabed (R/z « 1), the structure is unaffected by the hydrodynamic force. Once close to the seabed, the increasing hydrodynamic force decelerates the structure, resulting in a decrease of velocity and acceleration of the structure just before set-down.
- The crane tip heave motion affects the hydrodynamic force and therefore also the set-down of the structure. Due to this, weather conditions will affect the set-down as well. Crane tip heave motions caused by a short period and a high amplitude can be critical for structure installation. In this study, the weather conditions resulting in favourable crane tip heave motions are considered as a combination of a high period and a low amplitude. In the base case, $T = 10$ s and $A = 0.5$ m are considered as favourable weather conditions.
- Phasing will have a significant effect on the set-down of a subsea structure. Even in favourable weather conditions, there are phases for which the structure reaches the seabed with a high impact instead of having a smooth landing. This means that even with a high crane tip heave motion there is a phase for which a smooth landing is possible..
- The structural mass will have a small influence on the hydrodynamic force. A lower structural mass is expected to correspond to a slightly lower hydrodynamic force.
- The type of soil, among things characterized by the soil stiffness, will influence the set-down of the subsea structure. The hydrodynamic force is expected to be higher for stiffer soils.

SOIL DISTURBANCE

- The hydrodynamic force or hydrodynamic pressure acts onto the soil, resulting in soil deformation. A lower hydrodynamic force is expected to result in a lower soil disturbance.
- In this thesis, the soil displacement is calculated with three methods: Bernoulli equation together with Design Profile, maximum hydrodynamic force together with Design Profile and the a method based on the conservation of energy.
- The soil displacement calculated with Bernoulli equation is expected to be the most conservative.
- The method based on the maximum magnitude of the hydrodynamic force is expected to be less conservative than the Bernoulli equation. Because the maximum force only acts for a short period of time, the estimation is still not very realistic.
- Calculating the soil displacement based on conservation of energy engenders the lowest estimation of soil disturbance compared to the Bernoulli equation and maximum hydrodynamic force. The calculation based on the conservation of energy is expected to be the least conservative approach.

The results for the base case situation of this structural model for a closed disk and a disk with one symmetric valve are discussed in chapter 6.

6

BASE CASE RESULTS

This chapter discusses the results for the base case situation for the 1D and 2D model. First the results of the 1D model of both the closed and open disk (R_v = 0.75 m) are discussed. Next, the results of the 2D model are analyzed and compared with the 1D model.

6.1. 1D MODEL: CLOSED & OPEN DISK

In this section, the results of the 1D model with the closed and open (R_v = 0.75 m) disk are given and discussed.

6.1.1. INITIAL CONDITIONS

In the base case situation, a disk with a diameter of 5.5 m and a structural mass of 222 ton is positioned 2 meters above the sea floor. It is lowered towards the seabed with an initial velocity of 0.41 m/s. This velocity is derived from the initial heave motion and the constant crane lowering velocity of 0.1 m/s. There is no initial soil displacement. The timing of the set-down is difficult and is represented as the phase difference ϕ in the line force. A slight change in phase can result in a different output. In this case, ϕ has been chosen to be 0 rad.

Input condition	Value
Elevation	z = 2 m
Velocity	$\dot{z}$ = -0.41 m/s
Soil displacement	z_{soil} = 0 m
Phase difference	ϕ = 0 rad

Table 6.1: 1D model: initial conditions

6.1.2. RESULTS BASE CASE

The structure's motion behaviour, corresponding hydrodynamic force and soil force for the closed disk are shown in figure 6.1. Figures 6.1a, 6.1b and 6.1c show the displacement, velocity and acceleration, respectively, during the lowering and settling phase. The transition from the lowering into the settling phase can be seen around 22 s. During the first phase, the hydrodynamic force acts on the structure, as seen in figure 6.1d. During this phase, the soil and the hydrostatic pressure are in equilibrium.

Within 25 s, the structure has moved towards the soil and is slowed down as it gets closer to the seabed. Due to the increase in proximity, the hydrodynamic force increases as is illustrated in figure 6.1d. As explained earlier, the hydrodynamic force acts as a resistance force on the structure. Just before set-down, there is a sudden increase in acceleration. This development is also reflected in the sudden decrease of velocity. As expected, the soil has a noticeable impact on the hydrodynamic force and the structure's motion.

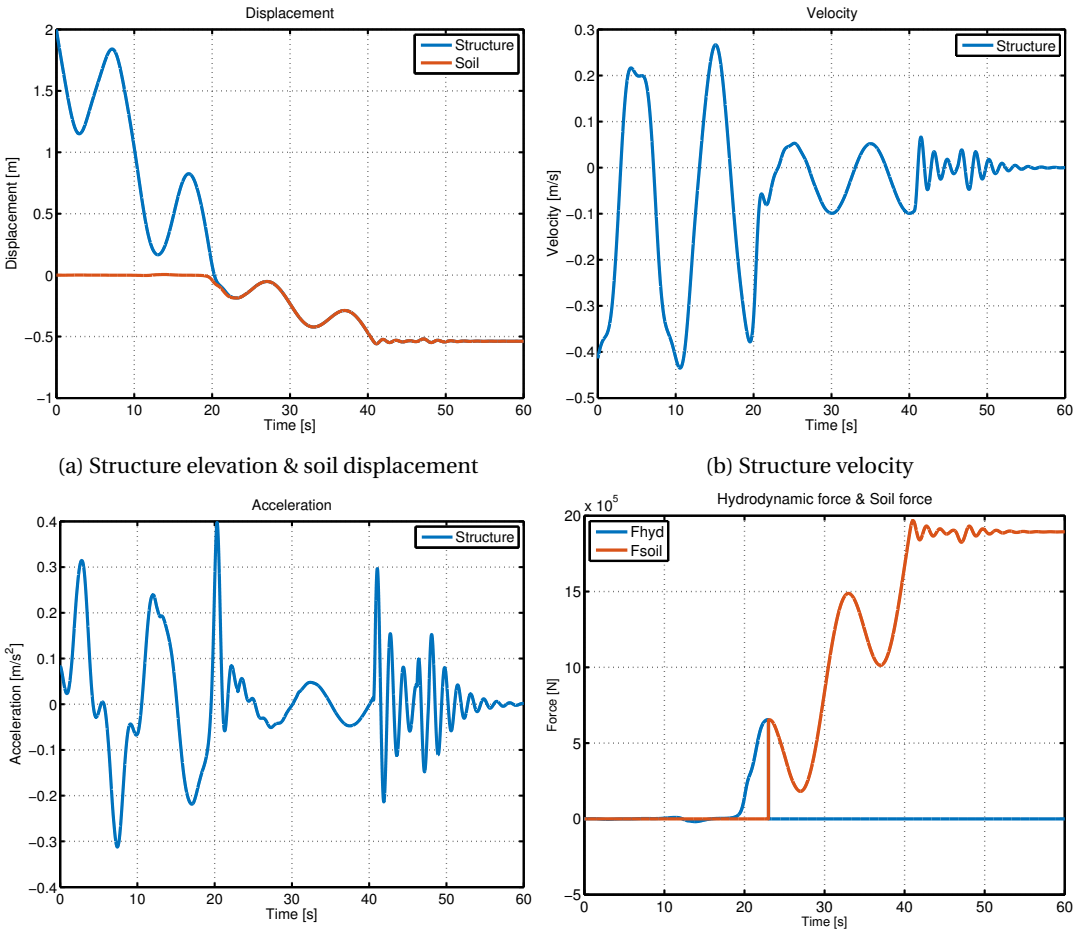

(a) Structure elevation & soil displacement

(b) Structure velocity

(c) Structure acceleration

(d) Hydrodynamic force & soil force

Figure 6.1: 1D model without valve: results base case, part 1

Figure 6.2 shows the horizontal fluid flow velocity $u(r,t)$ and pressure distribution $p(r,t)$ under the closed disk. As the disk is assumed to be symmetric, for simplicity only one side is shown.
In figure 6.2a, it is observed that the fluid velocity in the middle under the disk is zero and increases towards the outside. The fluid velocity is always maximum at the outside of the disk, at $R = 2.75$ m. As the structure gets closer to the seabed, similar to the hydrodynamic force $u(r,t)$ increases.
In figure 6.2b, it can be seen that the maximum pressure occurs at the middle of the disk and it is zero at the outside. This is expected as we assumed the outside pressure to be equal to the ambient pressure. The development is opposite to $u(r,t)$ and thus in line with the Bernoulli principle. Similar to $u(r,t)$, $p(r,t)$ rises as the proximity to the seabed increases. The behaviour of the fluid is in line with what was predicted by Brennen.

At the moment the structure and soil get in contact and the hydrodynamic force becomes zero, the system transitions to phase 2. This is seen after ~ 22 s in figure 6.1d. At that point, the soil force replaces the hydrodynamic force and the structure and soil will move together. They are connected in a kinematic way. When the contact force, i.e. soil force, becomes zero, there is a chance that the soil and structure disconnect. This is assumed to be a dynamic separation and can happen in case of e.g. unfavourable phasing. It would mean that the structure would disconnect from the soil and would move away from the seabed again. As seen in the figure 6.1, this does not happen in the base case situation.
While the structure settles on the seabed, the soil force rises, as is illustrated in figure 6.1d. After around 60 s, the structure has settled, meaning that the soil fore is in equilibrium with the structure's submerged weight.

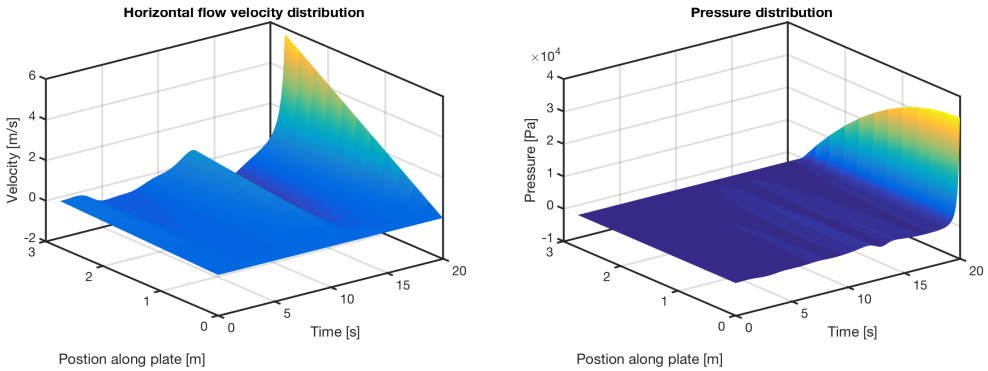

(a) Horizontal fluid flow velocity (b) Pressure distribution

Figure 6.2: 1D model without valve: results base case, part 2

The same analysis has been done for the 1D model with a valve of 0.75 m in radius (27 % opening). The results were similar, so for simplicity they are shown in appendix H.1.
The physical difference between both cases is the surface area where the hydrodynamic force acts on and thus the magnitude of the force is expected to be generally lower for larger valves. A slightly lower force was indeed observed for the disk with valve, seen in figure 6.3a. Figure 6.3b zooms in on both the hydrodynamic force for the open and closed 1D model just before the set-down. The magnitude of the force for the disk with 27% opening is slightly lower compared to the closed disk. In the 1D model, a valve with $R_v = 0.75$ m does not have a significant impact on the structure's motion behaviour.

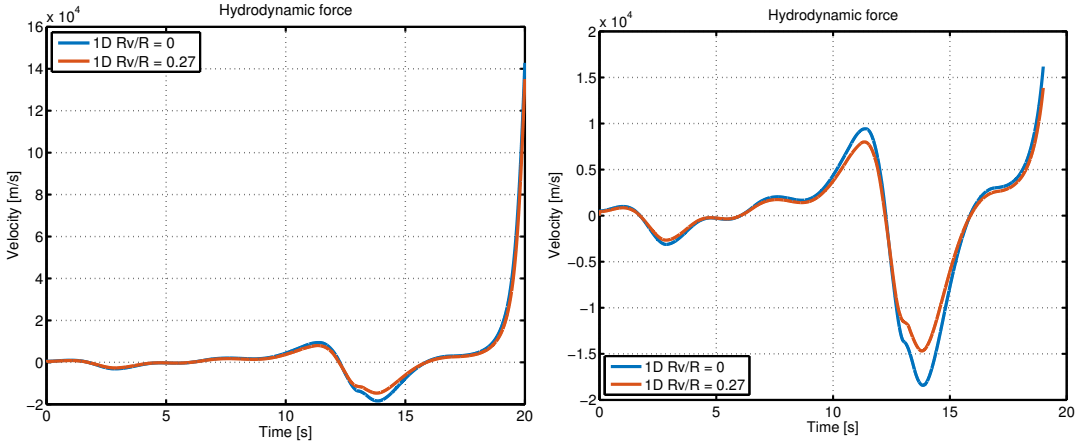

(a) Comparison of hydrodynamic forces (b) Comparison of hydrodynamic forces, zoomed in

Figure 6.3: 1D model: hydrodynamic force

6.1.3. RESULTS SOIL DISTURBANCE

Three methods for calculating the soil displacement were discussed in section 3.3. Based on the base case situation, the result calculated with the Bernoulli equation is constant for the 1D and 2D model: the maximum soil displacement is 0.61 m. The two other methods are differ for both models and are thus separately discussed. Eventually, the results of all three methods are compared.

METHOD BASED ON DESIGN PROFILE

Equation 3.8 together with the Design Profile has been used to convert the maximum of the hydrodynamic force into its corresponding soil disturbance. In figure 6.4, it is visualized that a closed disk, lowered with a velocity of ~ 0.40 m/s, from an initial elevation of 2 m from the seabed, results in a maximum soil displacement of ~ 0.50 m. This is a conservative estimation, since the maximum hydrodynamic force only acts for a small duration.

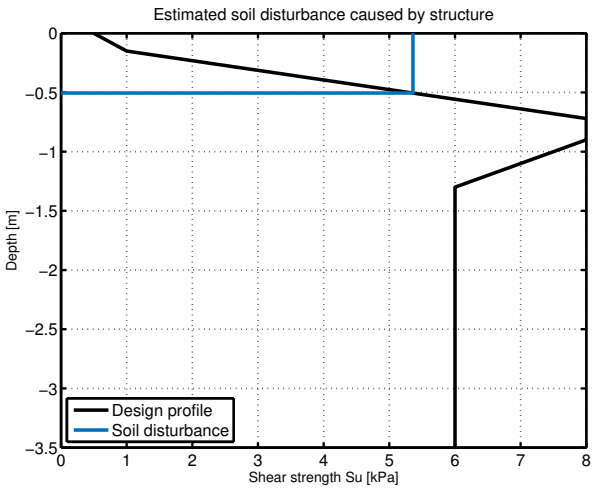

Figure 6.4: 1D model without valve: soil disturbance

Since the maximum magnitude of the hydrodynamic force for the open disk is comparable, similar results were obtained for the open disk.

METHOD BASED ON CONSERVATION OF ENERGY

In a less conservative method, the soil disturbance is based on the conservation of energy. Equation 3.13 is used to calculate the soil disturbance at time of collision for the closed and the open disk. For the damping ratio, the values of 0.7, 1 and 1.3 have been taken as upper, median and lower bound, respectively. The values have been given in the appendix H.

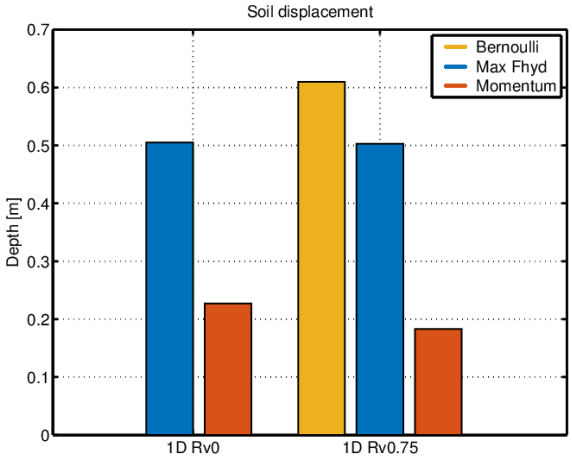

Figure 6.5: Comparison of soil displacement between three methods

Figure 6.5 compares the soil displacements calculated with the Bernoulli equation, given in equation 3.2 with the values based on the maximum hydrodynamic force and based on the conservation of energy. For this last method, the values for ζ are used. As the Bernoulli formula is not valid for a closed disk, it is not compared in the closed 1D model.
From figure 6.5 can be seen that the result of the Bernoulli equation is the hight and thus most conservative. The results of the conservation of energy for both the open & closed 1D model are clearly less conservative. For the Bernoulli equation, the soil disturbance of the open 1D model is 3 times as high compared to the conservation of energy. The figure also indicates that the open 1D model results in lower estimations of the soil displacement compared to the closed 1D model for the conservation of energy.

6.2. 2D MODEL: DISK WITH ONE SYMMETRIC VALVE

In this section, the results for the 2D model are given and discussed. The expression from equation 4.66 has been used for the hydrodynamic force. The results are given for a disk with a valve with $R_v = 0.75$ m.

6.2.1. INITIAL CONDITIONS & INITIALISATION

Again the structure starts at a position of 2 m above the seabed. The expression for the hydrodynamic force, derived in section 4.4.1, includes the vertical fluid flow velocity $v(t)$ going through the valve. It is expected that $v(t)$ has an influence on the magnitude of the hydrodynamic force. The initial vertical fluid floe velocity through the valve is difficult to obtain from calculations, because $v(t)$ arises as a result of the structure's motion. Therefore the system is first initialized before actual lowering. The system is brought into a steady-state before the constant crane lowering velocity is added to the system. This could give a shock to the system, bringing the system out of equilibrium. The initialisation has been taken into account for the results of the 2D model. In the results, the first 80 s are added for the initialisation of the system and afterwards the crane starts to lower with a constant velocity of 0.1 m/s. This is the reason why the plots start at 80 s.

6.2.2. RESULTS BASE CASE

Using the data from table 5.1, the following results for the base case for the 2D model, including $v(t)$, were generated. The results for the full run are given in appendix H.2.

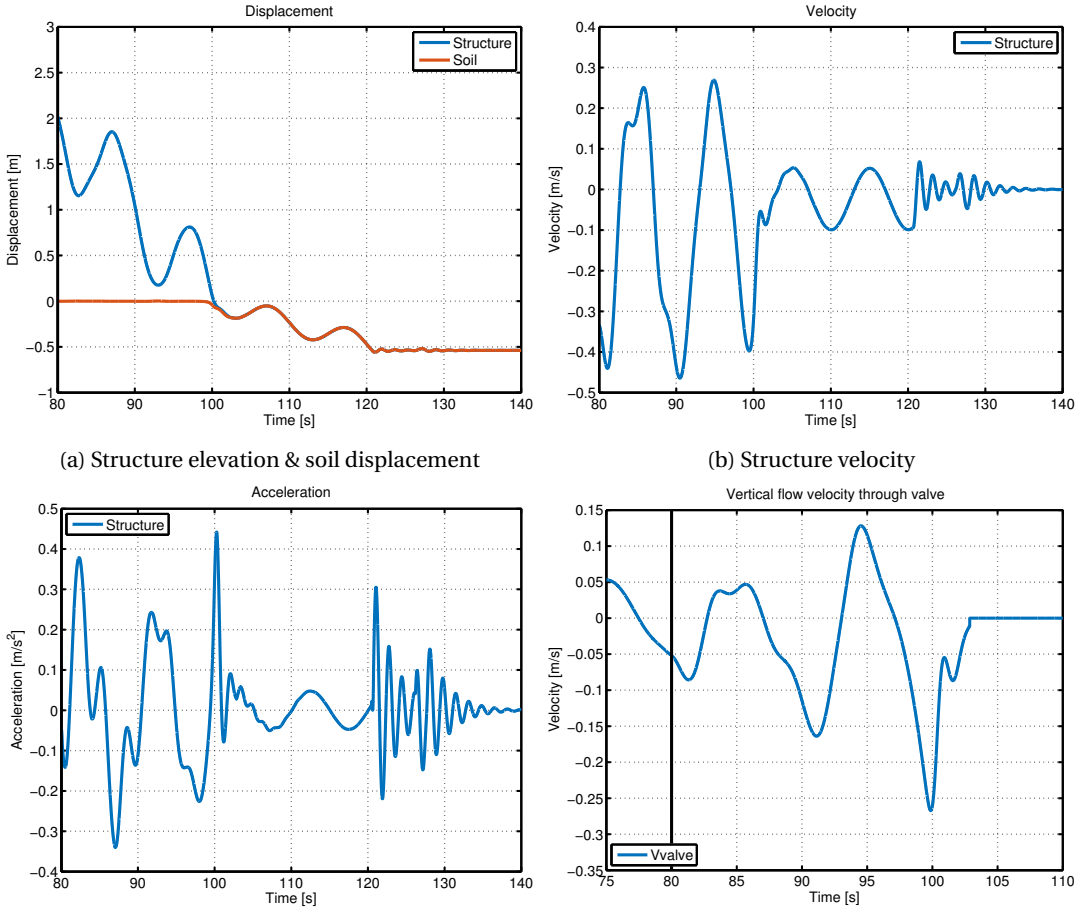

(a) Structure elevation & soil displacement

(b) Structure velocity

(c) Structure acceleration

(d) Vertical fluid flow velocity

Figure 6.6: 2D model: results base case, part 1

As was seen in section 6.1.2, the results for the 1D model, with and without valve, were similar i.e. the valve with $R_v = 0.75$ m had little influence on the motion behaviour. From the expectations, the hydrodynamic force in the 2D model is expected to be more realistic since the fluid velocity through the valve is included. The results for the displacement, velocity and acceleration, given in figure 6.6, seem similar to the results for

the 1D model. A different development and magnitude for the motion behaviour was predicted as the presence of the valve is expected to function as a pressure relief.
Figure 6.6d shows the results for the vertical fluid flow velocity. The $v(t)$ is assumed to be independent of the position. This is reflected in the 2D graph, instead of 3D, in figure 6.6d. Once the crane starts lowering (at 80 s), fluid flows through the valve with velocities between ~ 0.12 and -0.26 m/s. Since the flow can move through the valve, change in direction is expected. $v(t)$ increases as the structure gets closer to the seabed. This increase is expected, because the area under the disk for the fluid to escape horizontally becomes smaller close to the seabed and water is forced through the valve.

The development of the hydrodynamic force and consequently the soil force is much like the 1D model, as can be seen figure 6.7. In line with the expectations, a lower hydrodynamic force is observed for the 2D model. The maximum magnitude for the hydrodynamic force is similar to the one in figure 6.1d. However, the magnitude of the force before the set-down is lower for the 2D model. Figure 6.8 zooms in on all three hydrodynamic forces. The force from the 2D model is lower compared to the forces from the 1D model. Including $v(t)$ in the model indeed has an effect on the magnitude of the force. Before the set-down, the 2D model with an opening of 27% has a lower resistance force. However as the proximity to the seabed increases, the effect of the valve velocity is not significant anymore and the force results in a similar magnitude as for the 1D model.

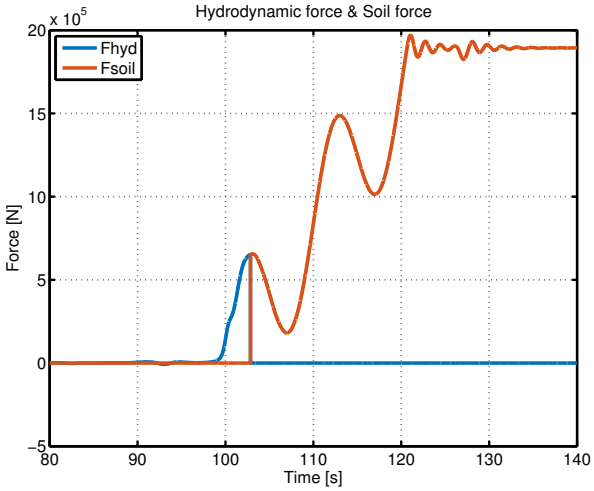

Figure 6.7: 2D model: hydrodynamic force & soil force

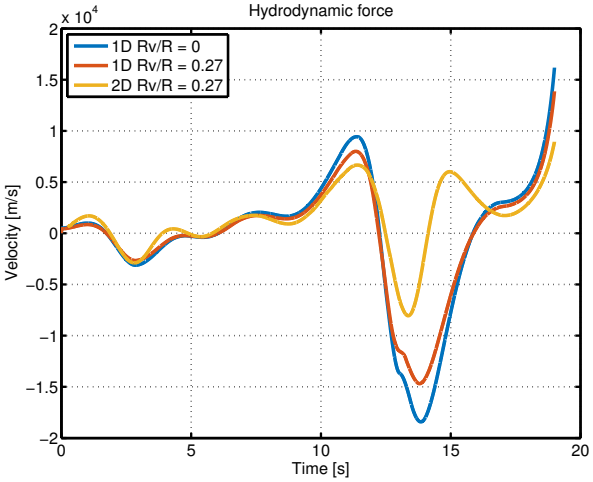

Figure 6.8: Comparison 1D & 2D hydrodynamic force, zoomed in

It is anticipated that $v(t)$ results in a lower horizontal flow velocity $u(r,t)$ and pressure distribution $p(r,t)$. They have been visualized in figure 6.9 for the 2D model.

Velocity $u(r,t)$ is maximum on the outside and increases as the structure gets closer to the seabed. The velocity is lower than seen in the 1D model. The slope from the disk outside radius R towards the valve radius R_v is steeper compared to the one from the 1D model, indicating a quicker change in velocity. This is expected to be due to the presence of the valve. $u(r,t)$ is nearly zero at the valve radius, indicating that the stagnation point is at $r = R_v$.
Pressure $p(r,t)$ is shown in figure 6.9b. Also here, the magnitude is lower compared to the one seen in figure 6.2b. Again zero pressure is observed on the outside and maximum at $r = R_v$, indicating that the stagnation point occurs at $r = R_v$.

As explained in section 4.4.1, due to the assumption made regarding the connection between the valve and plate side, the stagnation point was expected to be fixed on $r = R_v$. This is indeed observed for both $u(r,t)$ and $p(r,t)$ in figure 6.9.

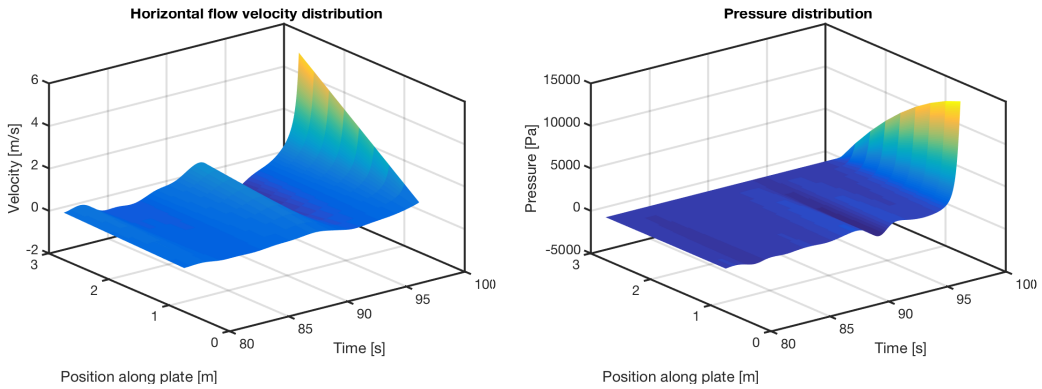

(a) Horizontal fluid flow velocity (b) Pressure distribution

Figure 6.9: 2D model: results base case, part 2

6.2.3. RESULTS SOIL DISTURBANCE

Again both methods are used to calculate the soil disturbance resulting from the 2D model.

METHOD BASED ON DESIGN PROFILE

A maximum soil disturbance of ~ 0.50 m is expected, when a 222 ton structure with an 27% opening and an initial velocity of ~ 0.40 m/s is set down on the seabed. As the maximum hydrodynamic force of the 1D and 2D model were alike, this value was expected. and for simplicity the graph has been left out of this report.

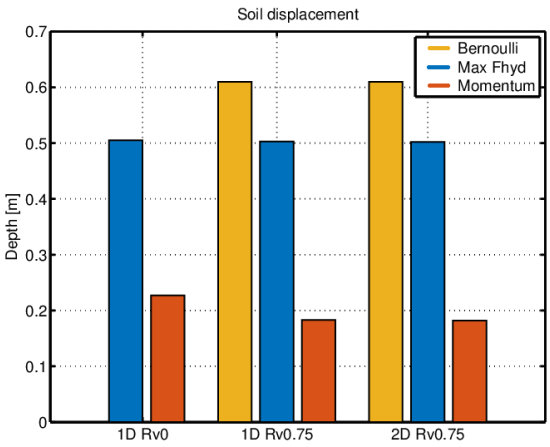

Figure 6.10: Comparison of soil displacement between three methods

METHOD BASED ON CONSERVATION OF ENERGY

Again the soil disturbance, corresponding to the impact of the hydrodynamic force in the 2D model, can be calculated for different damping ratio's and can be compared with the soil displacement based on the Bernoulli equation and the maximum force. Figure 6.10 measures the results of the closed/open 1D model and the open 2D model for all three calculation methods. As shown before, the results based on Bernoulli clearly are the most conservative. The calculation based on conservation of energy is clearly the least conservative. Based on the last two methods, the soil disturbance of the 2D model is lower compared to the closed 1D model and comparable to the open 1D model.

To make an estimation for the soil displacement in the preparation phase of an installation procedure, the method based on the conservation of energy would result in a more realistic and less conservative estimation. Due to this, it is likely that with this second method an increase in workability of a subsea installation could be realized.

6.3. CONCLUSIONS

Based on the base case results, the following is concluded about the impact the hydrodynamic force has on the set-down of the structure .

1D MODEL: CLOSED DISK

- During the lowering of a disk to the seabed, water escapes horizontally generating a pressure distribution acting underneath the structure. This pressure distribution is converted into a point force: the hydrodynamic or added mass force. This force works as a resistance force on the structure.
- In line with the literature, far away from the seabed ($R/z << 1$) the hydrodynamic force does not affect the structure's motion behaviour.
- In close proximity to the seabed, the fluid particles accelerate, resulting in an increase in the fluid flow velocity, pressure and hydrodynamic force.
- The stagnation point for a closed disk, indicated by zero fluid velocity and maximum pressure, is positioned right in the middle of the disk.
- The soil disturbance based on the Bernoulli equation is the most conservative. Based on the Design Profile, the maximum hydrodynamic force results in a maximum soil disturbance of 0.50 m. The method based on conservation of energy correspond to lower values, confirming it is less conservative. Under these circumstance the soil will not fail and the structure can safely be installed.

1D MODEL: DISK WITH ONE SYMMETRIC VALVE

- For a disk with 27% opening, the hydrodynamic force in the set-down phase is slightly lower compared to the closed disk. This is not reflected in the structure's motion behaviour and soil displacement.
- This intermediate step confirms that including a valve, by means of vertical flow velocity, is expected to result in a lower hydrodynamic force.

2D MODEL: DISK WITH ONE SYMMETRIC VALVE

- This model includes a disk with a symmetric valve with physical fluid flowing through it. The valve functions as a pressure relief during the lowering of the structure and has an impact on the magnitude of the hydrodynamic force. The vertical fluid flow velocity was assumed to be uniform in the valve.
- Like the 1D model, a lower horizontal fluid velocity and pressure under the disk occurs. The stagnation point is recognized at $r = R_v$ and therefore fixed. This is expected considering the assumptions made in chapter 4.
- Physically, the 2D model is more in line with reality than the 1D model. Including a valve in the model, allows for more water to escape underneath the disk resulting in a lower hydrodynamic resistance force. Initially, the force is indeed lower, but close the seabed the force rises significantly to a value similar to the one for the 1D model. It is thought that this is related to the function derived for the vertical fluid flow velocity in chapter 4. Possibly, too many assumption are made concerning the valve. This means that the values for the hydrodynamic force, derived in this thesis, are possibly higher compared to the actual ones.
- Compared to the 1D model, no significant change in the structure's motion behaviour occurs.
- The results for the 2D model are comparable to the 1D model, resulting in a soil disturbance of 0.5 m based on the Design Profile. The method based on the conservation of energy indicates values of lower soil displacement compared to the 1D model. This method is less conservative and therefore more realistic soil displacement estimations is made. In the preparation phase of an offshore installation project, it is likely that by using this method an increase in workability is gained.

From these conclusions, general understanding is gained on how the set-down of structures on the seabed was affected by the soil. As was seen in section 4.3.2, the hydrodynamic force is sensitive to different phases and frequencies. This will have an effect on the set-down of structures and the related soil displacement. Therefore, a sensitivity analysis has been performed, which is described in chapter 7.

7

SENSITIVITY ANALYSIS

The input data used to generate the results for the base case situation, described in chapter 6, were based on favourable (weather) conditions corresponding to acceptable crane tip heave motions. It would be interesting to evaluate the system for various structural properties, crane tip heave motions and soil properties.
This chapter describes the sensitivity analysis done for the 2D model. As the 2D model is expected to be more realistic, the 1D model has not been included in this analysis. The influence of the structural properties, in particular the size of valve and structural mass, have been analyzed. Thereafter, an analysis for variable periods, amplitudes and phases has been conducted for several valve sizes. Finally, a variable soil stiffness has been evaluated.

7.1. INPUT DATA

The variables for the period and amplitude are defined from the sea state given for HMC's Kaombo project. As it is hard to time a lowering installation, the analysis has been done for all phases. The soil stiffness has been varied with a lower and upper bound stiffness, from the soil data specification report from the Kaombo project. An overview of the base case values and variable values is given in table 7.1.

Input parameter		Base case value	Variable value
Structural properties	Valve radius	$R_v = 0.75$ m	$0 : 0.25 : 2.75$
	Structural mass	$M = 222$ ton	167, 229
Weather conditions	Period	$T = 10$ s	8, 12, 14, 16
	Amplitude	$A = 0.5$ m	0.25, 0.75, 1, 1.25
	Phase difference	$\phi = 0$ rad	$0 : 0.06 : 2\,\pi$
Soil properties	Soil stiffness	$k_{soil} = 3.52$ MN/m	1.76, 7.04

Table 7.1: Overview of input data for the sensitivity analysis

7.2. STRUCTURAL PROPERTIES

This section describes the influence of the structural properties, i.e. the valve size and the structural mass, on the set-down of structures onto the seabed.

7.2.1. VALVE SIZE

It is expected that a closed disk will behave differently than a disk with a valve. To investigate the valve influence, tests have been performed for various valve sizes. They have been labelled as a fraction of R: R_v/R. The results of some fractions are given here. The results of other fractions are given in appendix I.

RIGID UNDERGROUND

Two simple tests for variable valve sizes on a rigid underground have been analyzed: the free fall test and the constant lowering test. This section discusses the results of these tests.

Free fall test

Figures 7.1 and 7.2 illustrate the results for the free fall test. From figure 7.1a it can be seen that, the larger the valve, the quicker the structure reaches the seabed. A disk with a large valve is expected to relief more pressure, resulting in a lower hydrodynamic force and thus less resistance acts on the structure. In case of the free fall test, a structure with a lower resistance reaches the seabed with a higher velocity, as was seen in figure 7.1b.

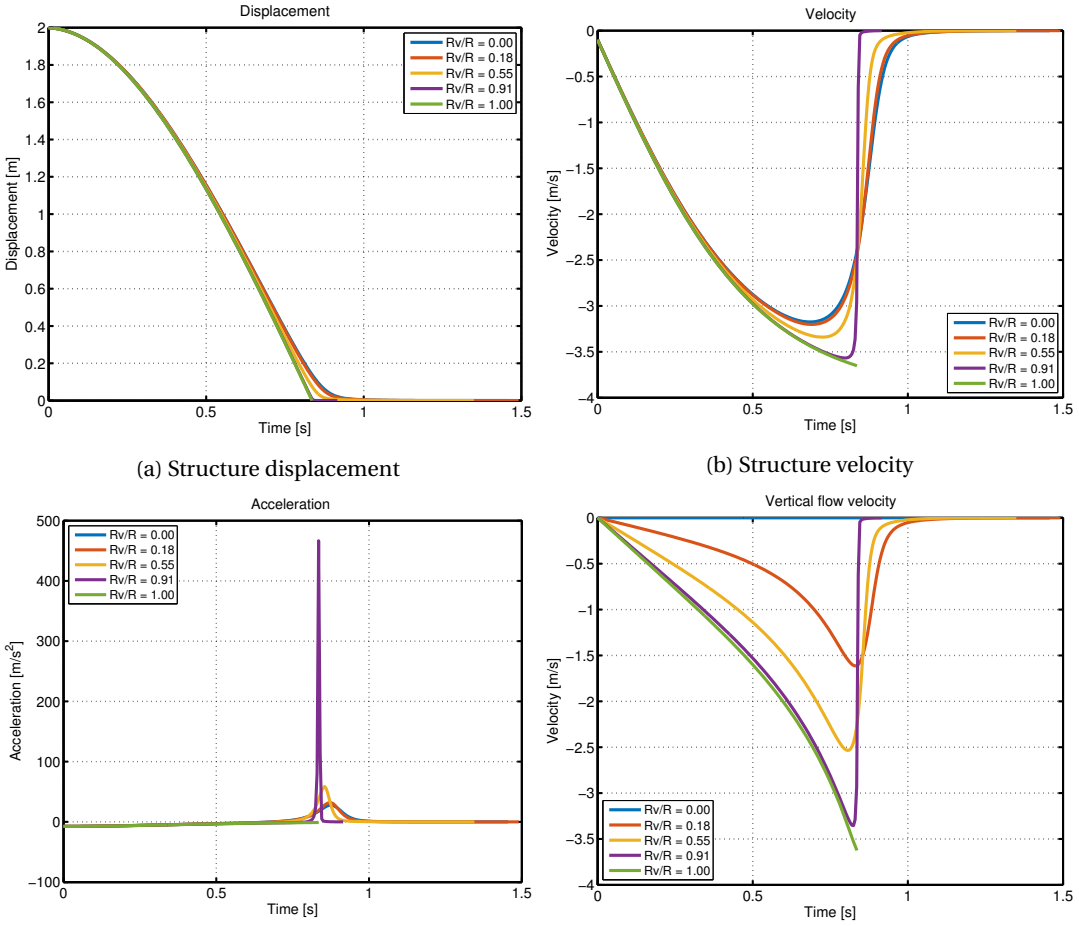

(a) Structure displacement

(b) Structure velocity

(c) Structure acceleration

(d) Vertical fluid flow velocity

Figure 7.1: Free fall test, part 1

For larger valves, the structure will experience less cushioning before encountering the impact of landing on the seabed. This results in a narrower and higher peak in hydrodynamic force, seen in figure 7.2a. Due to the higher velocity for larger valves, the kinetic energy of the structure is also higher when hitting the seabed. This is reflected in the structure acceleration in figure 7.1c. Thus, the impact force is higher when the kinetic energy with respect to the disk is higher. As for the valve radius in figure 7.1d, it is seen that as R_v goes to R, the vertical flow velocity $v(t)$ goes to the structure velocity (figure 7.1b).
When zooming in on the hydrodynamic force, done in figure 7.2b, it can be observed the structure with the largest valve corresponds to the lowest force. A lower force will result in a lower momentum (area under the force) and thus lower soil disturbance is predicted.

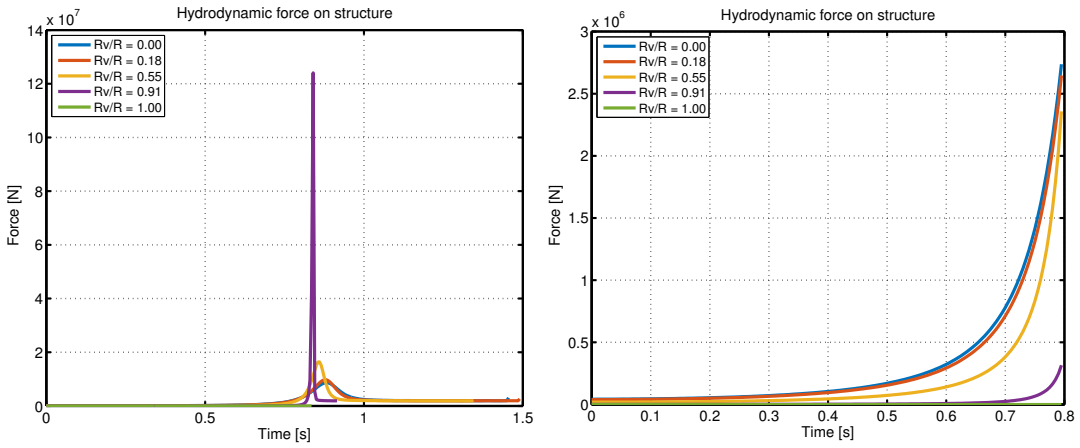

(a) Hydrodynamic force

(b) Zoomed in on hydrodynamic force

Figure 7.2: Free fall test, part 2

Figure 7.3 illustrates the horizontal fluid flow velocity $u(r,t)$ close before the set-down for two extreme cases: for a disk with a valve with $R_v = 0.5$ m (18% opening) and $R_v = 2.5$ m (91% opening), respectively. In line with the expectation, $u(r,t)$ for a structure with a large valve is lower than for a disk with a smaller valve. The same development was seen for the pressure distribution and the plots are therefore given in appendix I.

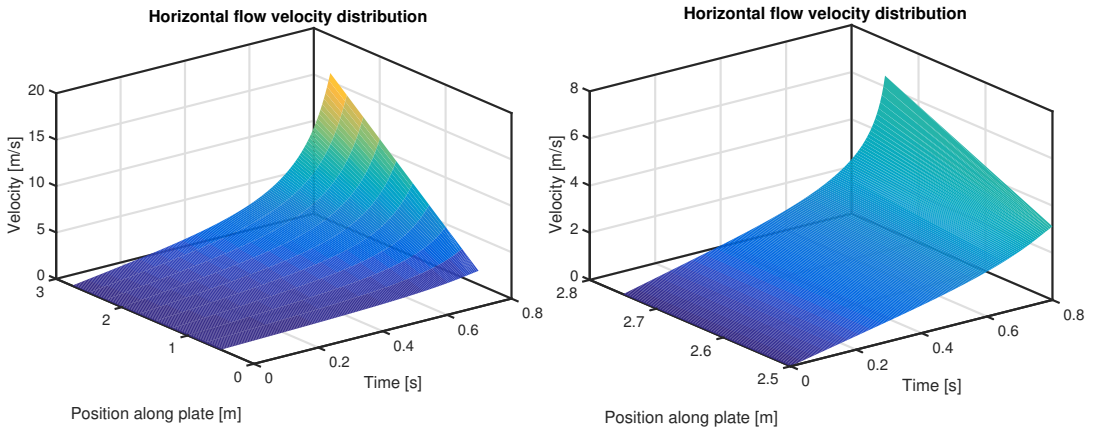

(a) Horizontal fluid flow velocity for Rv = 0.5m

(b) Horizontal fluid flow velocity for Rv = 2.5m

Figure 7.3: Free fall test

Constant lowering test

In the constant lowering test, similar behaviour in the magnitude of the hydrodynamic force for different valve sizes was seen. In this test, the structure is lowered with a constant velocity. Again, the hydrodynamic force suddenly rises, due to the occurrence of the rigid boundary, seen in figure 7.4a. Also for this test and illustrated in figure 7.4b, a lower resistance force was observed for larger valves. This corresponds to a smaller momentum and thus lower soil disturbance.

Since the structure is lowered with a constant velocity of 0.1 m/s, the results of the structure velocity in figure 7.4c are expected. During the lowering, the velocity is constant for all valve sizes and once the structure reaches the seabed, the velocity quickly decreases to zero. The results for the vertical fluid velocity through the valve show some unexpected results. The fluid velocity flowing through a valve with $R_v > 2$ m is expected to be nearly equal to the lowering velocity. This is not observed when comparing the results in figures 7.4c and 7.4d. As described in section 6.2.1, the system is first initialized before actual lowering occurs. Bringing the system into a steady oscillating state, does not apply for this constant lowering test as it would include an unwanted oscillating motion when introducing the constant velocity. Therefore the system has not been initialized, this is assumed to be related to the unexpected results.

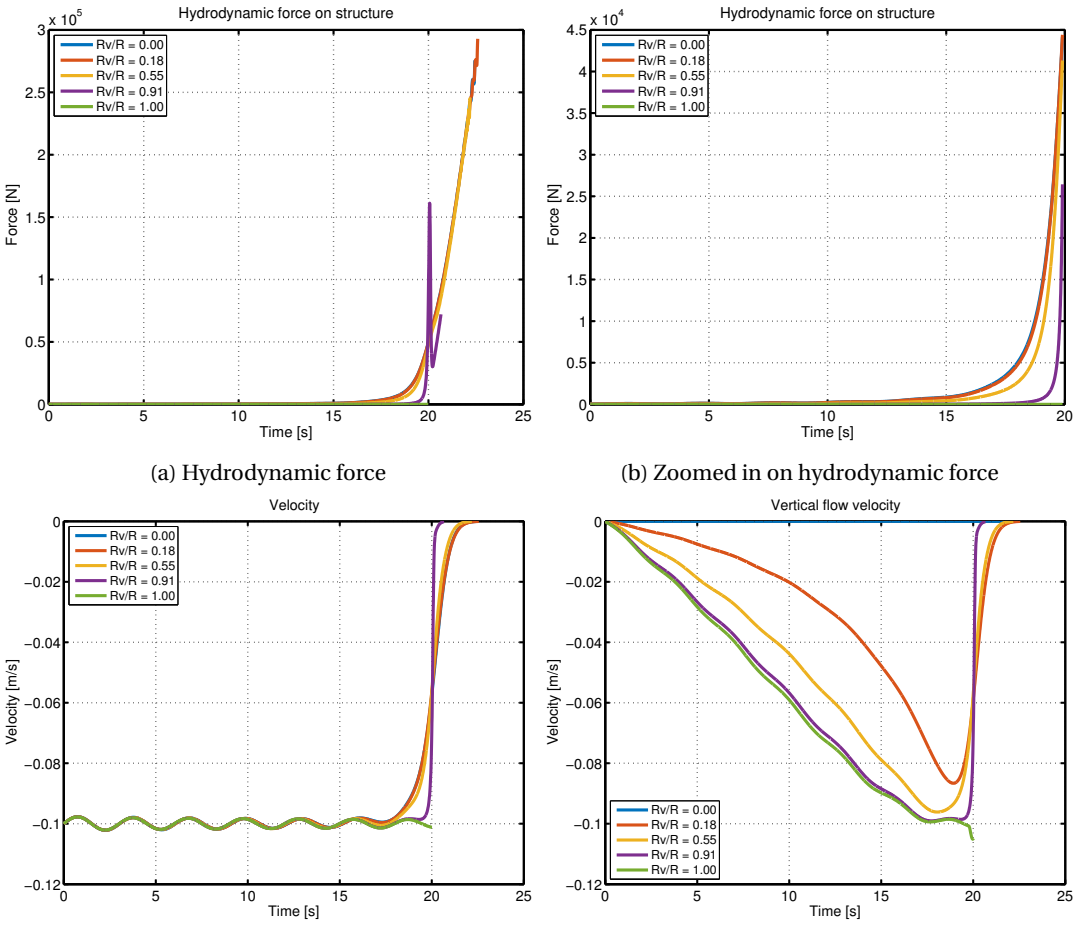

(a) Hydrodynamic force

(b) Zoomed in on hydrodynamic force

(c) Structure velocity

(d) Vertical fluid flow velocity

Figure 7.4: Constant lowering test

In this test, the results for the horizontal flow velocity and pressure for a large valve were also lower than for a smaller valve. The results for the horizontal fluid flow velocity for $R_v = 0.5$ m and $R_v = 2.5$ m can be found in appendix I. For simplicity, the pressure distribution corresponding to $R_v = 0.5$ m and $R_v = 2.5$ m been left out of this report.

SOIL UNDERGROUND

In this section, the results of the base case situation for various valve sizes have been analyzed. For simplicity the ratio for $R_v = 2.75$ m has been left out of this analysis. The graphs have been plotted from the moment the crane starts to lower at 80 s.

Similar to the results seen in 7.1a, increasing the valve radius has no significant effect on the motion behaviour of the structure. Just before the set-down, the velocity for a disk with 91% opening is slightly higher compared to smaller valves, see figure 7.5a. This, also seen in the results in section 7.2.1, is explained by the fact that a disk with a larger valve experiences a lower hydrodynamic resistance force.
In figure 7.5b, the results for the vertical flow velocity $v(t)$ are given for various valve sizes. In line with the expectations, large valves correspond to large vertical flow velocities. The change in magnitude of the vertical flow velocity for decreasing valve size is smaller than expected. Decreasing the opening of the disk from 91% to 55% results in a slide decrease in vertical flow velocity. The impact of decreasing the valve size on the vertical velocity was expected to be higher. This is assumed to be due to the assumptions made regarding the valve.

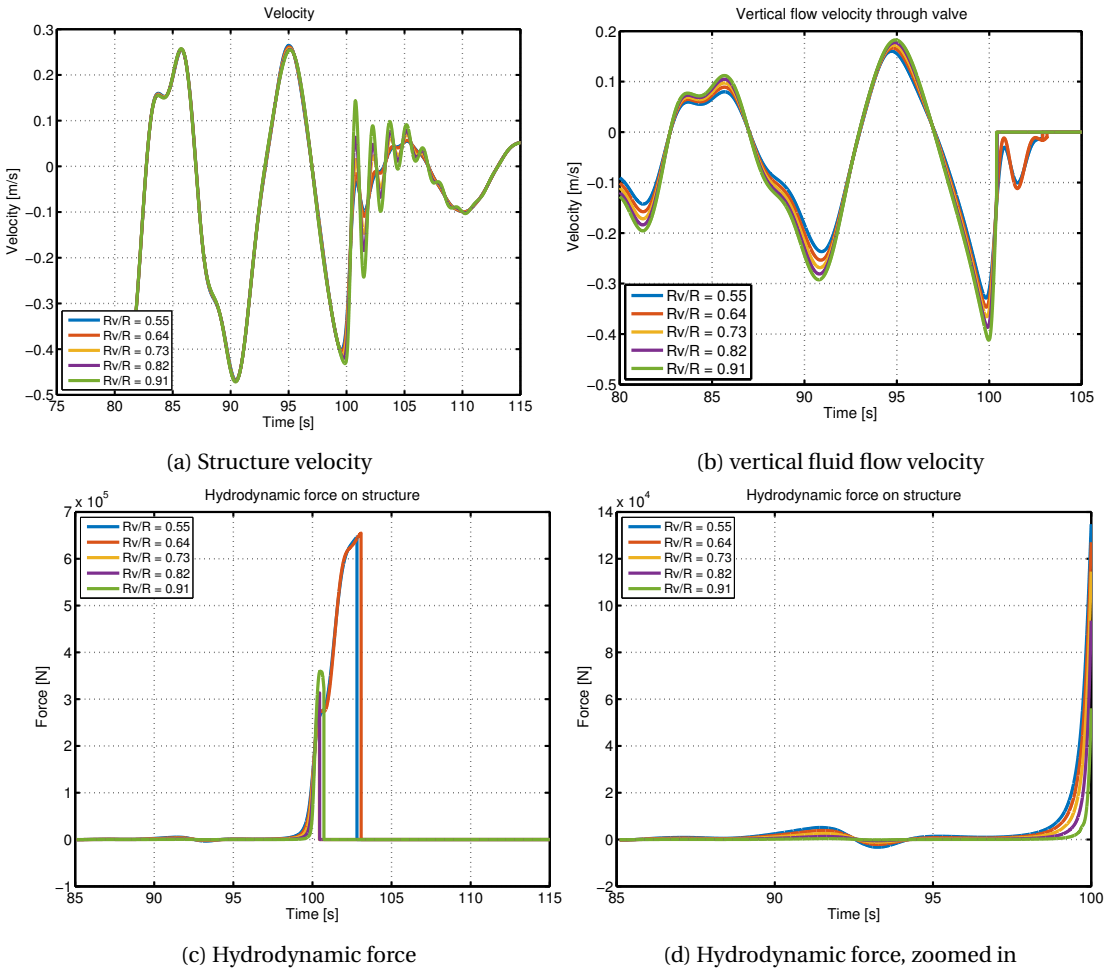

(a) Structure velocity

(b) vertical fluid flow velocity

(c) Hydrodynamic force

(d) Hydrodynamic force, zoomed in

Figure 7.5: Base case for various valve sizes

Figure 7.5c indicates a quick jump in the maximum magnitude of the hydrodynamic force for a disk with 73% to 82% opening, respectively. While indeed structures with larger valves correspond to lower magnitudes of the hydrodynamic force, this explicit jump is assumed to be a result of the cut-off point in the Matlab simulation. When zooming in on the hydrodynamic force, done in figure 7.5d, also here a large valve results in a lower resistance force. Based on the Design Profile for the soil, a soil displacement of 0.5 m for a R_v = 0.5 m and 0.3 m for a R_v = 2.5 m, respectively, correspond to the maximum magnitude of these forces. As the hydrodynamic force for structures with large valves is lower, so it its momentum. Based on the conservation of energy, less soil displacement was seen for a lower momentum.

7.2.2. STRUCTURAL MASS

The values for the structural mass analysis come from the Kaombo project. The difference between the values, which are expected to be realistic, is not very large, but still the analysis gives some insight into the impact of the structural mass. The maximum hydrodynamic forces for all phases were calculated, illustrated in figure 7.6. From this, the P90 value for the hydrodynamic force was calculated. P90 means 10% of the calculated values exceed the P90 estimate. Considering the base case situation with different masses for all phases, the following P90 values for the hydrodynamic force are found:

Mass M	P90 F_{hyd}
167 ton	542 kN
222 ton	545 kN
229 ton	547 kN

Table 7.2: P90 values for hydrodynamic force for various structural masses

The mass does not have a significant influence on the hydrodynamic force. A lower mass results in a slightly lower P90 value. If more extreme values for the masses would have been used, the fact that a lower structural mass will result in a slightly lower hydrodynamic force would have been emphasized even more.
In this case, it is more interesting to observe that phasing has a significant influence on the magnitude of the hydrodynamic force. This is visualized in figure 7.6. With this graph the phases dependency of the hydrodynamic force is clearly emphasized. This figure confirms that considering all phases in the preparation phase of an offshore installation procedure is advised.

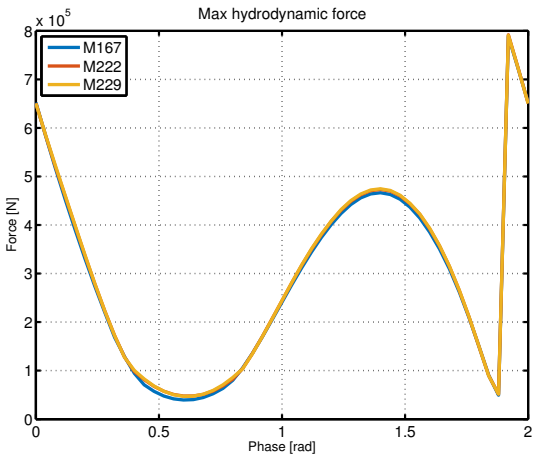

Figure 7.6: Mass influence for all phases

7.3. CRANE TIP HEAVE MOTION

Offshore weather causes motions which are characterized by period, amplitude and phase difference. These motion characteristics vary simultaneously. Consequently, the crane tip heave motion, affecting the motion behaviour of the structure, also varies for different motion characteristics. Both the crane tip and the subsea structure have a natural period. It is crucial that these do not get into resonance, because this could result in large heave motions and affect the structural integrity and stability of a subsea structure.
Timing of the set-down is difficult, therefore the impact of different periods and amplitudes has been analyzed for all phases. Considering all phases, the P90 value's of the hydrodynamic force have been obtained and reported for different combinations of period and amplitude.

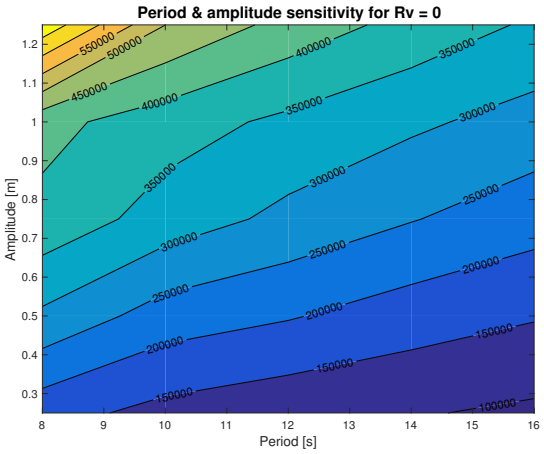

(a) Weather sensitivity on hydrodynamic force for closed disk

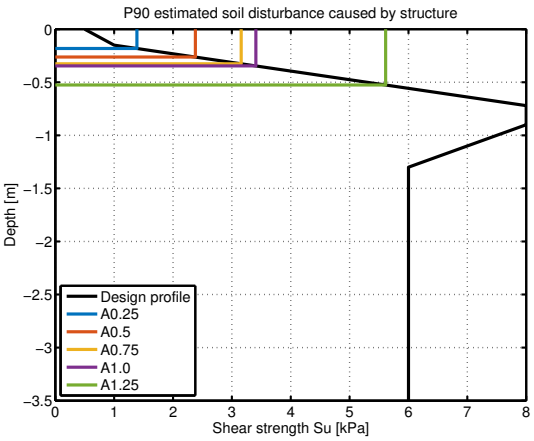

(b) Estimated soil disturbance for closed disk with $T = 8s$ and variable A

Figure 7.7: Weather sensitivity analysis for closed disk

Figure 7.7a shows a contour plot of the sensitivity results corresponding to a closed disk. As expected, the combination of higher periods and lower amplitudes leads to lower crane tip heave motions and thus to lower P90 values.
The P90 values can be converted into a corresponding soil disturbance using the Design Profile. In figure 7.7b, the estimated soil disturbance corresponding to T = 8 s and variable amplitudes is given. As predicted, the combination of T = 8 s & A = 1.25 m results in the highest soil displacement. These plots were also made for the other periods, which showed the same trend and for simplicity have been left out of here.

In the sensitivity analysis on the influence of the valve, it was seen that the maximum hydrodynamic force differs per valve size. Therefore, the same analysis has been performed for disks with valves with a radius of R_v = 0.5 m, R_v = 1.5 m and R_v = 2.5 m, respectively.

Figure 7.8a shows the contour plot of the P90 values for a disk with a valve of 0.5 m radius. The presence of the valve engenders a lower pressure under the disk. This is reflected in the magnitude of the hydrodynamic force. The P90 values are generally lower compared to the ones seen in figure 7.7a. Also the soil disturbance based on the Design Profile, seen in figure 7.8b, is generally lower compared to the closed disk.

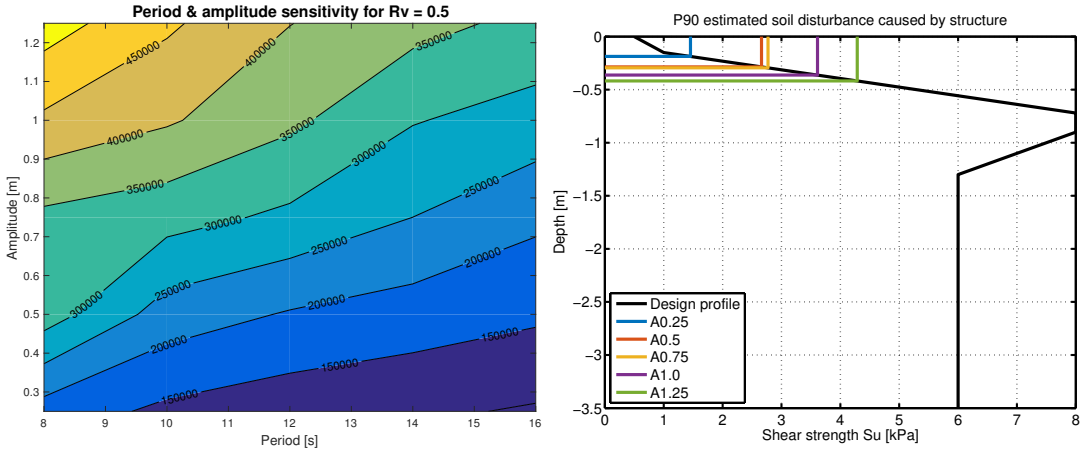

(a) Weather sensitivity on hydrodynamic force for disk with $R_v = 0.5m$

(b) Estimated soil disturbance for disk with $R_v = 0.5m$, $T = 8s$ and variable A

Figure 7.8: Weather sensitivity analysis for disk with $R_v = 0.5m$

Including a valve of R_v = 0.5 m decreases the hydrodynamic force, especially for the combination of short periods and high amplitudes. The results for R_v = 1.5 m and R_v = 2.5 m are given in appendix I. From those plots, it was interesting to see that the P90 values corresponding to the R_v = 1.5 m were not much lower compared to the values for the R_v = 0.5 m. For R_v = 2.5 m, a significant decrease in hydrodynamic force and soil disturbance was seen. It is thought that the soil will deform differently for a disk with such big valve (radius of disk is R_v = 2.75 m). In such a case, it can be understood that the soil will move in upward direction through the valve, which makes the Design Profile not valid anymore.

The conservative values for the estimated soil displacement based the maximum magnitude of the hydrodynamic force, derived with the Design Profile, are again compared with the values derived by the method of conservation of energy. For simplicity the results of the Bernoulli equation are left out of this comparison, as they are the most conservative. In figure 7.9, the results of the closed disk and the disk with 0.5 m radius for ζ = 1, T = 8 s and various amplitudes are compared with the ones based on the Design Profile.

The results of the second method are clearly lower compared to the more conservative method of the Design Profile. Especially for the higher amplitudes the conservatism of the Design Profile is clearly visible. Based on the second calculation method, the maximum soil disturbance generated in weather conditions with T = 8 s and A = 1.25 m for a disk with 18% opening is only ± 0.18 m. This is more than half of what was estimated with the Design Profile (0.42 m).

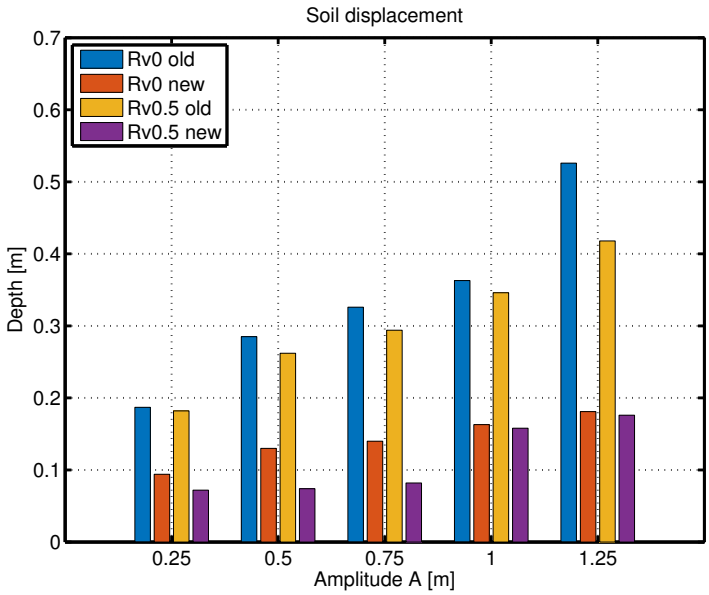

Figure 7.9: Comparison of soil displacement between the two methods

Overall, the model does what is expected when varying weather conditions. A high heave motion results in system with more energy, resulting in a bigger impact: more soil displacement. This analysis has been conducted for a disk and therefore it is assumed that the results for a real suction pile will be somewhat different.

7.4. SOIL PROPERTIES

As described in section 3.3, the behaviour for each soil type is different and each type deforms in a different way. Like the structural mass, a P90 value for the maximum hydrodynamic force for all phases can be calculated. Considering the base case situation for different soil stiffnesses, the following P90 values for the hydrodynamic force are found:

Soil stiffness k_{soil}	P90 F_{hyd}
1.76 MN/m	412 kN
3.52 MN/m	545 kN
7.04 MN/m	607 kN

Table 7.3: P90 values for various soil stiffnesses

Difference between the P90 values for different soil stiffnessess is noticed in table 7.3. The hydrodynamic force increases for stiffer soil.
At real offshore locations, exact soil behaviour is difficult to predict. The results from table 7.3 might be different with what is seen in reality, but it gives a good idea on how different soil types can affect the set-down of a structure. As is observed here, it is predicted that the hydrodynamic force on soft soils will be lower than for stiffer soils.

7.5. CONCLUSIONS

Based on the sensitivity analysis, the following is concluded:

VALVE SIZE

- The size of the valve influences the hydrodynamic force. A disk with a large valve will relieves more pressure and therefore the magnitude of the hydrodynamic force is lower compared to a closed disk and/or a disk with a smaller valve. A lower maximum hydrodynamic force corresponds with a lower estimated soil disturbance, seen in both the conservative Design Profile and the more realistic method based on the momentum of the force. The effect of the valve is greater for larger valves. The valve size is recognized as an influential parameter.

- It must be stated that no significant change in the structure's motion behaviour is observed when increasing the valve size. This is expected to be a result of the assumptions made concerning the valve.

STRUCTURAL MASS

- The structural mass has a small influence on the magnitude of the hydrodynamic force. A lower structural mass results in a slightly lower hydrodynamic force. The structural mass does not apply as one of the most influential parameters.

CRANE TIP HEAVE MOTION

- The crane tip heave motions are affected by and sensitive to weather conditions. This is directly reflected to the hydrodynamic force. The combination of a short period (T = 8 s) and high amplitude (A = 1.25 m), critical for a structure installation, results in the highest P90 value for the hydrodynamic force. According to both methods uses to calculate the soil disturbance, this corresponds to the deepest estimated soil disturbance. Increasing the valve size in the situation of the rough weather conditions engenders a lower P90 value, corresponding to a generally lower hydrodynamic force and lower momentum.

- Even for extreme motions, there are phase differences for which the structure can be set down smoothly, with minimal soil displacement. Timing the lowering operation to achieve this is subject to crane operator skills. To account for the difficulty in timing, the P90 of all phases is considered.

SOIL PROPERTIES

- The analysis showed that the magnitude of the hydrodynamic force increases for stiffer soils. Horizontal soil displacement, i.e. washing away of soil, is not included in the model.

Based on what was noticed from the sensitivity analysis, the size of the valve and the weather conditions can be considered to have the biggest impact on the set-down of structures onto the seabed.

8

CFD VERIFICATION

CFD tests have been conducted to verify the analytical expression for the hydrodynamic force of the 1D model, based on Brennen's flat plate analogy. The results of the closed 1D model were compared with the results from CFD tests.

For the verification an oscillating motion and lowering motion, for $T = 10$ s and $R = 2.75$ m, have been applied:

- $z(t) = 0.5sin(\omega t) + 1$
- $z(t) = 0.5sin(\omega t) - 0.1t + 2$

As described by Brennen [22], the hydrodynamic force is an extra added mass term. Half of the drag and inertia forces, representing the contribution of the hydrodynamics of the upper part of the disk, is included in the plots for 1D model [24]. The part beneath the disk is corresponding to the derived hydrodynamic force. The results of the CFD tests and the 1D model are given in figure 8.1.

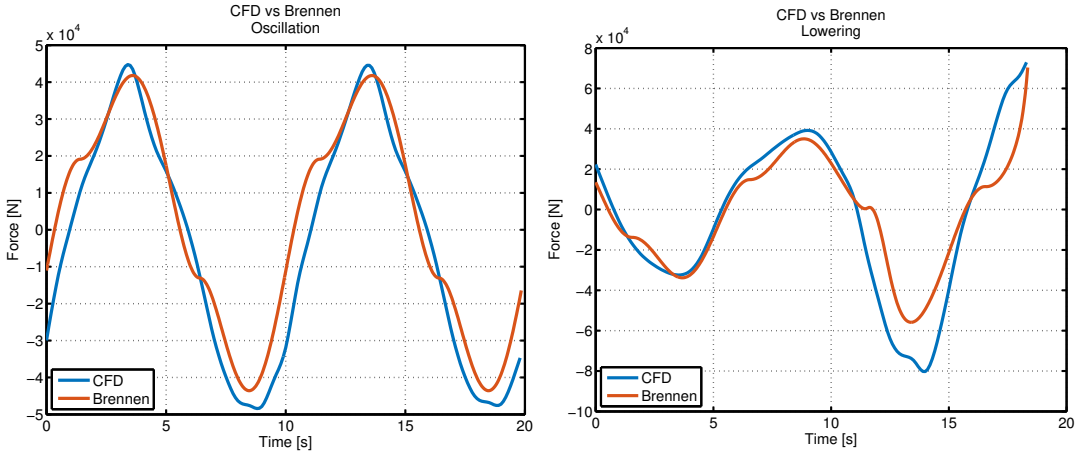

(a) Results oscillating motion

(b) Results lowering motion

Figure 8.1: Validation of hydrodynamic force

Figure 8.1a shows the results for an oscillating motion at a position of 1 m from the seabed. The development of both forces is in line, however the results from the 1D model are slightly lower. The difference could be explained by different assumptions made concerning both methods. The occurrence of vorticity and turbulence is not included in Brennen's derivation. It seems that the hydrodynamic force from the 1D model is slightly conservative compared to the one seen in the CFD tests.

In the results based on the oscillating motion, the impact of the hydrodynamic force close to the seabed is not evidently visible. The results for the lowering motion, starting at a position of 2 m above the seabed, are

shown in figure 8.1b. Again the development is comparable and the results based on Brennen are somewhat lower. For this imposed motion, a clear increase in the hydrodynamic force is observed as the structure gets closer to the seabed. Here the extra added mass term starts to become dominant. Apart from the assumptions just discussed, a slight difference in phasing could result in somewhat different magnitudes of the hydrodynamic force. That could be a reason why the results deviate somewhat. Overall the general development, corresponding to a lowering motion, is in line with what was expected from the literature.

Although there is a slight difference seen between CFD and Brennen, the general behaviour of both forces is in line. It can be stated that the analytical expression for the hydrodynamic force based on Brennen's flat plate analogy is verified by the conducted CFD tests.

9

CONCLUSIONS AND RECOMMENDATIONS

9.1. CONCLUSIONS

The objective of this research was to increase the understanding of how the set-down of structures on the seabed is influenced by the soil. The most important conclusions are discussed in this chapter.

9.1.1. BASE CASE SITUATION

The set-down of a structure onto the seabed has been modelled in a dynamic system. This model describes the system of a disk being lowered onto the seabed. The input for the hydrodynamic or added mass force for a closed disk was derived from literature. The fundamental equations are described by the mass and momentum conservation. They have been used to derive an expression for the hydrodynamic force for a disk including a valve with fluid flowing through it. This expression has been used as input for the 2D model.

1D MODEL

The following conclusions are made with respect to the closed model:

- Far away from the seabed ($R/z << 1$), the structure is not influenced by the hydrodynamic force. Close to the seabed, the hydrodynamic force is dominated by the solid boundary and therefore it increases significantly once it gets in proximity with the seabed.
- As expected, the hydrodynamic force for a closed disk generally has a larger magnitude compared to a disk with a valve (in this case no fluid flow is included).
- The closed disk has a clear stagnation point right in the middle underneath the disk. In line with the Bernoulli equation, the horizontal fluid flow velocity is zero and the pressure maximum at that point.

2D MODEL

Regarding the 2D model, including the vertical fluid flow in the hydrodynamic force, the following is concluded:

- The presence of an actual valve relieves pressure underneath the structure, producing a lower horizontal flow velocity and pressure compared to the 1D model. In line with the expectation, a valve engenders a lower hydrodynamic force. A lower hydrodynamic force or momentum corresponds to lower amount of soil disturbance.
- Compared to the 1D model, the same behaviour for the hydrodynamic force in close proximity with the seabed is observed in the 2D model. Just before the set-down, an increase in the vertical and horizontal fluid flow velocity, pressure and finally the hydrodynamic force occurs.
- Due to the assumptions made concerning the force derivation, the stagnation point has been fixed at the valve radius. At this point, the pressure is maximum and the horizontal flow velocity zero.
- Two approaches have been used to make an estimation for the soil disturbance: one is based on the maximum magnitude of the hydrodynamic force and one on the conservation of energy. This last method, assumed to be more realistic and less conservative, resulted in lower soil displacement estimations. This confirmed the conservatism of this method.

9.1.2. SENSITIVITY

To gain understanding on which parameters have impact on the set-down of structures onto the seabed, a sensitivity analysis has been conducted. The 2D model has been analyzed for various structural properties, crane tip heave motions and soil types. The following conclusions are drawn:

- A rough crane tip heave motion, caused by a short period and a high amplitude, results in a velocity amplitude corresponding to the highest hydrodynamic forces. Under these circumstances the hydrodynamic force or its momentum engenders the highest amount of soil disturbance. A probabilistic approach will remove conservatism with respect to an approach where worst phase is considered.
- The hydrodynamic force is sensitive to phasing. Even for weather conditions causing favourable crane tip heave motions, the force varies considerably for different phases.
- The size of the valve has an impact on the hydrodynamic force. Larger valves result in lower magnitudes of the hydrodynamic force, corresponding to a smaller amount of soil displacement. In the 2D model, no significant change in the structure's motion behaviour was observed when increasing the valve size. In the assumptions made regarding the valve, possibly mass flow has been lost resulting in a lower impact of the valve on the hydrodynamic force.
- The influence of the structural mass and the soil type is small compared to the impact of the crane heave motions and the valve size.

9.2. RECOMMENDATIONS

The model designed in this study provides a first step into an analytical method for describing the set-down operation of a subsea structure onto the seabed and how this operation is affected by the soil. An attempt has been made in providing a realistic expression for the hydrodynamic force, including the occurrence of 2D fluid flow. In order to use this equation for analysis purposes, additional research is necessary to obtain the required accuracy and reliability. All the recommendations are presented in this section.

9.2.1. HYDRODYNAMIC FORCE

Additional research on the derivation of the hydrodynamic force including vertical flow is advised. The following aspects should be further analyzed/improved:

1. The derived expression for the hydrodynamic force is as function of the motion behaviour and the vertical flow velocity. Similar to Brennen's flat plate analogy, an expression as function of only motion behaviour initially was expected. Further research in defining a set of fundamental equations, generating a hydrodynamic force independent of the valve velocity, is advised.

2. In the current model the stagnation point has been fixed. To make this stagnation point variable, an an extra boundary in the derivation of the force is necessary. With this improved expression, two stagnation points are expected to be seen: on both sides of the valve one.

3. In this thesis, the results of the fluid flow through the valve showed some unexpected behaviour. It is likely that once the above two improvements have been accomplished, the results for the flow through the valve will be more in line with the expectation made in the beginning of this thesis.

Before this model can actually be used in the preparation phase of an offshore installation project, further validation is necessary. This can be done by conducting (more) extensive CFD tests and model test to validate the derived expression for the hydrodynamic force.

IMPROVE HYDRODYNAMIC FORCE

An attempt has been made to improve the hydrodynamic force by taking an extra boundary equation into account. This section discusses the extra boundary equation and the several approaches tried to improve the hydrodynamic force.

In the derivation of the hydrodynamic force the stagnation point has been fixed at the valve radius, $r = R_v$. To make this point variable, an extra boundary condition has been derived. The extra boundary condition is based on a global equilibrium, which must hold at the edges of the disk. Figure 9.1 illustrates the system with the vertical velocity $v(t)$, independent of the position, and the horizontal flow velocity $u(R,t)$ at $r = R$.

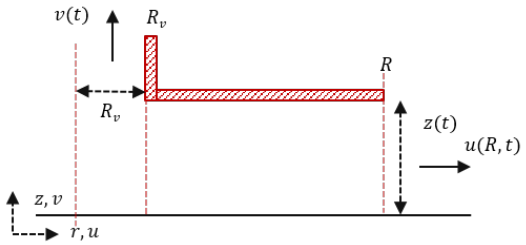

Figure 9.1: Global equilibrium

The global equilibrium, which is independent of the position, is given in equation 9.1. The equilibrium can be rewritten into an expression for $v(t)$, see equation 9.2. The full derivation is given in appendix J.

$$2\pi Rz\rho u(R,t)^2 = \rho\pi R_v^2 v(t)^2 \tag{9.1}$$

$$v(t) = \sqrt{2Rz}\left(\frac{u(R,t)}{R_v}\right) \tag{9.2}$$

As expected, this global expression for $v(t)$ is a function of $u(R,t)$ and R_v. This expression needs to be connected to the local equations derived in chapter 4. Several approaches have been made, they are explained in appendix J. None of these approaches resulted in a better description of the hydrodynamic force. As became clear from approach 2 & 3, described in the appendix, the valve radius was omitted from the momentum equation. This is impossible, since R_v represents the presence of the valve in the hydrodynamic force.

A possible next step in improving the force is to reanalyze the derived fundamental expressions, especially the horizontal fluid flow velocity. Possibly $u(r,t)$ should contain R_v^2, which would mean that, as expected, the R_v remains present in $u(r,t)$ and therefore in the expression for the pressure and hydrodynamic force.

9.2.2. SET-DOWN OF AN ACTUAL SUCTION PILE

The set-down of a disk has been analyzed in this study. By including actual skirts and adding length to the disk, a more realistic analysis of the set-down of a suction pile on the seabed can be obtained. From this analysis, the following is expected to be observed:

1. As the skirts start penetrating the soil, they will generate an extra resistance force acting on the suction pile. It is likely that the pile will come to rest before actually reaching the top.
2. The inside of the suction pile will fill up with water. Since water is assumed to be incompressible, the tip of the pile is expected to have the same characteristics as a closed disk.
3. For a tall pile, it is thought that the tip is not influenced by the valve, meaning the tip could be compared with a closed disk with uniform pressure underneath. A stagnation in the middle of the pile is expected to be present.
4. The top of the pile will be influenced by the valve, as water can only escape through the valve in vertical direction. For larger valves, water can flow easier through it, relieving the pressure underneath the top of the pile quicker. Right underneath the top of the pile, at some position left and right of the valve a stagnation point is expected.

After implementing an actual suction pile into the dynamic model, the set-down velocity can be analyzed more extensively. It is recommended to study/compare the structure velocities derived with the simplified method based on Bernoulli, the DNV iteration analysis and from the established dynamic model to detect whether any conservatism is included.

In this model a perfectly vertical set-down was assumed, neglecting the horizontal forces acting on the structure. In reality, the set-down of a suction pile can happen under a small angle. In this case, the horizontal forces acting on the suction pile need to be accounted for. It is expected that the hydrodynamic force will also act in horizontal direction on the structure and thus should be considered in the derivation of the hydrodynamic force.

9.2.3. OPTIMIZATION

To ensure a safe subsea installation operation and to minimize the costs, decisions concerning the influential parameters need to be well considered. To optimize the set-down of a suction pile, the following parameters need to be further analyzed, individually and together:

1. The amount and size of valves. This thesis indicates that the larger the valve, the lower the hydrodynamics force and thus the lowest soil displacement is expected. Suction piles can have several valves instead of one big one in the middle. Generally valves are quite expensive. A well considered decision between the allowable soil deformation and the costs spent on the amount and size of valves is recommended.

2. The constant crane lowering velocity. During this study a value of 0.1 m/s for the constant crane lowering velocity has been used. To optimize the set-down of structures, the impact of variable constant crane lowering velocities is advised. Especially in combination with irregular waves, it is not straightforward whether fast or slow lowering is favourable.

3. The crane tip heave motion. Maximizing these heave motions together with the constant crane lowering velocity will ensure to acquire an optimum set-down velocity for the suction pile. With this velocity the pile should maintain enough holding capacity in the soil guaranteeing a safe installation.

BIBLIOGRAPHY

[1] BP, *BP energy outlook 2016,* (2016).

[2] A. Arapogianni and A. Genachte, *Deep Water The next step for offshore wind energy,* (2013).

[3] J. P. De Vries, J. Drunen, R. Dijk, and R. Zoontjes, *OTC 21291 Offshore Monitoring Campaign on Installation of Suction Piles in Deep Water Fields,* (2011).

[4] Recommended practice DNV-RP-H103, *Modelling and analysis of marine operations,* (2011).

[5] T. Inge Tjelta Statoil Stavanger, *Suction Piles: Their Position and Application Today,* Set **1**, 51 (2001).

[6] S. Bang, K. D. Jones, Y. Cho, and D. J. Kwag, *Suction Piles and Suction Anchors for Offshore Structures,* DFI JOURNAL **33** (2009).

[7] K. Andersen, *Suction anchors for deepwater applications,* .

[8] Recommended practice DNV-RP-H201, *Lifting appliances used in subsea operations,* (2014).

[9] J. M. J. Journée and J. Pinkster, *Introduction in ship hydromechanics,* (2002).

[10] Heerema Marine Contractors, *HMC rewrite into Technip,* (2014).

[11] Heerema Marine Contractors, *Soil data specification Kaombo project*, Tech. Rep.

[12] R. D. Blevins, *Applied Fluid Dynamics Handbook* (Krieger publishing Company, 1984).

[13] F. White, *Fluid mechanics*, 7th ed. (2011) pp. 150 – 158.

[14] S. K. Chakrabarti, *Handbook of offshore engineering,* (2005).

[15] J. R. Morison, *The forces exerted by surface waves on piles* (1950).

[16] G. His, H. Keulegan, and L. H. Carpenter, *Forces on Cylinders and Plates in an Oscillating Fluid 1,* Journal of Research of the Na tional Bureau of Standards **60** (1958).

[17] A. Verruijt, *Soil Mechanics,* (2001).

[18] NORSOK STANDARD, *Marine soil investigations,* (2004).

[19] Recommended Practice DNV-RP-E303, *Geotechnical and Foundation Design Considerations ISO 19901-4:2003 (Modified), Petroleum and natural gas industries—Specific requirements for offshore structures, Part 4—Geotechnical and foundation design considerations,* (2005).

[20] A. V. Metrikine, *Dynamics, Slender Structures and an Introduction to Continuum Mechanics CT 4145 Module Dynamics of Mechanical Systems and Slender Structures,* (2014).

[21] A. V. Metrikine, *Lecture Slides Structural Dynamics, Lecture 3,* (2014).

[22] C. Brennen, *A review of added mass and fluid inertial force,* (1982).

[23] J. M. J. Journée and W. W. Massie, *Offshore hydromechanics,* (2001).

[24] C. A. Garrido-Mendoza, K. D. Thiagarajan Alston, and A. Lee Correll, *Hydrodynamic forces on heave plates for offshore systems oscillating close to the seabed or the free surface,* (2015).

A

DNV ITERATION ANALYSIS

This appendix describes the iterative analysis procedure established by Det Norske Vertias [4]. With this method the velocity of a suction pile can be calculated. The procedure, consisting of 11 steps, takes the non-linear behaviour of soil resistance into account.

1. Assume an incremental soil displacement $\Delta\delta_{soil}$ $[m]$.

2. Calculate clearance $h_i[m]$ between skirt tip and seabed. The clearance h_i becomes negative when the skirts start penetrating into the soil.

$$h_i = h_{i-1} - \Delta z_i + \Delta\delta_{soil} \quad \text{where } \Delta z_i = v_{c_i}\Delta t\ [m]$$

3. Calculate the area for water to escape $A_{flow_i}[m^2]$, consisting of the valve area A_v and the area under the pile till the seabed:

$$A_{flow_i} = A_v + \pi D h_i$$

4. Calculate the water pressure $P_{w_i}[N/m^2]$, the flow velocity $v_{flow_i}[m/s]$ and the water pressure force $Q_{w_i}[N]$ on the suction pile and the soil:

$$P_{w_i} = 0.5 k_{flow}\rho\left(v_{flow_i}\right)^2$$

$$\text{with } v_{flow_i} = \left(\frac{A_{sp}}{A_{flow_i}}\right)\left(v_{c_i} - \frac{\Delta\delta_{soil_i}}{\Delta t}\right)$$

$$Q_{w_i} = P_{w_i} A_{sp}$$

5. Calculate the total force on the soil $Q_{soil_i}[N]$, consisting of the water pressure force Q_{w_i} and the skirt force Q_{skirt_i}:

$$Q_{soil_i} = Q_{w_i} + Q_{skirt_i}$$

6. Calculate the soil displacement $\delta_{soil_i}[m]$ and the change in soil displacement $\Delta\delta_{soil_i}[m]$. There are three situation possible:

   (a) For $Q_{soil_i} < Q_{sd}$, which means 'elastic' soil deformation

$$\delta_{soil_i} = \delta_{mob}\left(\frac{Q_{soil_i}}{Q_{sd}}\right)$$

$$\Delta\delta_{soil_i} = \delta_{soil_i} - \delta_{soil_{i-1}}$$

   (b) For $Q_{soil_i} \geq Q_{sd}$ or $\frac{Q_{soil_i} - Q_{sd}}{Q_{sd}} \geq -0.0001$, which means 'permanent' soil deformation

   For $h_i > 0$, skirts are not yet penetrated:

$$A_{flow_i} = \left(v_{c_i} - \frac{\Delta\delta_{soil}}{\Delta t}\right) A_{sp} \sqrt{\frac{k_{flow} A_{sp} \rho}{2Q_{sd}}}$$

$$h_i = \frac{A_{flow_i} - A_h}{\pi D}$$

$$\Delta\delta_{soil_i} = -h_{i-1} + \Delta z_i + h_i$$

$$\delta_{soil_i} = \delta_{soil_{i-1}} + \Delta\delta_{soil_i}$$

For $h_i \leq 0$, skirts are penetrating:

$$\Delta\delta_{soil_i} = \left(v_{c_i} - \left(\frac{A_{flow_i}}{A_{sp}}\right) \sqrt{\frac{2\left(Q_{sd} - Q_{skirt_i}\right)}{k_{flow} A_{sp} \rho}}\right) \Delta t$$

7. Step 1 to 6 are repeated until convergence is reached.

8. Calculate the change in crane wire length $\delta_{line_i}[m]$, where v_c represents the constant crane lowering velocity:

$$\delta_{line_i} = \sum \Delta z_i - \left(V_c t + d_0 \frac{1}{M_f} \left(sin(\omega t + \phi) - sin\phi\right)\right)$$

9. Calculate the new line force $Q_{line_i}[N]$, where k_{line} is the crane wire stiffness:

$$Q_{line_i} = Q_{line,0} + k_{line} \delta_{line_i} \geq 0$$

10. Calculate loss in kinetic energy $\Delta E_{k_i}[Nm]$ and the remaining kinetic energy E_{k_i}:

$$\Delta E_{k_i} = \left(Q_{w_i} \left(\frac{A_{sp} - A_v}{A_{sp}}\right) + Q_{skirt_i} + Q_{line_i} - Q_{subm}\right) \Delta t$$

$$E_{k_i} = E_{k_{i-1}} - \Delta E_{k_i}$$

11. Calculate the new velocity $v_{c_{i+1}}[m/s]$:

$$v_{c_{i+1}} = \sqrt{\frac{2E_{k_i}}{m_d}}$$

B

SOIL DISTURBANCE

This appendix explains the method based on the conservation of energy for describing the soil disturbance resulting from the hydrodynamic force. The method includes the inertia of the soil. The soil is modelled as a 1 DOF mass spring system with viscous damping, on which a general disturbing force is acting: the hydrodynamic force. The situation is illustrated in figure B.1.

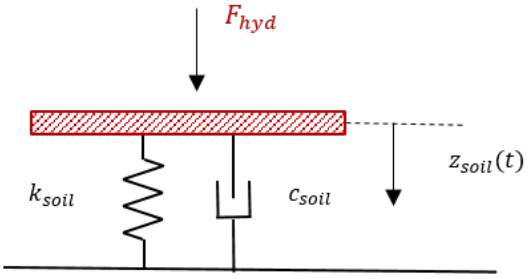

Figure B.1: 1 DOF system with viscous damping under general disturbing force

The 1 DOF system with viscous damping under a general disturbing force [20] can be explained by the equation of motion given in equation B.1 and can be rewritten into equation B.2. The terms m, c and k are related to the soil in this case.

$$m\ddot{z}_{soil} + c\dot{z}_{soil} + kz_{soil} = F_{hyd}(t) \tag{B.1}$$

$$\ddot{z}_{soil} + 2\zeta\omega_0\dot{z}_{soil} + \omega_0^2 z_{soil} = \frac{1}{m}F_{hyd}(t) \tag{B.2}$$

With

ω_0 : Natural frequency of soil, $\omega_0 = \sqrt{\frac{k_{soil}}{m}}$ [rad/s]
ζ : Damping ratio, $\zeta = 0.7 - 1.3$ [-]

The mass of the soil is calculated using the formula in equation B.3. Assuming that the soil under the disk with a depth of R can be affected by the momentum, the soil volume is calculated as $V = \pi R^2 R$. The density of the soil is taken as 2600 kg/m^3. The soil stiffness k_{soil} is equal to the one taken for the linear spring in the structural model.

$$m = \rho_{soil} V \tag{B.3}$$

To describe the maximum soil displacement, equation B.2 is integrated between the starting time t_0 and the collision time t_{col}. The collision time t_{col} is the moment at which the hydrodynamic force is maximum. This is just before the structure lands on the seabed. With respect to the starting time t_0, the following requirement should hold:

$$(t_{col} - t_0) < T_0 \tag{B.4}$$

The natural period T_0 is calculated by $\frac{2\pi}{\omega_0}$. By taking requirement B.4 into account, the integration is described by the following equation:

$$\int_{t_0}^{t_{col}} \ddot{z}_{soil} + 2\zeta\omega_0\dot{z}_{soil} + \omega_0^2 z_{soil} = \frac{1}{m}F_{hyd}(t)\,dt \tag{B.5}$$

The left-hand side of the equation describes the behaviour of the soil, including the inertia of the soil. The right-hand side of the equation describes the momentum or impulse coming from the hydrodynamic force. The impulse can be derived by means of the trapezoidal rule in the following manner:

$$\int_{t_0}^{t_{col}} \frac{1}{m}F_{hyd}(t)\,dt = \frac{(t_{col}-t_0)}{m}\left(\frac{F_{hyd}(t_0)+F_{hyd}(t_{col})}{2}\right) \tag{B.6}$$

This expression describes the total impulse of the hydrodynamic force that is exerted onto the soil during the landing procedure. The integration of the first two terms on the left-hand side can be derived as follows:

$$\int_{t_0}^{t_{col}} \ddot{z}_{soil}\,dt = \dot{z}_{soil}(t_{col}) - \dot{z}_{soil}(t_0) = -\dot{z}_{soil}(t_0) \tag{B.7}$$

$$\int_{t_0}^{t_{col}} 2\zeta\omega_0\dot{z}_{soil}\,dt = 2\zeta\omega_0\left(z_{soil}(t_{col}) - z_{soil}(t_0)\right) \tag{B.8}$$

It is assumed that the velocity of the soil is zero at the time of collision. Therefore $\dot{z}_{soil}(t_{col})$ is set equal to zero and equation B.7 results in $-\dot{z}_{soil}(t_0)$. The integration of the third term on the left-hand side is slightly more complex. The soil displacement at a variable time $z_{soil}(t)$, valid for $t_0 \le t \le t_{col}$, can be explained by function B.10. This expression is integrated in equation B.11.

$$\int_{t_0}^{t_{col}} \omega_0^2 z_{soil}\,dt \tag{B.9}$$

$$z_{soil}(t) = z_{soil}(t_0) + (t-t_0)\,\alpha \tag{B.10}$$

$$\int_{t_0}^{t_{col}} \left(z_{soil}(t_0) + (t-t_0)\,\alpha\right)dt = \left(z_{soil}(t_0) - \alpha t_0\right)(t_{col}-t_0) + \frac{\alpha}{2}\left(t_{col}^2 - t_0^2\right) \tag{B.11}$$

The α term, eventually inserted into equation B.11, can be found in the following way:

$$z_{soil}(t_{col}) = z_{soil}(t_0) + (t_{col}-t_0)\,\alpha \tag{B.12}$$

$$\alpha = \frac{z_{soil}(t_{col}) - z_{soil}(t_0)}{t_{col}-t_0} \tag{B.13}$$

Next, equations B.6, B.7, B.8, B.11 and B.13 can be substituted into the energy balance of equation B.5 and the equation can be solved for the soil displacement at time of collision t_{col}. This has been done in Maple and resulted into the following expression for $z_{soil}(t_{col})$:

$$z_{soil}(t_{col}) = \frac{-\left(m\omega_0^2 z_{soil}(t_0)\,(t_{col}-t_0) - 4m\omega_0 z_{soil}(t_0) + \left(F_{hyd}(t_0)+F_{hyd}(t_{col})\right)(t_0-t_{col}) - 2m\dot{z_{soil}}(t_0)\right)}{m\omega_0\left(-\omega_0 t_0 + \omega_0 t_{col} + 4\zeta\right)} \tag{B.14}$$

Based on conservation of energy, the expression in equation B.14 represents the maximum soil displacement which results from the momentum of the hydrodynamic force. The result from equation B.14 can be compared with the Design Profile. Compared to the Design Profile, this is expected to be a less conservative method to estimate the maximum soil disturbance.

C

DERIVATION BRENNEN

In this two dimensional model, Brennen considers a flat plate of width $2a$ and length l lying on the ocean floor. This plate is lifted away from the floor by a vertically upward force F and rises to a uniform height $h(t)$ above the floor at time t. Figure C.1 illustrates the situation.

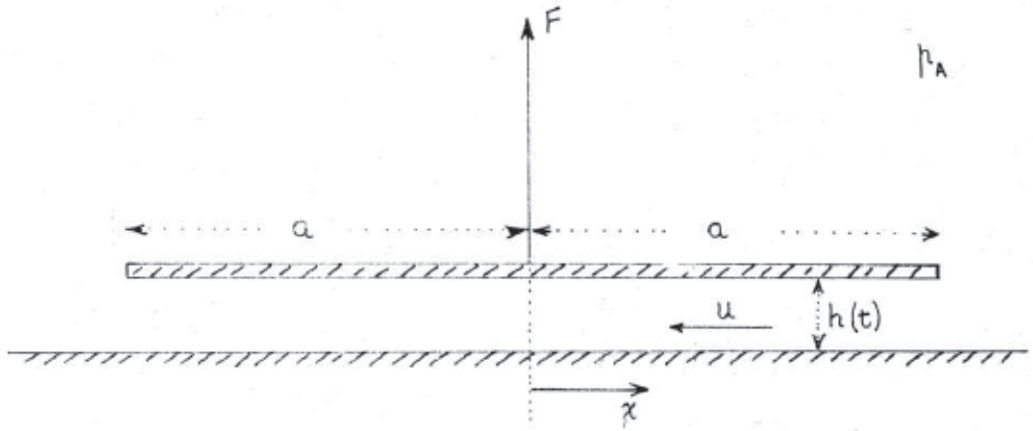

Figure C.1: Brennen's flat plate near ocean floor

Once the plate is lifted, the proximity increases and therefore the inflow of water increases. This approach is only applicable when the structure is in close proximity with the seabed, $a/h >> 1$. In this section, an explanation of the derivation of the obtained equations is given. As Brennen explains in his paper, the force can be derived by making use of the laws of conservation [22].

CONSERVATION OF MASS

According to White, the law of mass conservation for a fixed control volume is described in terms of volume V, surface area A and pressure p, as was seen in figure 4.3. The volume of the fluid is defined as V and varies over time t and position x. The surface area is derived between boundaries x and $x+\Delta x$ and for p the pressure at those boundaries is taken. Similar to the volume, the pressure varies over time and position. In both cases, V and p are treated uniform over the vertical cross section A. The mass conservation law by White is given as:

$$\frac{\partial}{\partial t}\iiint_V \rho dV + \iint_A \rho(\vec{u} * \vec{n}) dA = 0 \tag{C.1}$$

Physically this equilibrium answers the questions 'how much mass will flow through the channel with cross-sectional area A in time Δt?'. In this equilibrium equation, the first term describes the change in mass over time and the second term the in and out flow of mass in the control volume of length Δx. Thus the equilibrium can be rewritten into equation C.2. If a plate with width, $2a$, and length, l, is considered, the change in mass over time is given as in equation C.3.

$$\frac{\partial}{\partial t}\iiint_V \rho dV + (\rho Au)_{out} - (\rho Au)_{in} = 0 \tag{C.2}$$

$$\frac{\partial}{\partial t}\iiint_V \rho dV = \frac{\partial}{\partial t}\int_0^{h(t)} \rho l \Delta x dz = \rho l \Delta x \frac{dh}{dt} \tag{C.3}$$

Next, the in and out flow of mass over the control volume is determined. The mass entering the system at point x is described as $(\rho Au)_x$. Similarly, the mass leaving the system at point $x+\Delta x$ is given by $(\rho Au)_{x+\Delta x}$. The quantity ρAu is the mass flow passing through the system in kg/s. To solve this equation, use is made of the Taylor expansion [1].

$$(\rho Au)_{out} - (\rho Au)_{in} = \rho hl\,(u(x+\Delta x) - u(x)) \approx \rho hl\left(\left(u(x) + \frac{\partial u}{\partial x}\Delta x\right) - u(x)\right) \tag{C.4}$$

$$(\rho Au)_{out} - (\rho Au)_{in} = \rho hl \frac{\partial u}{\partial x}\Delta x \tag{C.5}$$

The above obtained equations can be substituted into the law for conservation of mass of equation C.1, which results into the following:

$$\rho l \Delta x \frac{dh}{dt} = -\rho hl \frac{\partial u}{\partial x}\Delta x \tag{C.6}$$

By rearranging and clearing the equilibrium of mass conservation, an expression for the velocity gradient is found in equation C.7. The horizontal fluid flow velocity underneath the plate can be found by integrating the velocity gradient with respect to x, given in equations C.8 and C.9.

$$\frac{\partial u}{\partial x} = -\frac{1}{h}\frac{dh}{dt} \tag{C.7}$$

$$\int_0^x \frac{\partial u}{\partial x} dx = \int_0^x -\frac{1}{h}\frac{dh}{dt} dx \tag{C.8}$$

$$\int_0^x -\frac{1}{h}\frac{dh}{dt} dx \rightarrow u(x,t) - u(0,t) = -\frac{x}{h}\frac{dh}{dt} \tag{C.9}$$

One of boundary conditions Brennen addresses in his paper is the fact that the flow velocity in the middle of the plate has to be zero, $u(0,t) = 0$. Thus the remaining equation describing the horizontal fluid flow velocity underneath the plate becomes:

$$\boxed{u(x,t) = -\frac{x}{h}\frac{dh}{dt}} \tag{C.10}$$

Equation C.10 describes the horizontal flow velocity underneath the plate appearing in the gap between the plate and the seabed. Since the flow is considered to be 1D, the vertical flow velocity can assumed to be zero, $u_z(x,t) = 0$.

[1] Taylor series: $u(x+\Delta x) \approx u(x) + \frac{\partial u}{\partial x}\Delta x$

To give an idea of the behaviour of the fluid flow velocity, equation C.10 has been plotted for an imposed oscillating motion of $z(t) = 0.5sin(\omega t) + 2$, see figure C.2. The results for the sinusoidal development motion can be found in figure 4.4. As can be seen in the figure, the velocity in the middle of the plate is zero, which confirms the boundary condition. Furthermore, the figure indicates that the flow velocity is maximum at the edges of the plate.

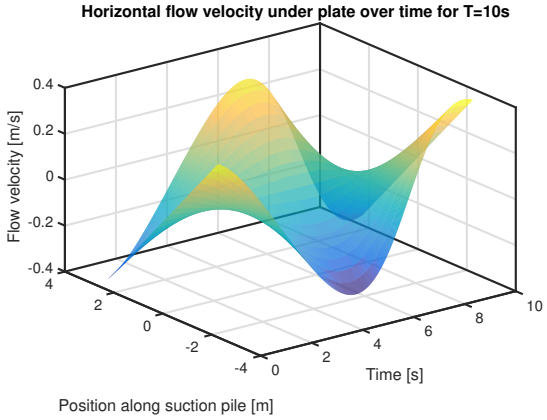

Figure C.2: Horizontal fluid flow velocity under plate

Conservation of momentum

As explained by White, the conservation of linear momentum, likewise to the conservation of mass, must also be applied to the system. It is described as:

$$\sum \vec{F} = \frac{d}{dt}(m\vec{u}) \tag{C.11}$$

The term $\sum F$ is the vector sum of all external forces acting on the structure. The law for momentum conservation is also known as Newton's second law. Similar to the mass conservation law, the conservation of momentum can be divided into an expression for the change of momentum over time and the momentum flux.

$$\sum F = \frac{\partial}{\partial t}\iiint_V \rho \vec{u} dV + \iint_A \rho(\vec{u}\cdot\vec{n})\vec{u} dA \tag{C.12}$$

The first term on the right-hand side of the equation describes the change of momentum over time. By examining a plate with width $2a$ and length l again, the following equation is obtained:

$$\frac{\partial}{\partial t}\iiint_V \rho \vec{u} dV = \frac{\partial}{\partial t}\int_0^{h(t)} \rho l \Delta x u dz = \rho l \Delta x \frac{\partial}{\partial t}(hu) \tag{C.13}$$

The second term on the right-hand side of the equation represents the momentum flux. In this equation the value for $\vec{u}$ is positive in the x-direction and the normal vector $\vec{n}$ is positive in outward direction. As stated by White, the inlet momentum will be negative and the outlet momentum positive. This is due to the dot product, seen in equation C.12. This term equals the vector sum of outlet momentum fluxes minus the vector sum of inlet fluxes.

$$\iint_A \rho(\vec{u}\cdot\vec{n})\vec{u} dA = (\rho A u)\vec{u}_{out} - (\rho A u)\vec{u}_{in} \tag{C.14}$$

To derive this equation, again use is made of the Taylor series[2] principle. The derived expression eventually describes the momentum flux.

$$= \rho h l(u(x+\Delta x)^2 - (u(x))^2) = \rho h l\left(\left(u(x) + \frac{\partial u}{\partial x}\Delta x\right)^2 - (u(x))^2\right) \tag{C.15}$$

[2]Taylor series: $(u(x+\Delta x))^2 \approx u^2 + 2u\frac{\partial u}{\partial x}\Delta x + \left(\frac{\partial u}{\partial x}\Delta x\right)^2$

$$\approx \rho h l \left(2u\frac{\partial u}{\partial x}\Delta x\right) \tag{C.16}$$

The equations for the change of momentum over time and the momentum flux describe the internal forces acting on the body. As explained above, $\sum F$ is the vector sum of all external forces. Since we are only considering horizontal flow, the gravitational forces can be neglected. Thus the only external force acting on the structure is due to the pressure of the surrounding fluid.

$$\sum F = \vec{F_{press}} = \iint_A p(-\vec{n})dA \tag{C.17}$$

As pointed out by White, the external pressure force acts normal to the surface and is directed inward. Again the unit vector $\vec{n}$ is defined positive in outward direction and thus always in opposite direction of the pressure. The force expression for the pressure over the surface area is given in equation C.18. The term $p(x+\Delta x)$ solved with the Taylor series[3].

$$\iint_A p(-\vec{n})dA = hl(p(x) - p(x+\Delta x) \approx -hl\frac{\partial p}{\partial x}\Delta x \tag{C.18}$$

Finally, the three expressions describing the conservation of momentum have been derived. Next, equations C.13, C.16 and C.18 can be substituted into equation C.12. Consequently, the momentum conservation law can be described by:

$$-hl\frac{\partial p}{\partial x}\Delta x = \rho l \Delta x \frac{\partial}{\partial t}(hu) + \rho h l \left(2u\frac{\partial u}{\partial x}\Delta x\right) \tag{C.19}$$

By dividing the whole equation by $\rho l h \Delta x$ and rearranging it, the following expression describing the conservation of linear momentum can be found.

$$\boxed{\frac{1}{\rho}\frac{\partial p}{\partial x} + 2u\frac{\partial u}{\partial x} + \frac{1}{h}\frac{\partial}{\partial t}(hu) = 0} \tag{C.20}$$

PRESSURE CALCULATION

The horizontal flow velocity from equation C.10 and its derivative with respect to x can be inserted into the momentum relation obtained in equation C.20.

$$\frac{1}{\rho}\frac{\partial p}{\partial x} + 2\left(-\frac{x}{h}\frac{dh}{dt}\right)\left(-\frac{1}{h}\frac{dh}{dt}\right) + \frac{1}{h}\frac{\partial}{\partial t}\left(-x\frac{dh}{dt}\right) = 0 \tag{C.21}$$

By multiplying the terms within the brackets with each other, eventually a simplified expression for the conservation of momentum can be found.

$$\frac{1}{\rho}\frac{\partial p}{\partial x} + \frac{2x}{h^2}\left(\frac{dh}{dt}\right)^2 - \frac{x}{h}\frac{d^2h}{dt^2} = 0 \tag{C.22}$$

Equation C.22 can be rewritten into an expression for the pressure gradient $\frac{\partial p}{\partial x}$, given in equation C.23. This pressure gradient can be used to find the expression for the pressure as function of time t and position x. To find an expression for the pressure, equation C.23 is integrated over its position, seen in equation C.24.

$$\frac{\partial p}{\partial x} = -\rho\left(\frac{2x}{h^2}\left(\frac{dh}{dt}\right)^2 - \frac{x}{h}\frac{d^2h}{dt^2}\right) \tag{C.23}$$

$$\int_x^a \frac{\partial p}{\partial x}dx = \int_x^a -\rho\left(\frac{2x}{h^2}\left(\frac{dh}{dt}\right)^2 - \frac{x}{h}\frac{d^2h}{dt^2}\right)xdx \tag{C.24}$$

$$p|_{x=a} - p(x,t) = -\frac{\rho}{2}(a^2 - x^2)\left(\frac{2}{h^2}\left(\frac{dh}{dt}\right)^2 - \frac{1}{h}\frac{d^2h}{dt^2}\right) \tag{C.25}$$

[3] Taylor series: $p(x+\Delta x) \approx p + \frac{\partial p}{\partial x}\Delta x$

One of the boundary conditions concerns the pressure at the outside of the plate, at $x = a$. It is assumed that the pressure at that point is equal to the ambient pressure, resulting in the assumption that $p|_{x=a} = 0$. Taking this boundary condition into account, equation C.25 can we rewritten into the following expression for the pressure underneath the flat plate:

$$\boxed{p(x,t) = p|_{x=a} + \frac{\rho}{2}\left(a^2 - x^2\right)\left(\frac{2}{h^2}\left(\frac{dh}{dt}\right)^2 - \frac{1}{h}\frac{d^2h}{dt^2}\right)} \tag{C.26}$$

The pressure distribution has been plotted in figure C.3. By looking at the figure, it can be seen that the pressure is zero at the outside $a = 2.25m$. The pressure is expected to be highest in the middle of the plate, this is also confirmed by the graph in the figure C.3.

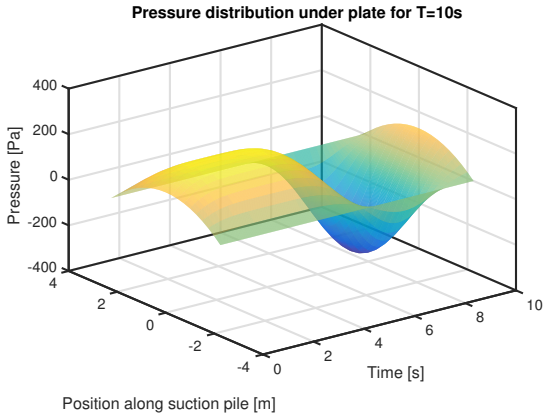

Figure C.3: Pressure distribution under plate

Force calculation

With equation C.26 the expression for the force exerting on the plate can be derived. Next, the pressure $p(x,t)$ is integrated over the whole surface area of the plate. This means that the pressure is integrated over twice the width a and over the length l. Since a unit plate length is considered the value $l = 1$ is used.

$$F = 2\int_0^1 \int_0^a p(x,t)\,dx\,dy \tag{C.27}$$

$$= 2\int_0^a \frac{\rho}{2}\left(a^2 - x^2\right)\left(\frac{2}{h^2}\left(\frac{dh}{dt}\right)^2 - \frac{1}{h}\frac{d^2h}{dt^2}\right)dx \tag{C.28}$$

Finally, the equation for the hydrodynamic force acting on a flat plate in proximity of a solid surface can be formulated as:

$$\boxed{F = \frac{2}{3}\rho\frac{a^3}{h}\left(\frac{2}{h}\left(\frac{dh}{dt}\right)^2 - \frac{d^2h}{dt^2}\right)} \tag{C.29}$$

The hydrodynamic force arises as a result of the fluid imposed on the plate in the proximity of a solid surface. It must be stated that Brennen displays it in a different way, i.e. the velocity squared term and acceleration term are switched in sign. This is correct, since Brennen indicates that he assumes the force to be directed downward.
In this force F, also known as the added mass force, clearly a velocity $\frac{dh}{dt}$ and an acceleration $\frac{d^2h}{dt}$ term can be seen. The force, related to the plate's motion behaviour, represents the hydrodynamic properties acting on the plate. Since the plate's motion changes over time, this hydrodynamic force changes over time and in proximity of a solid surface.

In his paper, Brennen mentions the initial force on the plate in absence of a solid boundary, i.e. freely moving in open water:

$$F_{free} = -\rho\pi a^2 \frac{d^2 h}{dt^2} \tag{C.30}$$

The reason is to illustrate what influence the presence of the boundary has on the magnitude of the force. The presence of the boundary results in an increase in the magnitude of the hydrodynamic force. As the assumption of $a/h >> 1$ should be satisfied, it can be stated that the presence of the solid boundary dominates the development of the hydrodynamic force imposed by the fluid on the plate.

The total hydrodynamic force, together with the velocity and acceleration term, has been plotted in figure C.4. In the figure, an overpressure in the first half of the period can be seen. In the second half, an underpressure can be seen. The progress of the acceleration term is dominant in the development of the total force.

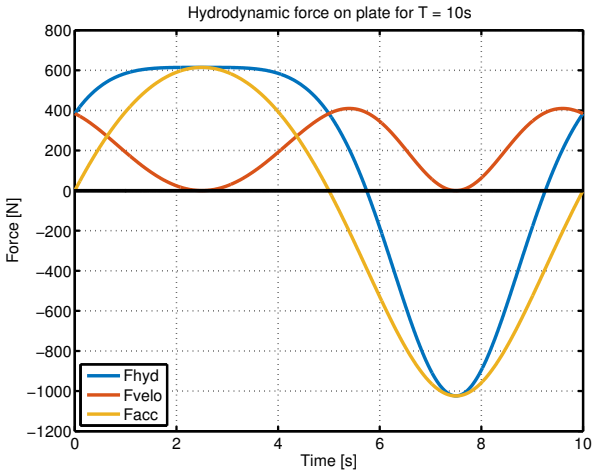

Figure C.4: Hydrodynamic force acting on the plate

D

BEHAVIOUR HYDRODYNAMIC FORCE

In this appendix, the results for the motion behaviour and hydrodynamic force for different imposed lowering motions on a rigid underground are given. The difference between the imposed lowering motions is the phasing. Whereas the first motion starts with zero phase difference, the second imposed motion has a phase difference of π.
Figure D.1 and D.2 correspond with the input motion of $z(t) = 0.5sin(\omega t) - 0.1t + 2$. Figure D.2a shows the results for the disk without valve and figure D.2b for a disk with valve. The influence of the valve is clearly visible: it decreases the magnitude of the force.

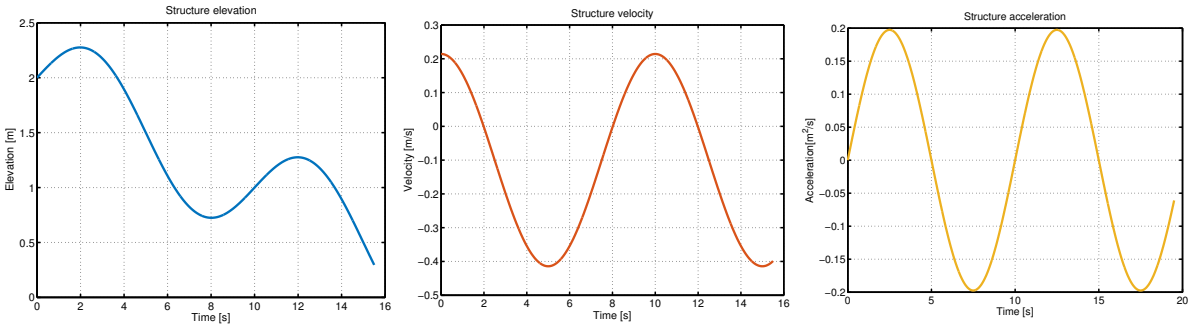

(a) Structure's elevation (b) Structure's velocity (c) Structure's acceleration

Figure D.1: Motion behaviour with input $z(t) = 0.5sin(\omega t) - 0.1t + 2$

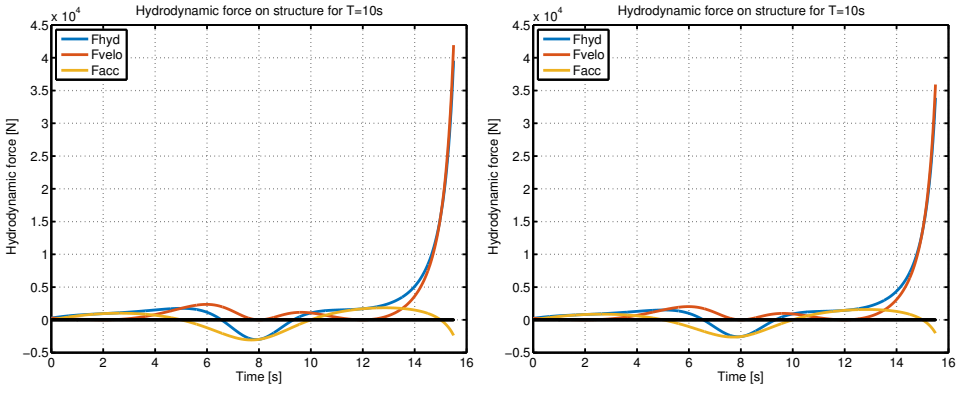

(a) Hydrodynamic force, without valve (b) Hydrodynamic force, with $R_v = 1m$

Figure D.2: Hydrodynamic force with input $z(t) = 0.5sin(\omega t) - 0.1t + 2$

Once the proximity increases, the velocity contribution to the force increases rapidly. As explained by Brennen, the presence of the boundary becomes dominant in the behaviour of the hydrodynamic force. This statement is confirmed by these graphs.

Figures D.3 and D.4 corresponds to the input motion of $z(t) = 0.5sin(\omega t+\pi)-0.1t+2$. The difference with the previous graphs is the starting direction of the oscillation, resulting from the phase difference. The intention of these different imposed motions is to show the phase dependency of the hydrodynamic force.

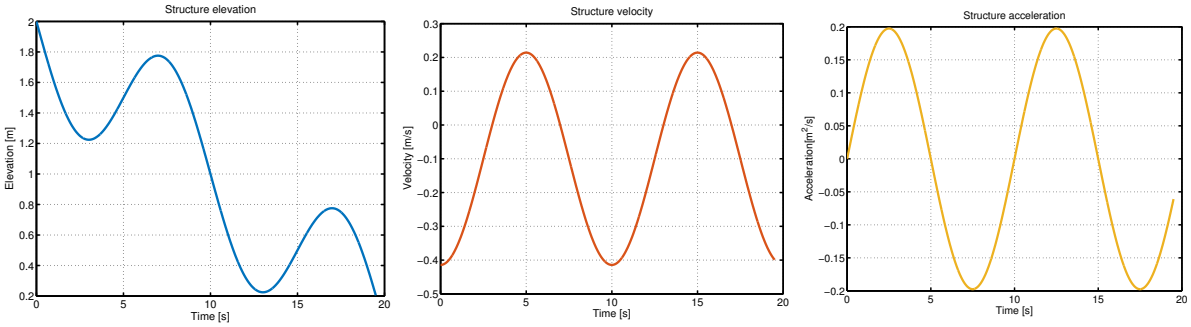

(a) Structure's elevation (b) Structure's velocity (c) Structure's acceleration

Figure D.3: Motion behaviour with input $z(t) = 0.5sin(\omega t+\pi)-0.1t+2$

Figure D.4a is the result for the disk without valve and figure D.4b results from the disk with valve. Again the influence of the valve is seen in the magnitude of the total force.

Around 13 s, the motion gets 0.2 m from the rigid underground. With this imposed motion, an increase from the acceleration term (yellow line) is observed at that moment in figure D.4. At this distance to the rigid underground, the presence of the boundary is not yet dominant in the magnitude of the hydrodynamic force, while this was the case in figure D.2. Since one term is quadratic and the other is not, the force is also frequency dependent. This is seen in the results from figure D.4.

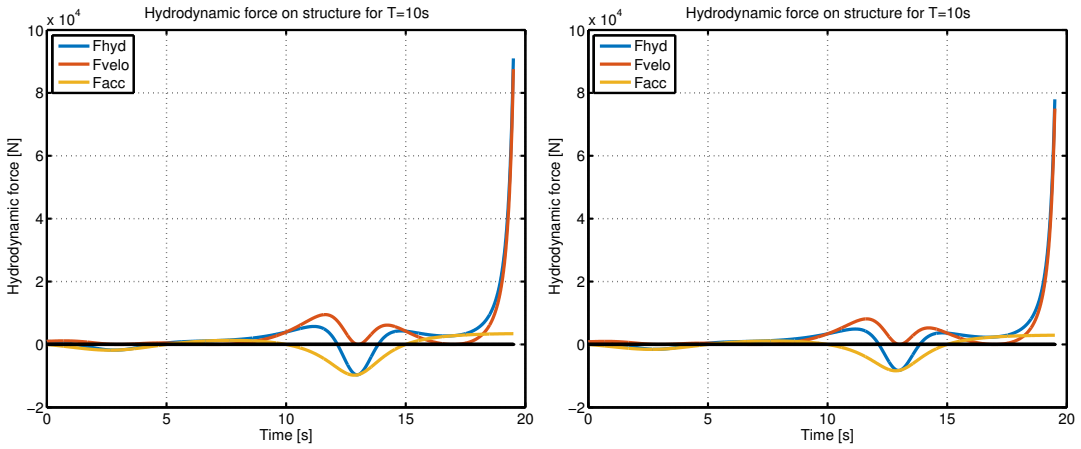

(a) Hydrodynamic force, without valve (b) Hydrodynamic force, with $R_v = 1m$

Figure D.4: Hydrodynamic force with input $z(t) = 0.5sin(\omega t+\pi)-0.1t+2$

E

2D MODEL: HYDRODYNAMIC FORCE

For the 2D model, the hydrodynamic force has been derived through the numerical software programme Maple. In this appendix the Maple code is given.

2D MODEL: DERIVATION HYDRODYNAMIC FORCE

This file gives a stepwise explanation of the derivation of the hydrodynamic force including a valve.

Conservation of mass: plate side

```
> restart
> Masschange + Massflow1 + Massflow2 = 0
```

$$Masschange + Massflow1 + Massflow2 = 0 \quad (1)$$

```
> Masschange := ρ·π·r·Δr·(d/dt) z(t)
```

$$Masschange := \rho\,\pi\,r\,\Delta r\left(\frac{d}{dt}z(t)\right) \quad (2)$$

```
> Massflow1 := 2·ρ·π·Δr·z(t)·u
```

$$Massflow1 := 2\,\rho\,\pi\,\Delta r\,z(t)\,u \quad (3)$$

```
> Massflow2 := -1·ρ·π·(Rv)·Δr·v(t)
```

$$Massflow2 := -\rho\,\pi\,Rv\,\Delta r\,v(t) \quad (4)$$

```
> ConsofMass := Masschange + Massflow1 + Massflow2 = 0
```

$$ConsofMass := \rho\,\pi\,r\,\Delta r\left(\frac{d}{dt}z(t)\right) + 2\,\rho\,\pi\,\Delta r\,z(t)\,u - \rho\,\pi\,Rv\,\Delta r\,v(t) = 0 \quad (5)$$

```
> u(r,t) := solve(ConsofMass, u)
```

$$u := (r,t) \rightarrow solve(ConsofMass, u) \quad (6)$$

```
> u(r,t)
```

$$-\frac{1}{2}\,\frac{\left(\frac{d}{dt}z(t)\right)r - v(t)\,Rv}{z(t)} \quad (7)$$

Conservation of mass: valve side

```
> restart
> Masschange2 := 0
```

$$Masschange2 := 0 \tag{8}$$

```
> Massflow12 := 2·π·ρ·Rv·z·u(Rv, t)
```

$$Massflow12 := 2\,\pi\,\rho\,Rv\,z\,u(Rv, t) \tag{9}$$

```
> Massflow22 := -ρ·π·(Rv)^2 v
```

$$Massflow22 := -\rho\,\pi\,Rv^2\,v \tag{10}$$

```
> ConsofMass2 := Masschange2 + Massflow12 + Massflow22 = 0
```

$$ConsofMass2 := 2\,\pi\,\rho\,Rv\,z\,u(Rv, t) - \rho\,\pi\,Rv^2\,v = 0 \tag{11}$$

```
> v(t) := solve(ConsofMass2, v)
```

$$v := t \rightarrow solve(ConsofMass2, v) \tag{12}$$

```
> v(t)
```

$$\frac{2\,u(Rv, t)\,z}{Rv} \tag{13}$$

Conservation of momentum: plate side

```
> restart
> Momentumchange1 := ρ · π·r·Δr·d/dt (z(t)·u(r, t))
```

$$Momentumchange1 := \rho\,\pi\,r\,\Delta r \left(\left(\frac{d}{dt} z(t) \right) u(r, t) + z(t) \left(\frac{\partial}{\partial t} u(r, t) \right) \right) \tag{14}$$

```
> Momentumflux1 := ρ ·2· π·r·z(t)·(2·u(r, t)·d/dr u(r, t)·Δr)
```

$$Momentumflux1 := 4\,\rho\,\pi\,r\,z(t)\,u(r, t) \left(\frac{\partial}{\partial r} u(r, t) \right) \Delta r \tag{15}$$

```
> External1 := -2· π·r·z(t)·dpdr·Δr
```

$$External1 := -2\,\pi\,r\,z(t)\,dpdr\,\Delta r \tag{16}$$

```
> Mom1 := Momentumchange1 + Momentumflux1 = External1
```

$$Mom1 := \rho\,\pi\,r\,\Delta r \left(\left(\frac{d}{dt} z(t) \right) u(r, t) + z(t) \left(\frac{\partial}{\partial t} u(r, t) \right) \right) + 4\,\rho\,\pi\,r\,z(t)\,u(r, t) \left(\frac{\partial}{\partial r} u(r, t) \right) \Delta r = -2\,\pi\,r\,z(t)\,dpdr\,\Delta r \tag{17}$$

```
> dpdr1 := solve(Mom1, dpdr)
```

$$dpdr1 := -\frac{1}{2} \frac{\rho \left(4\,z(t)\,u(r, t) \left(\frac{\partial}{\partial r} u(r, t) \right) + z(t) \left(\frac{\partial}{\partial t} u(r, t) \right) + \left(\frac{d}{dt} z(t) \right) u(r, t) \right)}{z(t)} \tag{18}$$

```
> dpdr11 := 1/ρ ∂/∂r p(r, t) + 2·u(r, t) (∂/∂r u(r, t)) + 1/(2 z(t)) · ∂/∂t (z(t)·u(r, t)) = 0
```

$$dpdr11 := \frac{\frac{\partial}{\partial r} p(r,t)}{\rho} + 2\,u(r,t)\left(\frac{\partial}{\partial r} u(r,t)\right) + \frac{1}{2}\,\frac{\left(\frac{d}{dt} z(t)\right) u(r,t) + z(t)\left(\frac{\partial}{\partial t} u(r,t)\right)}{z(t)} = 0 \quad (19)$$

Conservation of momentum: valve side

```
> # Conservation of momentum 2
> restart
> Momentumchange2 := -ρ ·π·Rv^2·Δr·d/dt v(t)
```

$$Momentumchange2 := -\rho\,\pi\,Rv^2\,\Delta r\left(\frac{d}{dt} v(t)\right) \quad (20)$$

```
> Momentumflux2 := ρ · π·Rv^2·(2·v(t)·d/dr v(t)·Δr)
```

$$Momentumflux2 := 0 \quad (21)$$

```
> External2 := -π·Rv^2 dpdr·Δr
```

$$External2 := -\pi\,Rv^2\,dpdr\,\Delta r \quad (22)$$

```
> Mom2 := Momentumchange2 + Momentumflux2 = External2
```

$$Mom2 := -\rho\,\pi\,Rv^2\,\Delta r\left(\frac{d}{dt} v(t)\right) = -\pi\,Rv^2\,dpdr\,\Delta r \quad (23)$$

```
> dpdr2 := solve(Mom2, dpdr)
```

$$dpdr2 := \left(\frac{d}{dt} v(t)\right)\rho \quad (24)$$

```
> dpdr22 := 1/ρ ∂/∂r p(r,t) - ∂/∂t (v(t)) = 0
```

$$dpdr22 := \frac{\frac{\partial}{\partial r} p(r,t)}{\rho} - \left(\frac{d}{dt} v(t)\right) = 0 \quad (25)$$

Insert Equilibrium between equations of conservation of momentum

```
> restart
> dpdr1 := (ρ(-2·u(r,t)(∂/∂r u(r,t)) - 1/(2 z(t))·∂/∂t (z(t)·u(r,t))))
```

$$dpdr1 := \rho\left(-2\,u(r,t)\left(\frac{\partial}{\partial r} u(r,t)\right) - \frac{1}{2}\,\frac{\left(\frac{d}{dt} z(t)\right) u(r,t) + z(t)\left(\frac{\partial}{\partial t} u(r,t)\right)}{z(t)}\right) \quad (26)$$

```
> u(r,t) := -1/2 ((d/dt z(t)) r - v(t) Rv)/z(t)
```

$$u := (r, t) \to -\frac{1}{2}\,\frac{\left(\frac{d}{dt} z(t)\right) r - v(t)\, Rv}{z(t)} \tag{27}$$

> $u(Rv, t)$

$$-\frac{1}{2}\,\frac{\left(\frac{d}{dt} z(t)\right) Rv - v(t)\, Rv}{z(t)} \tag{28}$$

> $diff(u(r, t), r)$

$$-\frac{1}{2}\,\frac{\frac{d}{dt} z(t)}{z(t)} \tag{29}$$

> $A := simplify\left(-\frac{\frac{d}{dt} z(t)}{z(t)}\right)$

$$A := -\frac{\frac{d}{dt} z(t)}{z(t)} \tag{30}$$

> $diff((z(t) \cdot u(r, t)), t)$

$$-\frac{1}{2}\left(\frac{d^2}{dt^2} z(t)\right) r + \frac{1}{2}\left(\frac{d}{dt} v(t)\right) Rv \tag{31}$$

> $B := simplify\left(-\frac{1}{2}\left(\frac{d^2}{dt^2} z(t)\right) Rv + \frac{1}{2}\left(\frac{d}{dt} v(t)\right) Rv\right)$

$$B := -\frac{1}{2}\, Rv \left(\frac{d^2}{dt^2} z(t) - \left(\frac{d}{dt} v(t)\right)\right) \tag{32}$$

> $dpdr1 := simplify\left(\rho\left(-2 \cdot u(Rv, t) \cdot A - \frac{1}{2\, z(t)} B\right)\right)$

$$dpdr1 := \rho\left(\frac{1}{4}\,\frac{1}{z(t)^2}\left(Rv\left(4\left(\frac{d}{dt} z(t)\right) v(t) + z(t)\left(\frac{d^2}{dt^2} z(t)\right) - z(t)\left(\frac{d}{dt} v(t)\right) - 4\left(\frac{d}{dt} z(t)\right)^2\right)\right)\right) \tag{33}$$

>

> $dpdr2 := \rho\, \frac{d}{dt} v(t)$

$$dpdr2 := \rho\left(\frac{d}{dt} v(t)\right) \tag{34}$$

> $C := simplify(dpdr1 - dpdr2 = 0)$

$$C := \rho\left(\frac{1}{4}\,\frac{1}{z(t)^2}\left(Rv\left(4\left(\frac{d}{dt} z(t)\right) v(t) + z(t)\left(\frac{d^2}{dt^2} z(t)\right) - z(t)\left(\frac{d}{dt} v(t)\right)\right)\right)\right) \tag{35}$$

$$-4\left(\frac{d}{dt}z(t)\right)^2\Big)\Big)\Big)-\rho\left(\frac{d}{dt}v(t)\right)=0$$

> $DPDR := F\cdot\frac{d}{dt}v(t)+G\cdot v(t)+H=0$

$$DPDR := F\left(\frac{d}{dt}v(t)\right)+G\,v(t)+H=0 \tag{36}$$

> $solve\left(DPDR,\ \frac{d}{dt}v(t)\right)$

$$-\frac{G\,v(t)+H}{F} \tag{37}$$

> $F := \left(-1-\frac{Rv}{4\,z(t)}\right)$

$$F := -1-\frac{1}{4}\frac{Rv}{z(t)} \tag{38}$$

> $G := \frac{Rv}{z(t)^2}\cdot\frac{d}{dt}z(t)$

$$G := \frac{Rv\left(\frac{d}{dt}z(t)\right)}{z(t)^2} \tag{39}$$

> $H := -\frac{Rv}{z(t)^2}\left(\frac{d}{dt}z(t)\right)^2+\frac{Rv}{4\,z(t)}\frac{d^2}{dt^2}z(t)$

$$H := -\frac{Rv\left(\frac{d}{dt}z(t)\right)^2}{z(t)^2}+\frac{1}{4}\frac{Rv\left(\frac{d^2}{dt^2}z(t)\right)}{z(t)} \tag{40}$$

> $solve\left(DPDR,\ \frac{d}{dt}v(t)\right)$

$$\frac{Rv\left(4\left(\frac{d}{dt}z(t)\right)v(t)+z(t)\left(\frac{d^2}{dt^2}z(t)\right)-4\left(\frac{d}{dt}z(t)\right)^2\right)}{z(t)\,(Rv+4\,z(t))} \tag{41}$$

Pressure calculation

> $restart$

> $u(r,t) := -\frac{1}{2}\frac{\left(\frac{d}{dt}z(t)\right)r-v(t)\,Rv}{z(t)}$

$$u := (r,t)\rightarrow -\frac{1}{2}\frac{\left(\frac{d}{dt}z(t)\right)r-v(t)\,Rv}{z(t)} \tag{42}$$

> $dpdr := \left(\rho\left(-2\cdot u(r,t)\left(\frac{\partial}{\partial r}u(r,t)\right)-\frac{1}{2\,z(t)}\cdot\frac{\partial}{\partial t}(z(t)\cdot u(r,t))\right)\right)$

$$dpdr := \rho\left(-\frac{1}{2}\,\frac{\left(\left(\frac{d}{dt}z(t)\right)r - v(t)\,Rv\right)\left(\frac{d}{dt}z(t)\right)}{z(t)^2} - \frac{1}{2}\,\frac{-\frac{1}{2}\left(\frac{d^2}{dt^2}z(t)\right)r + \frac{1}{2}\left(\frac{d}{dt}v(t)\right)Rv}{z(t)}\right) \tag{43}$$

```
> # Integrate first part of equation
```

```
> DPDR1 := (ρ(-2·u(r, t)(∂/∂r u(r, t))))
```

$$DPDR1 := \rho\left(-\frac{1}{2}\,\frac{\left(\left(\frac{d}{dt}z(t)\right)r - v(t)\,Rv\right)\left(\frac{d}{dt}z(t)\right)}{z(t)^2}\right) \tag{44}$$

```
> DPDR1A := -(1/2)ρ((d/dt z(t))^2/z(t)^2)·r
```

$$DPDR1A := -\frac{1}{2}\,\frac{\rho\left(\frac{d}{dt}z(t)\right)^2 r}{z(t)^2} \tag{45}$$

```
> INT1A := int(DPDR1A, r = r..R) assuming r > 0, R > 0
```

$$INT1A := -\frac{1}{4}\,\frac{\rho\left(\frac{d}{dt}z(t)\right)^2\left(R^2 - r^2\right)}{z(t)^2} \tag{46}$$

```
> DPDR1B := -(1/2)(-v(t) Rv)(d/dt z(t))/z(t)^2
```

$$DPDR1B := \frac{1}{2}\,\frac{v(t)\,Rv\left(\frac{d}{dt}z(t)\right)}{z(t)^2} \tag{47}$$

```
> INT1B := int(DPDR1B, r = r..R) assuming r > 0, R > 0
```

$$INT1B := \frac{1}{2}\,\frac{v(t)\,Rv\left(\frac{d}{dt}z(t)\right)(R - r)}{z(t)^2} \tag{48}$$

```
> INT1 := INT1A + INT1B
```

$$INT1 := -\frac{1}{4}\,\frac{\rho\left(\frac{d}{dt}z(t)\right)^2\left(R^2 - r^2\right)}{z(t)^2} + \frac{1}{2}\,\frac{v(t)\,Rv\left(\frac{d}{dt}z(t)\right)(R - r)}{z(t)^2} \tag{49}$$

```
> # Integrate second part of equation
```

> $DPDR2 := \rho\left(-\frac{1}{2\,z(t)}\cdot\frac{\partial}{\partial t}\left(z(t)\cdot u(r,t)\right)\right)$

$$DPDR2 := \rho\left(-\frac{1}{2}\,\frac{-\frac{1}{2}\left(\frac{d^2}{dt^2}z(t)\right)r+\frac{1}{2}\left(\frac{d}{dt}v(t)\right)Rv}{z(t)}\right) \tag{50}$$

> $DPDR2A := \frac{1}{4}\rho\,\frac{\left(\frac{d^2}{dt^2}z(t)\right)}{z(t)}\cdot r$

$$DPDR2A := \frac{1}{4}\,\frac{\rho\left(\frac{d^2}{dt^2}z(t)\right)r}{z(t)} \tag{51}$$

> $INT2A := int(DPDR2A, r = r..R)$ assuming $r > 0, R > 0$

$$INT2A := \frac{1}{8}\,\frac{\rho\left(\frac{d^2}{dt^2}z(t)\right)\left(R^2-r^2\right)}{z(t)} \tag{52}$$

> $DPDR2B := \rho\left(-\frac{1}{4}\,\frac{\left(\frac{d}{dt}v(t)\right)Rv}{z(t)}\right)$

$$DPDR2B := \rho\left(-\frac{1}{4}\,\frac{\left(\frac{d}{dt}v(t)\right)Rv}{z(t)}\right) \tag{53}$$

> $INT2B := int(DPDR2B, r = r..R)$ assuming $r > 0, R > 0$

$$INT2B := \rho\left(-\frac{1}{4}\,\frac{\left(\frac{d}{dt}v(t)\right)Rv}{z(t)}\right)(R-r) \tag{54}$$

> $INT2 := INT2A + INT2B$

$$INT2 := \frac{1}{8}\,\frac{\rho\left(\frac{d^2}{dt^2}z(t)\right)\left(R^2-r^2\right)}{z(t)}+\rho\left(-\frac{1}{4}\,\frac{\left(\frac{d}{dt}v(t)\right)Rv}{z(t)}\right)(R-r) \tag{55}$$

> $P(r,t) := (-1\cdot(INT1 + \mathrm{INT2}))$

$$P := (r,t)\rightarrow -INT1 - INT2 \tag{56}$$

> $P(r,t)$

$$\frac{1}{4}\,\frac{\rho\left(\frac{d}{dt}z(t)\right)^2\left(R^2-r^2\right)}{z(t)^2}-\frac{1}{2}\,\frac{v(t)\,Rv\left(\frac{d}{dt}z(t)\right)(R-r)}{z(t)^2}$$
$$-\frac{1}{8}\,\frac{\rho\left(\frac{d^2}{dt^2}z(t)\right)\left(R^2-r^2\right)}{z(t)}-\rho\left(-\frac{1}{4}\,\frac{\left(\frac{d}{dt}v(t)\right)Rv}{z(t)}\right)(R-r) \tag{57}$$

>

Calculate force F by integrating P from Rv..R and from 0 to 2pi

```
> F(t) := int(int(P(r, t)*r, r = Rv..R), theta = 0..2*Pi)
```

$$F := t \to \int_0^{2\pi} \int_{Rv}^{R} P(r, t)\, r \, dr\, d\theta \tag{58}$$

```
> F(t)
```

$$2\left(\frac{1}{4}\left(-\frac{1}{4}\frac{\rho\left(\frac{d}{dt}z(t)\right)^2}{z(t)^2}+\frac{1}{8}\frac{\rho\left(\frac{d^2}{dt^2}z(t)\right)}{z(t)}\right)\left(R^4-Rv^4\right)\right.$$
$$+\frac{1}{3}\left(\frac{1}{2}\frac{v(t)\,Rv\left(\frac{d}{dt}z(t)\right)}{z(t)^2}+\rho\left(-\frac{1}{4}\frac{\left(\frac{d}{dt}v(t)\right)Rv}{z(t)}\right)\right)\left(R^3-Rv^3\right)$$
$$+\frac{1}{2}\left(\frac{1}{4}\frac{\rho\left(\frac{d}{dt}z(t)\right)^2R^2}{z(t)^2}-\frac{1}{2}\frac{v(t)\,Rv\left(\frac{d}{dt}z(t)\right)R}{z(t)^2}-\frac{1}{8}\frac{\rho\left(\frac{d^2}{dt^2}z(t)\right)R^2}{z(t)}\right.$$
$$\left.\left.-\rho\left(-\frac{1}{4}\frac{\left(\frac{d}{dt}v(t)\right)Rv}{z(t)}\right)R\right)\left(R^2-Rv^2\right)\right)\pi \tag{59}$$

```
>
```

Calculate hydrodynamics force as function of z, dzdt, dz2dt2 & v

Insert the function of dvdt into the hydrodynamic force as it was derived earlier.

```
> restart
```

```
> diff(v(t), t) = (Rv*(4*(diff(z(t), t))*v(t) + z(t)*(diff(z(t), t$2)) - 4*(diff(z(t), t))^2))/(z(t)*(Rv + 4*z(t)))
```

$$\frac{d}{dt}v(t) = \frac{Rv\left(4\left(\frac{d}{dt}z(t)\right)v(t)+z(t)\left(\frac{d^2}{dt^2}z(t)\right)-4\left(\frac{d}{dt}z(t)\right)^2\right)}{z(t)\,(Rv+4\,z(t))} \tag{60}$$

```
> # Hydrodynamic force as function of oa v & dvdt (
```

```
> F(t) := (1/2)*((-1/4)*(rho*(diff(z(t), t))^2)/(z(t)^2) + (1/8)*(rho*(diff(z(t), t$2)))/z(t))*(R^4 - Rv^4)*Pi
  + (2/3)*((1/2)*(v(t)*Rv*(diff(z(t), t)))/(z(t)^2) + rho*(-(1/4)*((diff(v(t), t))*Rv)/z(t)))*(R^3 - Rv^3)*Pi
```

$$+\left(\frac{1}{4}\,\frac{\rho\left(\frac{d}{dt}z(t)\right)^2 R^2}{z(t)^2}-\frac{1}{2}\,\frac{v(t)\,Rv\left(\frac{d}{dt}z(t)\right)R}{z(t)^2}-\frac{1}{8}\,\frac{\rho\left(\frac{d^2}{dt^2}z(t)\right)R^2}{z(t)}-\rho\left(-\frac{1}{4}\,\frac{\left(\frac{d}{dt}v(t)\right)Rv}{z(t)}\right)R\right)\left(R^2-Rv^2\right)\pi$$

$$F := t\rightarrow\left(-\frac{1}{8}\,\frac{\rho\left(\frac{d}{dt}z(t)\right)^2}{z(t)^2}+\frac{1}{16}\,\frac{\rho\left(\frac{d^2}{dt^2}z(t)\right)}{z(t)}\right)\left(R^4-Rv^4\right)\pi \tag{61}$$

$$+\left(\frac{1}{3}\,\frac{v(t)\,Rv\left(\frac{d}{dt}z(t)\right)}{z(t)^2}+\frac{2}{3}\,\rho\left(-\frac{1}{4}\,\frac{\left(\frac{d}{dt}v(t)\right)Rv}{z(t)}\right)\right)\left(R^3-Rv^3\right)\pi$$

$$+\left(\frac{1}{4}\,\frac{\rho\left(\frac{d}{dt}z(t)\right)^2 R^2}{z(t)^2}-\frac{1}{2}\,\frac{v(t)\,Rv\left(\frac{d}{dt}z(t)\right)R}{z(t)^2}-\frac{1}{8}\,\frac{\rho\left(\frac{d^2}{dt^2}z(t)\right)R^2}{z(t)}-\rho\left(-\frac{1}{4}\,\frac{\left(\frac{d}{dt}v(t)\right)Rv}{z(t)}\right)R\right)\left(R^2-Rv^2\right)\pi$$

```
> # Hydrodynamic force as function of z, dzdt, dz2dt2 & v
> # dvdt inserted into hydrodynamic force equation
```

$$> dvdt := \frac{Rv\left(4\left(\frac{d}{dt}z(t)\right)v(t)+z(t)\left(\frac{d^2}{dt^2}z(t)\right)-4\left(\frac{d}{dt}z(t)\right)^2\right)}{z(t)\,\left(Rv+4\,z(t)\right)}$$

$$dvdt := \frac{Rv\left(4\left(\frac{d}{dt}z(t)\right)v(t)+z(t)\left(\frac{d^2}{dt^2}z(t)\right)-4\left(\frac{d}{dt}z(t)\right)^2\right)}{z(t)\,\left(Rv+4\,z(t)\right)} \tag{62}$$

$$dvdt \tag{63}$$

$$> Fhyd(t) := \frac{1}{2}\left(-\frac{1}{4}\,\frac{\rho\left(\frac{d}{dt}z(t)\right)^2}{z(t)^2}+\frac{1}{8}\,\frac{\rho\left(\frac{d^2}{dt^2}z(t)\right)}{z(t)}\right)\left(R^4-Rv^4\right)\pi$$

$$+\frac{2}{3}\left(\frac{1}{2}\,\frac{v(t)\,Rv\left(\frac{d}{dt}z(t)\right)}{z(t)^2}+\rho\left(-\frac{1}{4}\,\frac{(dvdt)\,Rv}{z(t)}\right)\right)\left(R^3-Rv^3\right)\pi$$

$$+\left(\frac{1}{4}\,\frac{\rho\left(\frac{d}{dt}z(t)\right)^2 R^2}{z(t)^2}-\frac{1}{2}\,\frac{v(t)\,Rv\left(\frac{d}{dt}z(t)\right)R}{z(t)^2}-\frac{1}{8}\,\frac{\rho\left(\frac{d^2}{dt^2}z(t)\right)R^2}{z(t)}-\rho\left(\right.\right.$$

$$\left. -\frac{1}{4}\ \frac{(dvdt)\ Rv}{z(t)}\right) R\Bigg]\left(R^2 - Rv^2\right)\pi$$

$$Fhyd := t \rightarrow \left[\left(-\frac{1}{8}\ \frac{\rho\left(\frac{\mathrm{d}}{\mathrm{d}t}\,z(t)\right)^2}{z(t)^2} + \frac{1}{16}\ \frac{\rho\left(\frac{\mathrm{d}^2}{\mathrm{d}t^2}\,z(t)\right)}{z(t)}\right)\left(R^4 - Rv^4\right)\pi \right. \tag{64}$$

$$+\left(\frac{1}{3}\ \frac{v(t)\ Rv\left(\frac{\mathrm{d}}{\mathrm{d}t}\,z(t)\right)}{z(t)^2} + \frac{2}{3}\ \rho\left(-\frac{1}{4}\ \frac{dvdt\ Rv}{z(t)}\right)\right)\left(R^3 - Rv^3\right)\pi$$

$$+\left(\frac{1}{4}\ \frac{\rho\left(\frac{\mathrm{d}}{\mathrm{d}t}\,z(t)\right)^2 R^2}{z(t)^2} - \frac{1}{2}\ \frac{v(t)\ Rv\left(\frac{\mathrm{d}}{\mathrm{d}t}\,z(t)\right) R}{z(t)^2} - \frac{1}{8}\ \frac{\rho\left(\frac{\mathrm{d}^2}{\mathrm{d}t^2}\,z(t)\right) R^2}{z(t)} - \rho\left(\right.\right.$$

$$\left.\left. -\frac{1}{4}\ \frac{dvdt\ Rv}{z(t)}\right) R\right]\left(R^2 - Rv^2\right)\pi$$

> $Fhyd(t)$

$$\left(-\frac{1}{8}\ \frac{\rho\left(\frac{\mathrm{d}}{\mathrm{d}t}\,z(t)\right)^2}{z(t)^2} + \frac{1}{16}\ \frac{\rho\left(\frac{\mathrm{d}^2}{\mathrm{d}t^2}\,z(t)\right)}{z(t)}\right)\left(R^4 - Rv^4\right)\pi + \left(\frac{1}{3}\ \frac{Rv\left(\frac{\mathrm{d}}{\mathrm{d}t}\,z(t)\right) v(t)}{z(t)^2}\right. \tag{65}$$

$$\left. + \frac{2}{3}\ \rho\left(-\frac{1}{4}\ \frac{Rv^2\left(4\left(\frac{\mathrm{d}}{\mathrm{d}t}\,z(t)\right) v(t) + z(t)\left(\frac{\mathrm{d}^2}{\mathrm{d}t^2}\,z(t)\right) - 4\left(\frac{\mathrm{d}}{\mathrm{d}t}\,z(t)\right)^2\right)}{z(t)^2\ (Rv + 4\,z(t))}\right)\right)\left(R^3\right.$$

$$\left. - Rv^3\right)\pi + \left(\frac{1}{4}\ \frac{\rho\left(\frac{\mathrm{d}}{\mathrm{d}t}\,z(t)\right)^2 R^2}{z(t)^2} - \frac{1}{2}\ \frac{Rv\left(\frac{\mathrm{d}}{\mathrm{d}t}\,z(t)\right) v(t)\ R}{z(t)^2}\right.$$

$$\left. - \frac{1}{8}\ \frac{\rho\left(\frac{\mathrm{d}^2}{\mathrm{d}t^2}\,z(t)\right) R^2}{z(t)} - \rho\left(\right.\right.$$

$$\left.\left. -\frac{1}{4}\ \frac{Rv^2\left(4\left(\frac{\mathrm{d}}{\mathrm{d}t}\,z(t)\right) v(t) + z(t)\left(\frac{\mathrm{d}^2}{\mathrm{d}t^2}\,z(t)\right) - 4\left(\frac{\mathrm{d}}{\mathrm{d}t}\,z(t)\right)^2\right)}{z(t)^2\ (Rv + 4\,z(t))}\right) R\right)\left(R^2 - Rv^2\right)\pi$$

>

F

INPUT DATA

The complete list of all the input data for the base case situation is given here.

	Input data	Value
General	Sea water density	ρ_w = 1025 kg/m^3
	Steel density	ρ_s = 7850 kg/m^3
	Soil density	ρ_{soil} = 2600 kg/m^3
	Gravitational acceleration	g = 9.81 m/m^2
Structural	Structural mass	M = 222 ton
	Radius	R = 2.75 m
	Valve radius	R_v = 0.75 m
	Submerged weight	F_{subm} = 1.90 MN
	Position from seabed	z_0 = 2 m
Crane	Period	T = 10 s
	Angular velocity	ω = 0.628 rad/s
	Amplitude	A = 0.5 m
	Initial crane wire length	L_0 = 1000 m
	Crane wire stiffness	k_{line} = 1.09 MN/m
	Crane lowering velocity	V_c = 0.1 m/s
Soil	Soil stiffness	k_{soil} = 3.52 MN/m
	Soil damping ratio	ζ = 0.7 - 1.3
	Soil mass	m_{soil} = 169.9 ton
Hydrodynamics	Added mass coefficient	C_A = 28.4 ton
	Drag coefficient	C_D = 10

Table F.1: All input data for the base case situation

The crane wire stiffness value is based on the crane wire stiffness from the Balder. The main hoist has an axial stiffness of 272 kN/m. In this case, a 4-fall crane wire was taken resulting in a crane wire stiffness of 1.09 MN/m, seen in table F.1. The soil stiffness of 3.52 MN/m was derived by making use of equations 3.6 and 3.7 for large strains and linear behaviour for the shear strength (S_u = 2).

The initial conditions differ for the 1D and 2D model. They are discussed for each model separately in sections 6.1 and 6.2, respectively.

G

VALIDATION

To investigate whether the obtained equations of motion are correct, some simple checks have been done. These checks were done to see if the system is consistently in equilibrium and if the results are in line with the expectation. In this section, the results of both the 1D model and the 2D model for the following tests are given:

- Free fall test
- Free decay test
- Constant lowering test

The results for the free fall test for both the 1D and the 2D model are given in figure G.1. In a free fall test, there is no line connected to the structure, so it should go to zero immediately. In figure G.1a, it can be seen that eventually the velocity and acceleration become zero. This is at the moment when the submerged weight is in equilibrium with the soil force.
The exact same is observed for the 2D model with $R_v = 0.75$ m in figure G.1b. Notice that the crane oscillation from the top right corner in figure G.1a has been replaced by the valve velocity in figure G.1b. As expect, the valve velocity quickly increase and immediately decreases back to zero again.

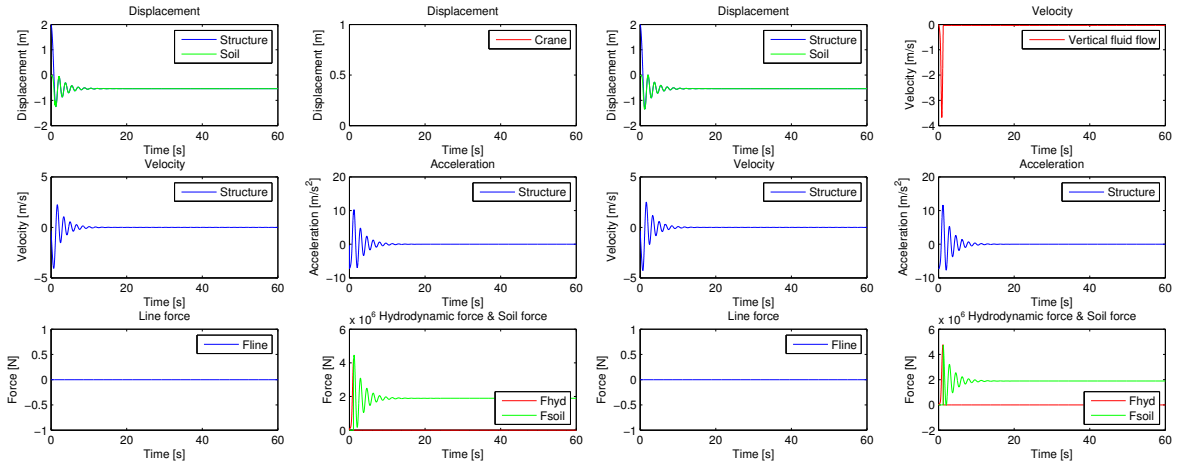

(a) Free fall test for 1D model

(b) Free fall test for 2D model

Figure G.1: Model validation: free fall test

The results for the free decay test for both models can be found in figure G.2. In a free decay test, the constant lowering speed of the crane and the amplitude are assumed to be zero. The system starts in an unbalanced situation (in this case 3 m above the seabed) and needs to get back into its equilibrium state. This is eventually achieved, as seen in the figure G.2.

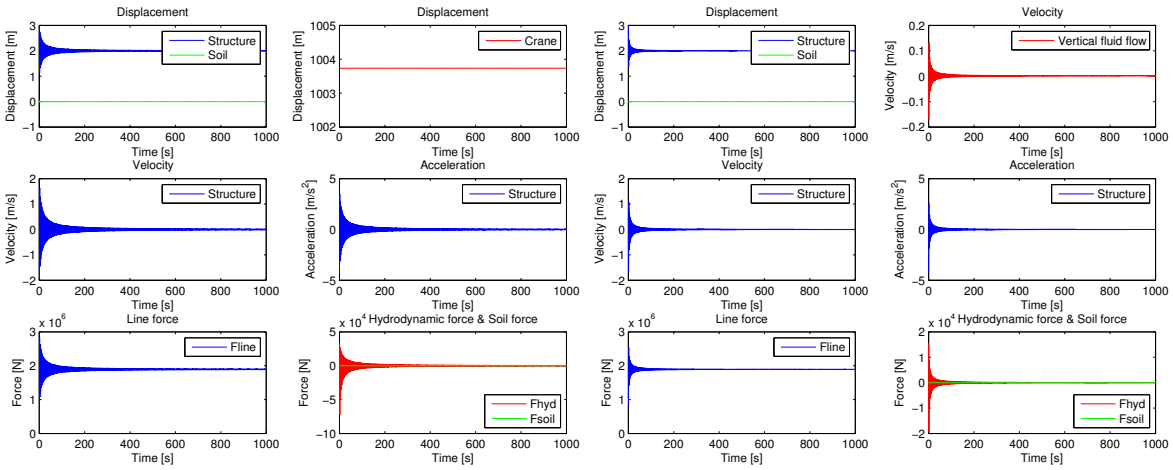

(a) Free decay test model for 1D model

(b) Free decay test for 2D model

Figure G.2: Model validation: free decay test

The results of the constant lowering test can be found in figure G.3. During this test, the amplitude and period are assumed to be zero. This means that the structure is lowered with the constant crane lowering velocity of 0.1 m/s. Basically the structure is pushed downwards with a constant velocity and once it reaches the soil, this velocity changes due to the soil reaction force. This can be seen in the figure below.
The behaviour for the closed disk, illustrated in figure G.3a, and for the disk with a valve radius of $R_v = 0.75$ m, are shown in figure G.3b, is expected.

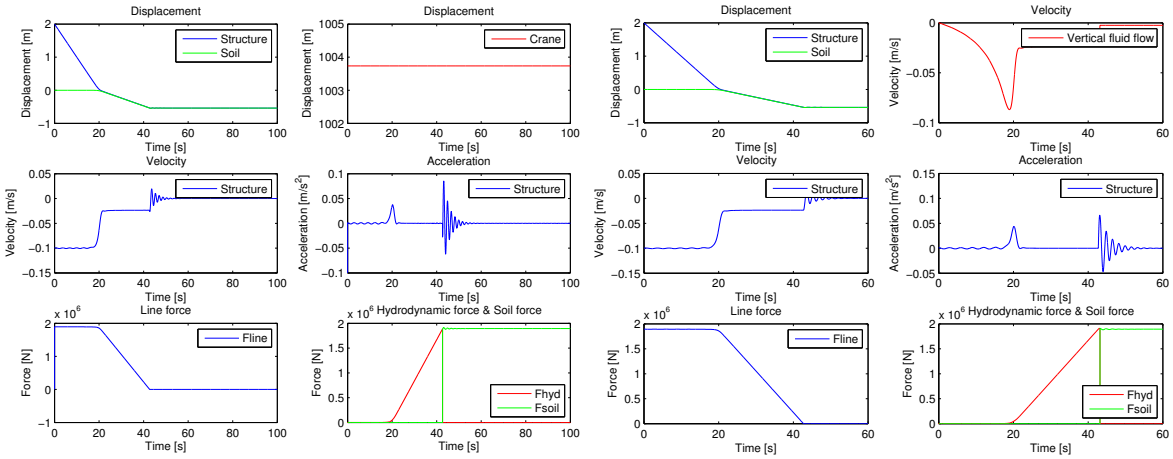

(a) Constant lowering test for 1D model

(b) No heave oscillation test for 2D model

Figure G.3: Model validation: constant lowering test

H

RESULTS BASE CASE

H.1. 1D MODEL: OPEN DISK

The results for the base case situation of the 1D model with a valve of $R_v = 0.75$ m are given here. Also here the structure decreases as it gets closer to the seabed and an increase in the acceleration and the hydrodynamic force is observed. The maximum hydrodynamic force is slightly lower compared to the closed disk.

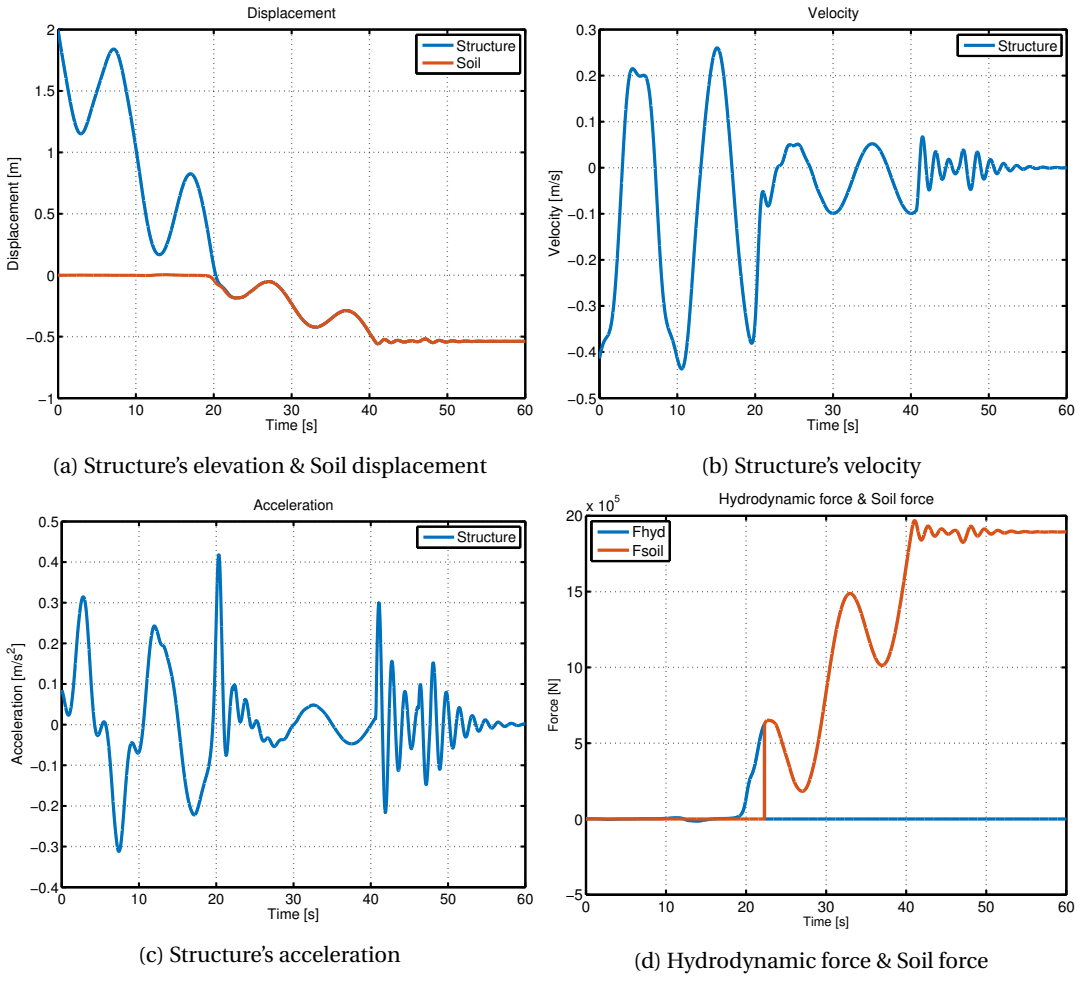

(a) Structure's elevation & Soil displacement

(b) Structure's velocity

(c) Structure's acceleration

(d) Hydrodynamic force & Soil force

Figure H.1: 1D model with valve with $R_v = 0.75m$: results base case

Since the development is similar to the closed disk for the 1D model, the graphs corresponding to the hor-

izontal fluid velocity, pressure distribution and estimated soil displacement are left out of here. Table H.1 shows the soil disturbance for different damping ratio's calculated with the conservation of energy method.

Model	Damping ratio ζ	Soil disturbance z_{soil}
Closed 1D model	0.7	0.276 m
	1	0.227 m
	1.3	0.189 m
Open 1D model	0.7	0.218 m
	1	0.182 m
	1.3	0.154 m
Open 2D model	0.7	0.219 m
	1	0.183 m
	1.3	0.153 m

Table H.1: 1D % 2D model: estimated soil displacement for various damping ratio's

H.2. 2D MODEL: DISK WITH ONE SYMMETRIC VALVE

The results for the 2D model including the initialisation are given in this section. As can be seen in figure H.2, the structure's velocity and acceleration and vertical fluid flow velocity start with an initial condition of zero. After 80 s the crane starts to lower with a constant velocity of 0.1 m/s.

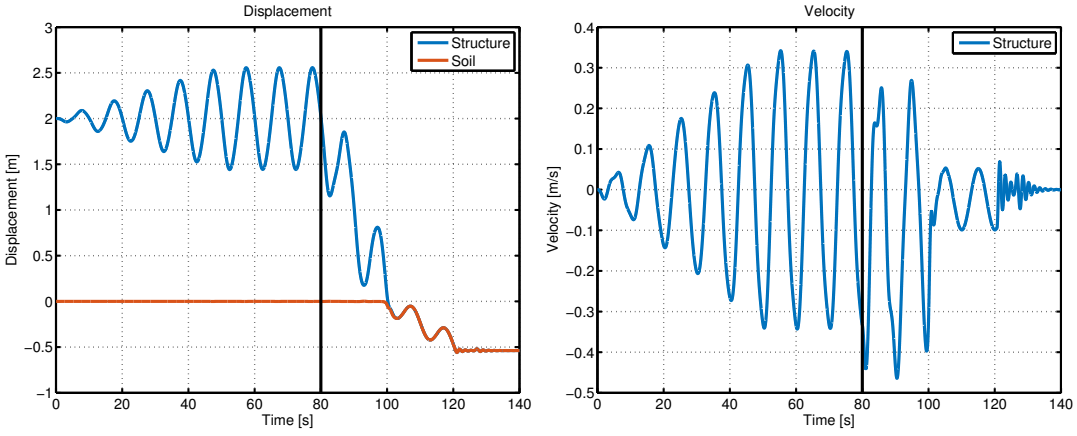

(a) Structure's elevation & Soil displacement

(b) Structure's velocity

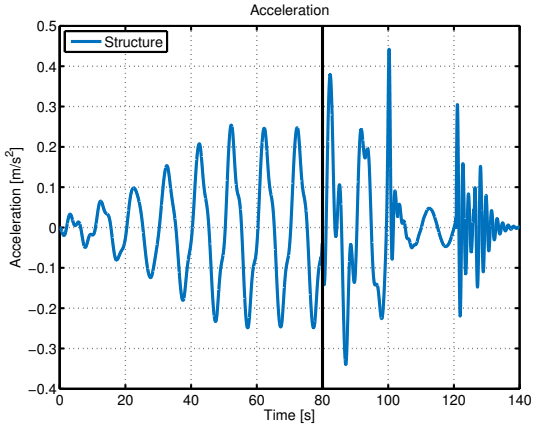

(c) Structure's acceleration

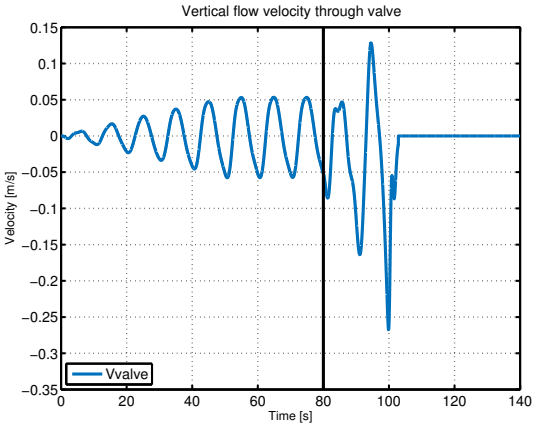

(d) Vertical fluid flow velocity

Figure H.2: 2D model with valve with $R_v = 0.75m$: results base case

I

RESULTS SENSITIVITY ANALYSIS

I.1. STRUCTURAL PROPERTIES: VALVE SIZE

RIGID UNDERGROUND

In figures I.1 and I.2, the results for all ratio's related to the free fall are shown. From figure I.1b and I.1d, a clear development for different valve sizes can be observed. Figure I.2b clearly indicates that a large valve results in a lower hydrodynamic force.

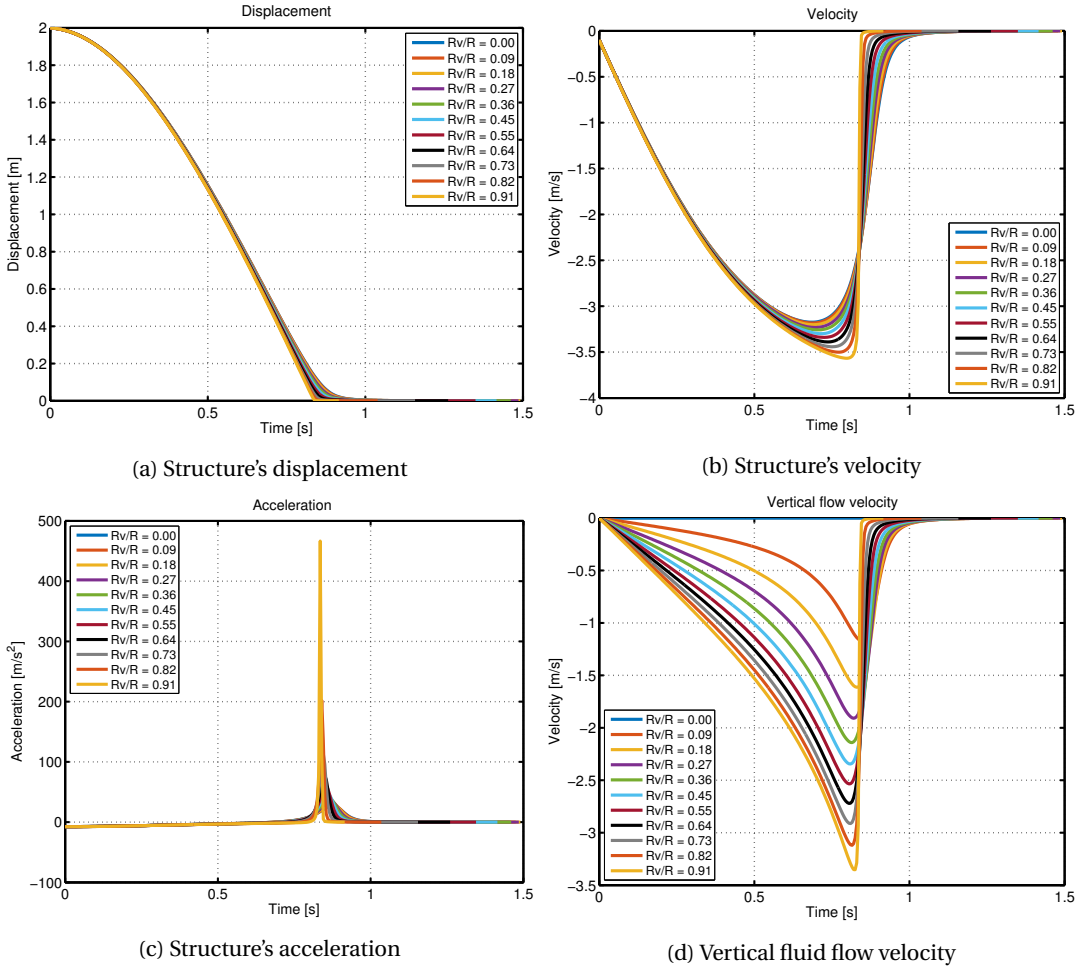

(a) Structure's displacement

(b) Structure's velocity

(c) Structure's acceleration

(d) Vertical fluid flow velocity

Figure I.1: Free fall test for all ratio's, part 1

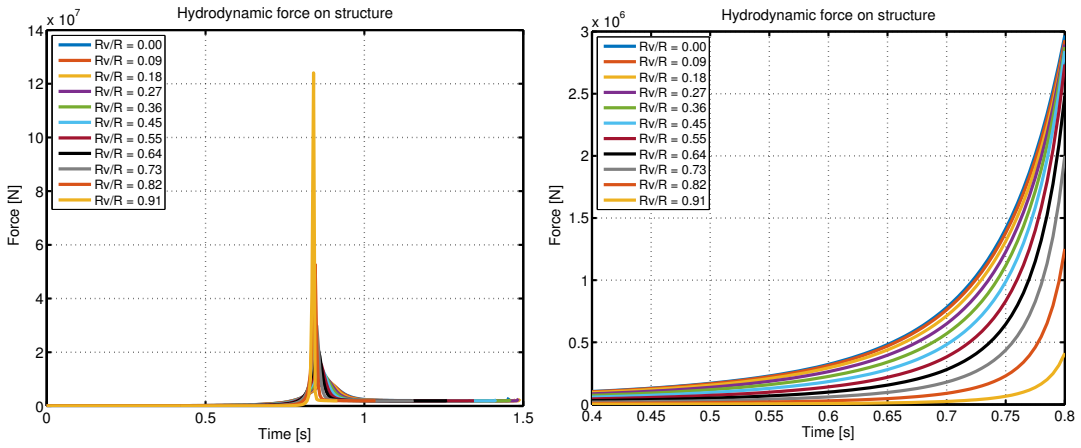

(a) Hydrodynamic force

(b) Zoomed in on hydrodynamic force

Figure I.2: Free fall test for all ratio's, part 2

The pressure distribution for a disk with valve with $R_v = 0.5$ m and $R_v = 2.5$ m, respectively, have been given in figure I.3. As expected, the pressure distribution underneath a disk with a large valve is lower compared to the disk with the smaller valve.

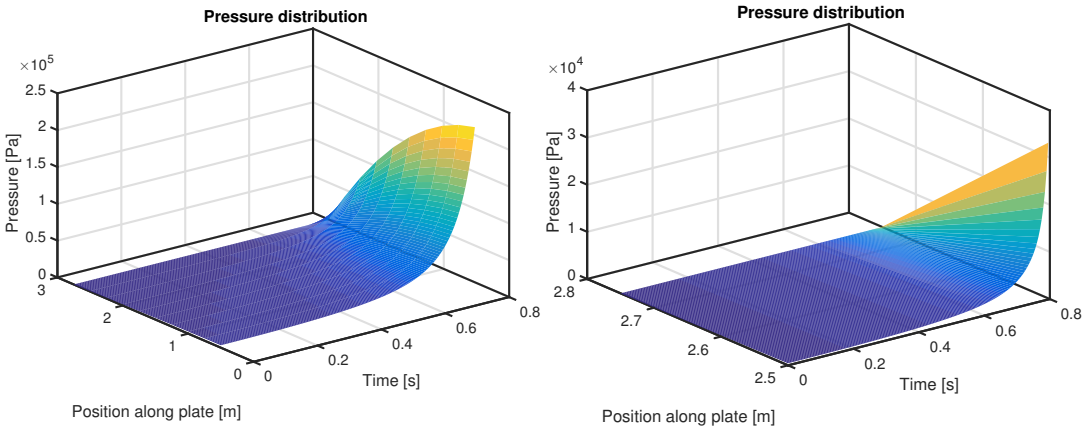

(a) Pressure distribution for Rv = 0.5m

(b) Pressure distribution for Rv = 2.5m

Figure I.3: Free fall test for $R_v = 0.5m$ and $R_v = 2.5m$

The results for the constant lowering test are given in figure I.4. Based on this test it can be stated that for a structure with a large valve, lowered with a constant velocity of 0.1 m/s, the hydrodynamic is lowest. This is in line with the expectation and also seen in the free fall test.
In figure I.4d, some unexpected results for the vertical fluid flow velocity were observed. The vertical fluid flowing through a valve with $R_v > 2$ m is expected to be nearly equal to the structure's velocity. This was not observed in this test.

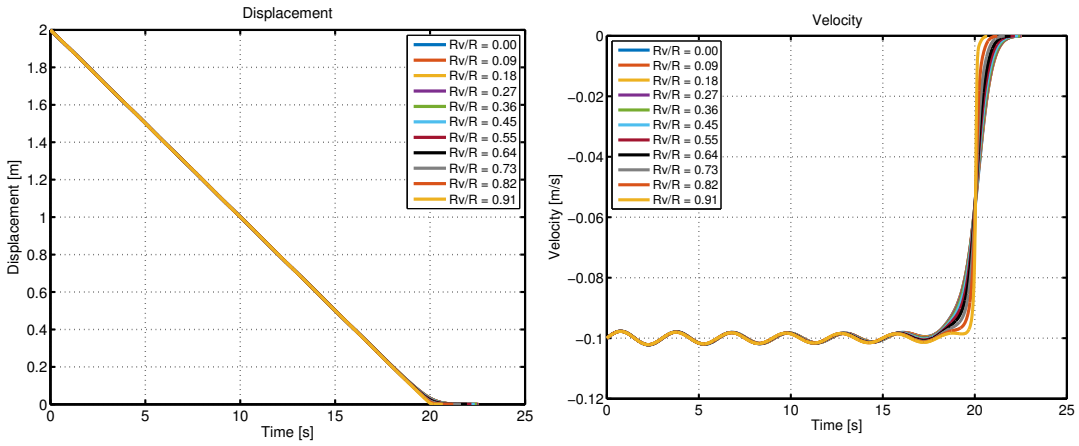

(a) Structure's displacement

(b) Structure's velocity

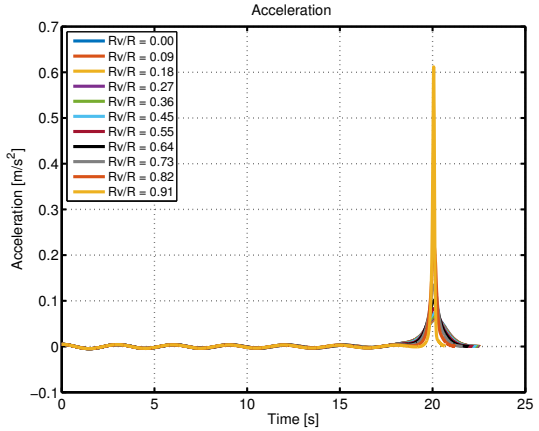

(c) Structure's acceleration

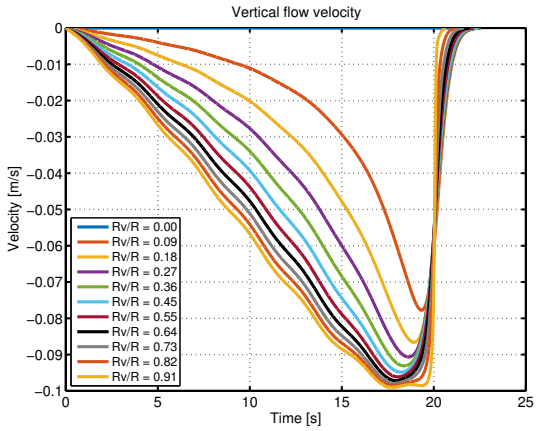

(d) Vertical fluid flow velocity

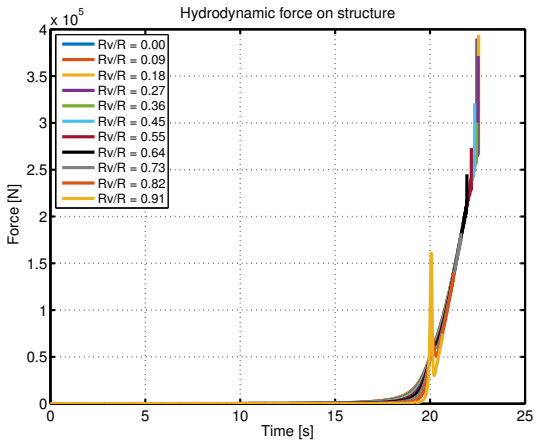

(e) Hydrodynamic force

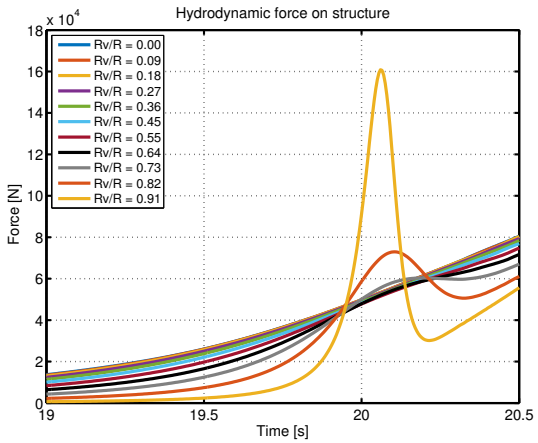

(f) Zoomed in on hydrodynamic force

Figure I.4: Constant lowering test for all ratio's, part 1

The horizontal fluid flow velocity for various valve sizes was evaluated. The results for a disk with valve radius of 0.5 m and of 2.5 m are given in figure I.5. As was expected, the horizontal flow velocity for the large valve is generally lower than for the smaller valve. Similar to the free fall test, a lower pressure distribution for the disk with R_v =2.5 m was observed and therefore has been left out of here.

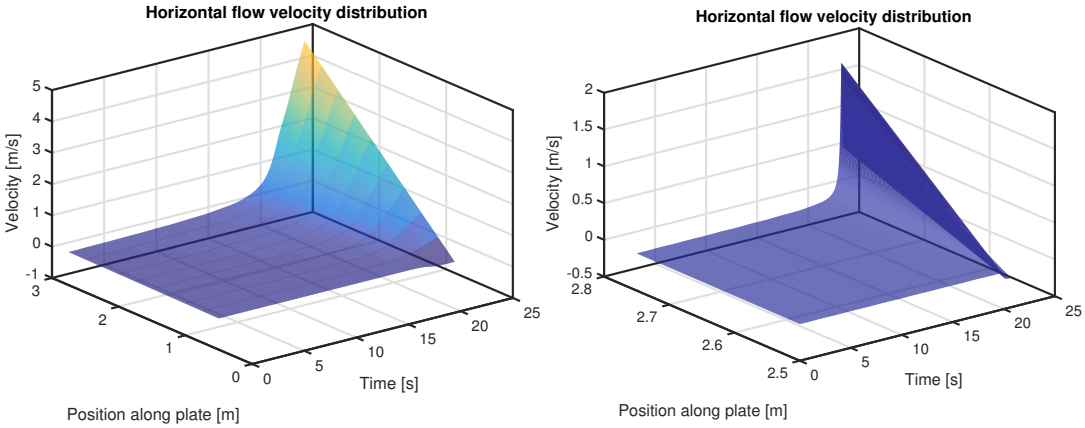

(a) Horizontal fluid flow velocity for Rv = 0.5m

(b) Horizontal fluid flow velocity for Rv = 2.5m

Figure I.5: Constant lowering test for $R_v = 0.5m$ and $R_v = 2.5m$

SOIL UNDERGROUND

The results for the base case situation for all valve ratio's can be found here. A clear development in the hydrodynamic force can be visualized in figure I.6d.

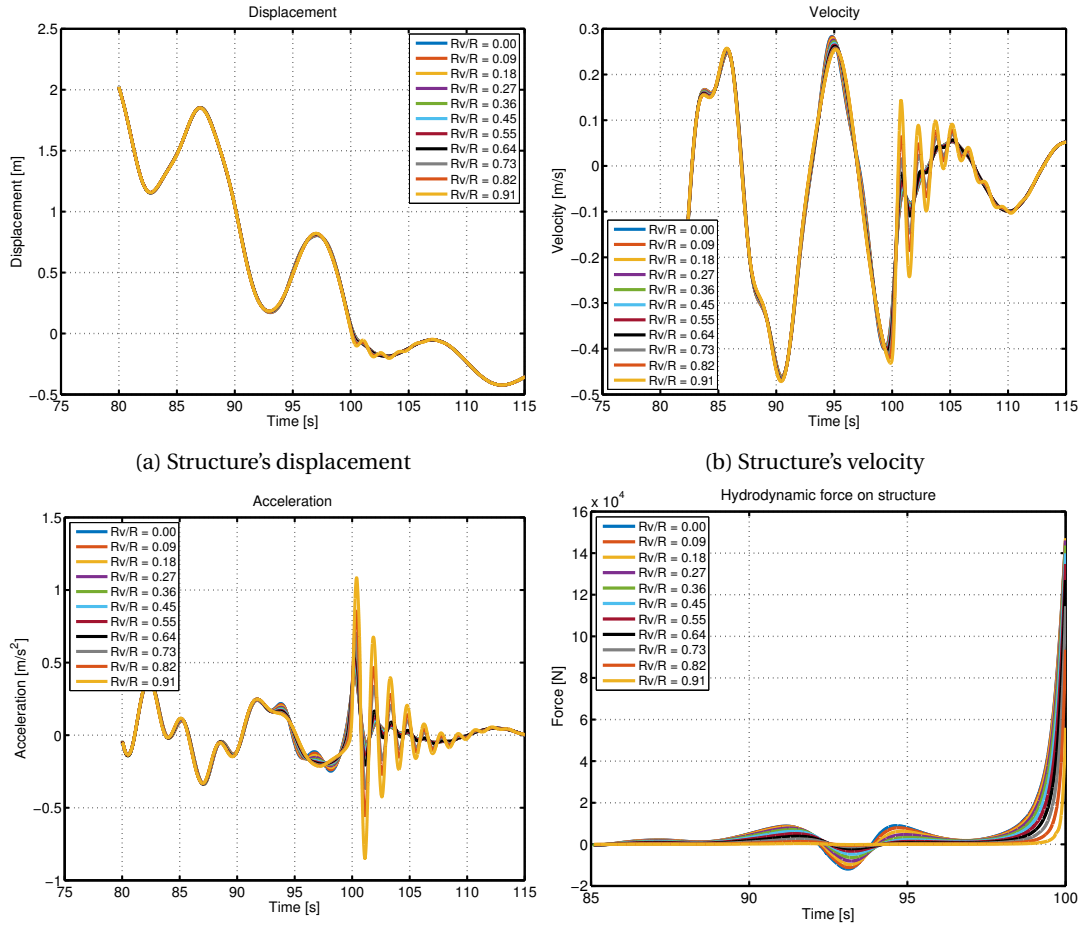

(a) Structure's displacement

(b) Structure's velocity

(c) Structure's acceleration

(d) Hydrodynamic force, zoomed in

Figure I.6: Base case for all valve ratio's

I.2. CRANE TIP HEAVE MOTION

The P90 values of the hydrodynamic force and the soil displacement for a disk with R_v = 1.5 m are given in figure I.7. The soil disturbance, based on the P90 values for T = 8 s, are given in figure I.7b. Also here the combination of T = 8 s and A = 1.25 leads to the largest soil displacement. The estimated soil disturbance graphs corresponding to a period of 10, 12, 14 & 16, respectively, have been left out of this report.

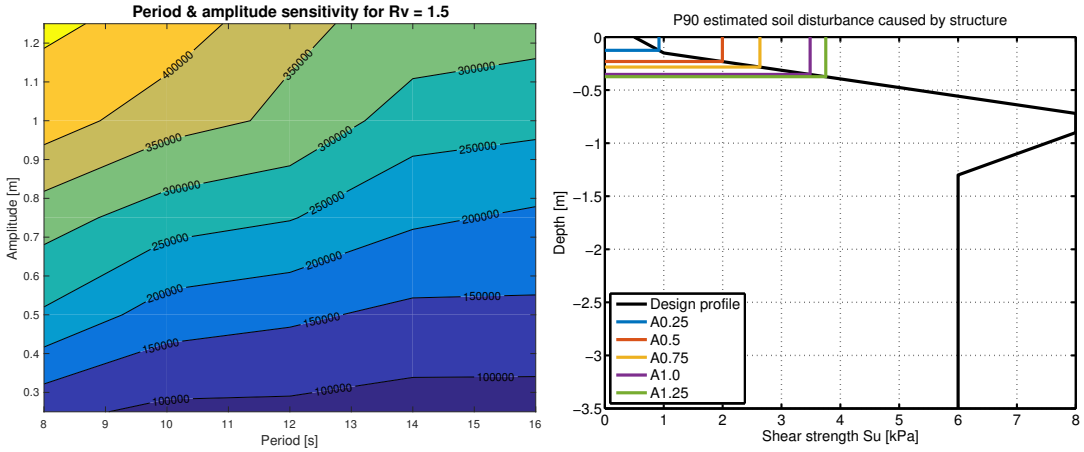

(a) Weather sensitivity on hydrodynamic force for disk with $R_v = 1.5m$

(b) Estimated soil disturbance for disk with $R_v = 1.5m$, $T = 8s$ and variable A

Figure I.7: Weather sensitivity analysis for disk with $R_v = 1.5m$

Figure I.8 shows the results for a disk with R_v = 2.5 m. It can be noticed that the P90 values for such a large valve are significantly lower compared to a valve with R_v = 1.5 m. According to the Design profile, a structure with this size in valve will displace nearly no soil. It is expected that the Design profile for structures with such large valves is not valid any more. In such a case, it is predicted that the soil will move in upward direction through the valve.

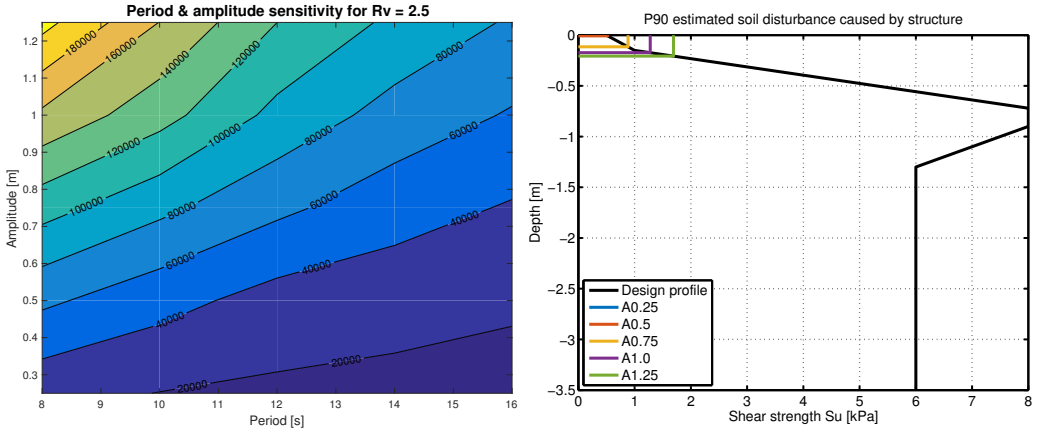

(a) Weather sensitivity on hydrodynamic force for disk with $R_v = 2.5m$

(b) Estimated soil disturbance for disk with $R_v = 2.5m$, $T = 8s$ and variable A

Figure I.8: Weather sensitivity analysis for disk with $R_v = 2.5m$

The conservation of energy method also has been used to calculate the soil displacement corresponding to the contour plots in figures I.7b and I.8b. The displacements coming from T = 8 s, ζ = 1 and various amplitudes for the disk with R_v = 1.5 m and R_v = 2.5 m are given in table I.1. The value for R_v = 0 m and R_v = 0.5 m are for simplicity also given in the table. As expected, they are more conservative compared to the Design Profile.

R_v	A = 0.25 m	A = 0.5 m	A = 0.75 m	A = 1 m	A = 1.25 m
0 m	0.094 m	0.130 m	0.140 m	0.163 m	0.181 m
0.5 m	0.072 m	0.074 m	0.082 m	0.158 m	0.176 m
R_v = 1.5 m	0.058 m	0.070 m	0.087 m	0.104 m	0.169 m
R_v = 2.5 m	0.035 m	0.060 m	0.075 m	0.091 m	0.106 m

Table I.1: 2D model: estimated soil displacement for ζ = 1, T = 8 s and various amplitudes

I.3. SOIL CONDITIONS

The maximum hydrodynamic force for all phases and estimated soil disturbance has been visualized for different soil stiffnesses in figure I.9. For soil with stiffness k_{soil} = 7.04 MN/m, the highest hydrodynamic forces and largest soil disturbance can be observed. This was expected and in correspondence to what was seen in the analysis on the valve influence on a rigid boundary, section 7.2.

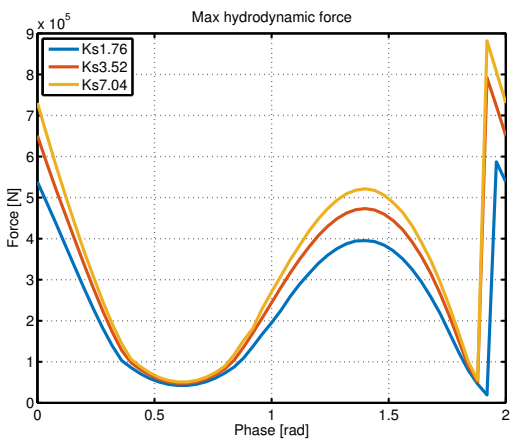

(a) Soil influence

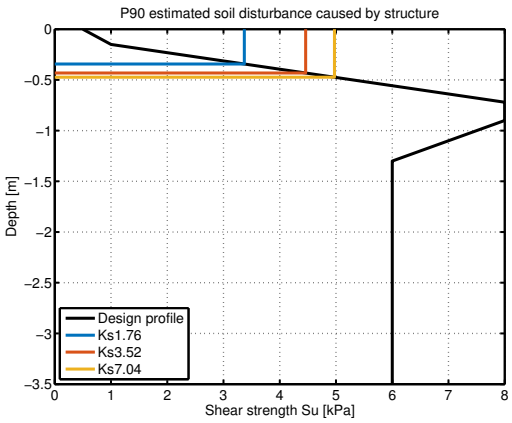

(b) Estimated soil disturbance for disk with $R_v = 0.75m$ and variable k_{soil}

Figure I.9: Sensitivity analysis soil conditions

J

GLOBAL EQUILIBRIUM

J.1. DERIVATION GLOBAL EQUILIBRIUM

This section explains the derivation of the global equilibrium. Global means the equilibrium is independent of the position. Thus, the global equilibrium must hold at the edges of the disk, see figure J.1.

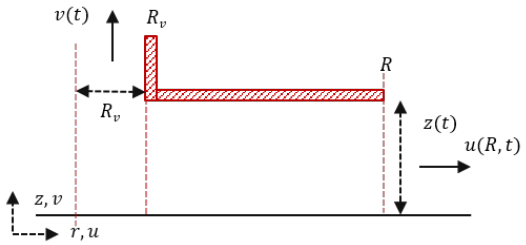

Figure J.1: Global equilibrium

This global equilibrium is derived by means of the conservation of momentum. Assuming there is no change in momentum, the momentum flux and external force for the plate side are described in equations J.1 and J.2 and for the valve in equations J.3 and J.4, respectively. The P^+ and P^- represent the pressure at the plate side and the valve, respectively.

$$\iint_A \rho\left(\vec{u}\cdot\vec{n}\right)\vec{u}\,dA = 2\pi Rz\rho u(R,t)^2 \tag{J.1}$$

$$\iint_A p\left(-\vec{n}\right)dA = P^+ 2\pi Rz \tag{J.2}$$

$$\iint_A \rho\left(\vec{u}\cdot\vec{n}\right)\vec{u}\,dA = \rho\pi R_v^2 v(t)^2 \tag{J.3}$$

$$\iint_A p\left(-\vec{n}\right)dA = P^-\pi R_v^2 \tag{J.4}$$

These equations can be substituted into the conservation of momentum, see equation J.5. In the derivation of the hydrodynamic force, the hydrostatic pressure at the outside was assumed to be zero: $P^+ = P^- = 0$. Finally, the global equilibrium is given in equation J.6.

$$P^+ 2\pi Rz + 2\pi Rz\rho u(R,t)^2 = P^-\pi R_v^2 + \rho\pi R_v^2 v(t)^2 \tag{J.5}$$

$$2\pi Rz\rho u(R,t)^2 = \rho\pi R_v^2 v(t)^2 \tag{J.6}$$

$$v(t) = \sqrt{2Rz}\left(\frac{u(R,t)}{R_v}\right) \tag{J.7}$$

J.2. ATTEMPTED APPROACHES

This section describes the attempted approaches on improving the hydrodynamic force by including an extra boundary equation.

BASED ON EQUILIBRIUM BETWEEN EQUATIONS OF MOMENTUM CONSERVATION

- The local equilibrium between the equations of momentum conservation, $\frac{\partial p}{\partial r}|_{plate} = \frac{\partial p}{\partial r}|_{valve}$, resulted in a local expression for $\frac{\partial v}{\partial t}$ in chapter 4.
- This expression was set equal to the global $\frac{\partial v}{\partial t}$, derived from equation J.7, and solved for an expression for the stagnation point R_s.
- The local $\frac{\partial v}{\partial t}$, global $v(t)$ and stagnation point R_s were inserted in the conservation of momentum. That equation, being a function of only know variables, was converted into an equation for the pressure and eventually the hydrodynamic force. The results generated were not realistic.
- When implementing a variable stagnation point, the connection made of $\frac{\partial p}{\partial r}|_{plate} = \frac{\partial p}{\partial r}|_{valve}$ at $r = R_v$ does not hold any more. It is thought that in this case you should remain with a conservation of mass of $u(r,t)$ (as function of i.a. R_v) and a conservation of momentum (instead of each equation double).
- It is expected that we remain with the global equation J.6 and the following two local equations:

$$u(r,t) = \frac{R_v v(t) - r\frac{dz}{dt}}{2z} \tag{J.8}$$

$$\frac{1}{\rho}\frac{\partial p}{\partial r} + 2u\frac{\partial u}{\partial r} + \frac{1}{2z}\frac{\partial}{\partial t}(zu) = 0 \tag{J.9}$$

- In the three other attempted approaches, only these three fundamental equations have been considered.

BASED ON EQUILIBRIUM $v(t)$

- The global equilibrium (equation J.6) was rewritten into $u(R,t)$ and set equal to the local horizontal velocity $u(r,t)$ at $r = R$.
- Solving this equilibrium for $v(t)$ and substituting that into $u(r,t)$ resulted in a function of $u(r,t)$ independent of R_v.
- Converting the conservation of momentum into the pressure, with substitution of $u(r,t)$ independent of R_v, resulted in a function for the pressure independent of R_v. This can not be correct, as R_v represents the presence of the valve in the hydrodynamic force.

BASED ON EQUILIBRIUM $u(R,t)$

- The local $u(r,t)$ was inserted into the global equilibrium (equation J.6) at $r = R_v$ and solved for $v(t)$. By inserting this $v(t)$ into $u(r,t)$ again the R_v was omitted from $u(r,t)$.
- Similarly, this ended in a function for the pressure independent of R_v.

BASED ON EQUILIBRIUM $\frac{du}{dr} = 0$

- At the position where the stagnation point occurs, the following should hold: $\frac{du}{dr} = 0$. By using J.8, this equilibrium results in $\frac{du}{dr} = -\frac{\frac{dz}{dt}}{2z} = 0$. The only possibility for this to hold is if z or $\frac{dz}{dt}$ were equal to zero. This seems unrealistic and thus expected to be incorrect.

List of Figures

List of Tables